FACULTÉ DES ÉTUDES SUPÉRIEURES ET POSTOCTORALES

uOttawa

L'Université canadienne
Canada's university

FACULTY OF GRADUATE AND POSDOCTORAL STUDIES

Jehad Saleh

AUTEUR DE LA THÈSE / AUTHOR OF THESIS

M.A.Sc. (Chemical Engineering)

GRADE / DEGREE

Department of Chemical Engineering

FACULTÉ, ÉCOLE, DÉPARTEMENT / FACULTY, SCHOOL, DEPARTMENT

A model of a partially flooded anode-backing layer (ABL) in a direct methanol fuel cell (DMFC)

TITRE DE LA THÈSE / TITLE OF THESIS

Marten Ternan

DIRECTEUR (DIRECTRICE) DE LA THÈSE / THESIS SUPERVISOR

Yves Bourgault

CO-DIRECTEUR (CO-DIRECTRICE) DE LA THÈSE / THESIS CO-SUPERVISOR

EXAMINATEURS (EXAMINATRICES) DE LA THÈSE / THESIS EXAMINERS

Xudong Cao

Marc Dubé

Gary W. Slater

LE DOYEN DE LA FACULTÉ DES ÉTUDES SUPÉRIEURES ET POSTDOCTORALES /
DEAN OF THE FACULTY OF GRADUATE AND POSTDOCORAL STUDIES

A model of a partially flooded anode-backing layer (ABL) in a direct methanol fuel cell (DMFC)

JEHAD SALEH

Thesis submitted to the
Faculty of Graduate and Postdoctoral Studies
in partial fulfillment of the requirements
for the degree of Master of Applied Science in Chemical Engineering

Department of Chemical Engineering
Faculty of Engineering
University of Ottawa

Your file Votre référence
ISBN: 0-494-14945-0
Our file Notre référence
ISBN: 0-494-14945-0

ABSTRACT

Direct methanol fuel cells (DMFCs) generate electrical energy from an electro-chemical reaction between methanol and oxygen in the presence of a platinum containing electro-catalyst. They normally have the following components: (a) the anode gas channel, (b) the anode backing layer (that distributes liquid methanol and water from the anode gas channel to the anode catalyst layer), (c) the anode catalyst layer (that performs the reaction, $CH_3OH + 2\ H_2O = CO_2 + 6\ H^+ + 6\ e^-$), (d) the electrolyte layer (that transports H^+ from the anode catalyst layer to the cathode catalyst layer), (e) the cathode catalyst layer (that performs the reaction $^3/_2\ O_2 + 6\ H^+ + 6\ e^- = 3\ H_2O$), (f) the cathode backing layer (that distributes oxygen from the cathode gas channel to the cathode catalyst layer and transports water formed in the cathode catalyst layer to the cathode gas channel), and (g) the cathode gas channel.

The direct methanol fuel cell being modeled in this project is being developed primarily for low power applications (lap-tops, PDA's) and to a lesser extent for transportation applications (automobiles, fork-lifts). A major problem in DMFC's is methanol crossover from the anode to the cathode without any electrochemical reaction. Species movements are controlled by four mechanisms, diffusion and convection for all species, plus migration of protons driven by the electrical potential gradient, and electro-osmotic drag of polar molecules by the protons.

A one-dimensional model of the anode-backing layer in a low temperature DMFC operating with a liquid feed has been developed. The model describes the flow of the liquid phase from the anode gas channel toward the anode catalyst layer and the simultaneous flow of the gas phase in the opposite direction.

The variables investigated include, current density, contact angle, methanol molarity, layer thickness, and the diameter of the CO_2 gas bubbles formed in the anode gas channel. It was found that the primary mechanism for flow was convection for the liquid phase water and methanol, and a combination of diffusion and convection for the CO_2 gas.

RÉSUMÉ

Les piles à combustible directes au méthanol (DMFCs) produisent de l'énergie électrique à partir d'une réaction électro-chimique entre le méthanol et l'oxygène en présence d'un électro-catalyseur à base de platine. Ces piles à combustible possèdent normalement les composantes suivantes : (a) un canal anodique pour le gaz, (b) une couche anodique poreuse de transport et de soutien (distribuant le méthanol et l'eau liquide du canal anodique vers la couche catalytique de l'anode), (c) une couche de catalyseur anodique (siège de la réaction, $CH_3OH + 2\ H_2O = CO_2 + 6\ H^+ + 6\ e^-$), (d) une couche électrolytique (transportant les ions H^+ de la couche de catalyseur anodique à la couche de catalyseur cathodique), (e) une couche de catalyseur cathodique (siège de la réaction $^3/_2\ O_2 + 6\ H^+ + 6\ e^- = 3\ H_2O$), (f) une couche cathodique poreuse de transport et de soutien (distribuant l'oxygène du canal cathodique vers la couche de catalyseur cathodique et transportant l'eau formée dans la couche de catalyseur cathodique vers le canal cathodique), et (g) un canal cathodique pour le gaz.

Les piles à combustible directes au méthanol faisant l'objet de la présente étude sont développées principalement pour alimenter les appareils à faible puissance (tel que les ordinateurs portables, les PDA's) et éventuellement pour des applications reliées au transport (tel que les automobiles, les chariots élévateurs). Un des plus grands problèmes des DMFC est la perte de performance résultant du passage de méthanol de l'anode vers la cathode sans qu'aucune réaction électro-chimique ne réduise ce méthanol. Plus généralement, le mouvement des espèces chimiques dans les DMFC est contrôlé par quatre mécanismes, soit la diffusion et la convection de toutes les espèces, la migration des protons induite par le gradient du potentiel électrique et la dérive électro-osmotique des molécules polaires par les protons.

Dans cette thèse, un modèle uni-dimensionnel de la couche anodique de transport d'une DMFC opérant à basse température avec une alimentation liquide a été développé. Le modèle décrit le flux de la phase liquide du canal anodique vers la couche de catalyseur anodique ainsi que le flux simultané de la phase gazeuse en sens inverse.

Les paramètres du modèle incluent la densité de courant, l'angle de contact, la molarité du méthanol, l'épaisseur de la couche anodique de transport et le diamètre des

bulles de CO_2 gazeux formées dans le canal anodique. Il a été constaté que le mécanisme principal de transport des espèces était la convection pour l'eau en phase liquide et le méthanol, et une combinaison de la diffusion et convection pour le gaz de CO_2.

ACKNOWLEDGEMENTS

I am deeply grateful to my thesis supervisor, Dr. Marten Ternan, for his continuous guidance, support and enthusiasm throughout this work, and for being an inspiring teacher for me.

I would also like to express my most sincere thanks to Dr. Yves Bourgault for supervising my work, for his generous help, and invaluable suggestions and advice.
I am grateful to my mother, my wife, and my kids for their endless love and support.

TABLE OF CONTENTS

CHAPTER ONE: INTRODUCTION

CHAPTER TWO: REVIEW OF DMFC MODELING LITERATURE

CHAPTER THREE: A model of a partially flooded anode-backing layer (ABL) in a direct methanol fuel cell (DMFC)

CHAPTER FOUR: Complete mathematical equations for ACL, ELL, CCL, and CBL

CHAPTER FIVE

CHAPTER SIX

APPENDICES

LIST OF FIGURES

LIST OF TABLES

CHAPTER ONE

INTRODUCTION

1.1 A Brief History of Fuel Cells

In 1839 Sir William Grove invented the fuel cell. He produced electricity by combining hydrogen and oxygen at electrodes that were separated by an aqueous liquid acid electrolyte. Subsequently, throughout the 19^{th} and 20^{th} centuries, a variety of researchers investigated fuel cell reactions for the conversion of chemical energy into electrical energy. The first practical application of fuel cells occurred during the Apollo space program from 1960 to 1965. Those fuel cells provided both drinking water and electricity. In 1970 Kordesch built a car that operated using the combination of an alkaline fuel cell and a lead acid battery. Recently environmental pollution issues have been the driving force for the development of fuel cells.

1.2 Fuel Cells - Definition, Composition, and Operating Principles

A fuel cell is a device that generates electricity and produces heat from an electro-chemical reaction using suitable catalysts. The most common fuel used in fuel cells is hydrogen. It is used in combination with oxygen to produce electricity based on the following overall chemical reaction

$$H_2 + \tfrac{1}{2} O_2 \rightarrow H_2O \qquad (1\text{-}1)$$

In general, a fuel cell assembly can be divided into five layers as shown in figure 1-1. On each side of the five layers there are flow channels that are usually machined into solid graphite plates. The anode side of the fuel cell includes the anode-backing layer (anode diffusion layer) and the anode catalyst layer. The cathode side includes the cathode backing layer (cathode diffusion layer) and the cathode catalyst layer. The electrolyte layer separates the anode side from the cathode side of the fuel cell. If the electrolyte is a membrane, the five layers are called a Membrane Electrode Assembly (MEA).

Hydrogen or a hydrocarbon-containing fuel such as methanol is supplied to the anode side and electrochemically oxidized. Oxygen or air is supplied to the cathode side and electrochemically reduced. The anode reaction that occurs at the anode side (anode catalyst layer) produces protons and electrons. Electrons flow through (a) the electronically conducting anode material, to (b) the external circuit that contains an electrical load, to (c) the cathode side. The protons travel through a specific electrolyte (such as a membrane), to (d) meet the electrons and oxygen at the cathode side, where the cathode reaction occurs.

Each of the fuel cell layers has individual characteristics. The backing layers in the anode and the cathode have several functions. They are the thickest of the layers and they provide the mechanical strength for the MEA that includes the other layers of the fuel cell. They are made from either carbon paper or carbon cloth composed of fibers that create a porous structure. The channels containing the flowing reactants are interspersed with "lands", or regions of the backing layers that are not exposed to reactants. The porous structures of the backing layers permit the reactants to diffuse in a direction perpendicular to the catalyst layers and thereby provide a more even concentration of reactants at the interface between the catalyst layer and the backing layer. The carbon backing layers also provide both good electronic conductivity for the electrons that participate in the electrochemical reactions and good heat conductivity for the heat released when the electrochemical reactions that occur. Often the backing layers are made hydrophobic by using Teflon, in order to avoid flooding that comes from water produced by the reaction. The need for hydrophobicity at the cathode is generally greater than that at the anode, as most of product water is produced at the cathode.

The next layer is the anode or cathode catalyst layer that is a thin porous solid. It is often composed of a precious metal (Pt, Ru) on a carbon support. The carbon support provides a large surface area on which the precious metal can be dispersed. This permits a large surface area of the precious metal to contact the reactants.

The last layer that separates the two sides is an electrolyte. The type of electrolyte is usually the characteristic that distinguishes the different fuel cell types. The purpose of the electrolyte is to transport ionic species (eg. H^+) from one side to the other.

1.3 Advantages of fuel cell compared to combustion

In principle fuel cells processes can have substantially greater energy efficiencies than combustion processes. During combustion a fuel is burned in the presence of an oxygen-containing gas (usually air) to produce heat (eg. burning gasoline inside the internal combustion engine of a car). The durability of materials at high temperatures limits the theoretical energy efficiencies of combustion processes to approximately 60%. The energy efficiencies obtained in practice are normally in the 30-40 % range. In fuel cells, the fuel reacts electrochemically to produce electricity. Fuel cells are not required to operate at temperatures as high as those in combustion processes. In contrast to combustion processes, the theoretical energy efficiencies of fuel cells can be above 90%. One of the goals of current fuel cell research is to demonstrate fuel cell energy efficiencies that exceed those of combustion processes.

1.4 Types of fuel cells

The direct methanol fuel cell (DMFC) is one of the six different fuel cell categories. Each of the other types will be described briefly before providing a more detailed description of the DMCF.

The categories are defined by both the type of the electrolyte used (liquid or solid) and by their operating temperature. The following list is arranged in order of ascending temperatures.

1) Alkaline fuel cell (AFC).
2) Direct Methanol Fuel Cell (DMFC).
3) Proton exchange membrane fuel cells or polymer electrolyte membrane fuel cells (PEMFC).
4) Phosphoric acid fuel cell (PAFC).
5) Molten carbonate fuel cell (MCFC).
6) Solid oxide fuel cell (SOFC).

1.4.1 Alkaline fuel cells

Alkaline fuel cells (AFC) have an aqueous potassium hydroxide electrolyte (KOH) and operate at temperatures of 50 – 200 °C. They are classified as low temperature fuel cells. The electrochemical reactions in an AFC are:

Anode Reaction:

$$H_2 + 2\ OH^- \rightarrow 2\ H_2O + 2e^- \qquad (1\text{-}2)$$

Cathode Reaction:

$$\tfrac{1}{2}\ O_2 + H_2O + 2e^- \rightarrow 2\ OH^- \qquad (1\text{-}3)$$

Overall Reaction:

$$H_2 + \tfrac{1}{2}\ O_2 \rightarrow H_2O \qquad (1\text{-}4)$$

Hydroxyl ions, OH^- species, are formed during the oxygen reduction reaction at the cathode, equation 1-3, and migrate through the electrolyte to the anode where they react with hydrogen, equation 1-2, to produce water and electrons. These electrons travel through the external circuit to the cathode where they react with oxygen and water. AFCs operate smoothly with pure H_2 and O_2. However, carbon dioxide impurities degrade their electrolyte performance by forming carbonate compounds. They have greater electrical efficiencies than any of the other fuel cells types. Different types of AFC electrodes have been investigated, such as platinum (Pt) promoted with Ni and Pt/Co alloys (Kiros, 1996), Ag/Co catalysts (Geeter et al., 1999), and Pt /Pd at the anode (Kiros, 2000).

The operating lifetimes of AFCs can be extended by circulating the electrolyte. It has several effects. Water produced at the anode can be removed. It can act as a cooling liquid to remove heat from the fuel cell. It is a method of removing carbonates that are produced by the reaction between the electrolyte and the CO_2 impurities that are in the air used at the cathode.

$$CO_2 + 2OH^- \rightarrow (CO_3)^{-2} + H_2O \qquad (1\text{-}5)$$

Carbonate compounds that are not removed in the aqueous phase can precipitate as solids that clog the pores of the gas diffusion layer and decrease the fuel cell performance (Kordesch et al., 1996, 1999, and 2000).

1.4.2 Polymer electrolyte membrane fuel cells (PEMFC)

As noted above, the first application of PEMFCs was in the US space program. Recently a number of PEMFCs have been used in demonstration vehicles. The electrolyte in PEMFCs is a polymer membrane that conducts protons. The membrane is an alternative to an aqueous liquid electrolyte. PEMFCs operate in a temperature range of 50 – 100 °C and are classified as low temperature fuel cells.

The electrochemical reactions in PEMFC's are:

Anode Reaction:

$$H_2 \rightarrow 2\,H^+ + 2\,e^- \qquad (1\text{-}6)$$

Cathode Reaction:

$$\tfrac{1}{2}\,O_2 + 2H^+ + 2e^- \rightarrow \quad H_2O \qquad (1\text{-}7)$$

Overall reaction:

$$H_2 + \tfrac{1}{2}\,O_2 \rightarrow H_2O \qquad (1\text{-}8)$$

At the anode, equation 1-6, hydrogen atoms are oxidized to form protons that migrate through a membrane to the cathode. In accordance with equation 1-6, the electrons flow through an external electrical circuit from the anode to cathode. At the cathode, equation 1-7, protons, electrons, and oxygen combine to form water.

Nafion is the membrane used in PEMFCs. It is polytetrafluoroethylene (PTFE) polymer containing sulphonic acid groups. The hydrophobic properties of PTFE are desirable for diminishing flooding by water. The transport of protons through Nafion is attributed to the concentration of the sulphonic acid groups. Because the water content of PEMFC membranes has a major impact on proton conductivity, water management in PEMFCs is one of the most important issues. Several investigations have been performed to improve the membrane structure and the conductivity (Nouel and Fedkiw, 1998; Abraham et al, 2000; Doyle et al., 2000; Peled et al., 1998). Although proton transport through the

membrane is desirable, the cross-over through the membrane of other species, such as methanol, hydrogen, and oxygen, should be minimized. Since both proton transport and species cross-over become easier as the membrane thickness decreases, optimization is required (Kordesch et al., 1996).

Platinum is the electro-catalyst most commonly used for the cathode. Unfortunately the fuel used at the anode often contains carbon monoxide (CO impurities in H_2 fuel, CO formed from methanol). CO is strongly adsorbed on Pt metal reaction sites and therefore is a poison for the Pt anode electro-catalysts that decreases reaction sites for fuel molecules, hydrogen or methanol. The uses of Pt-Ru alloy catalysts have diminished this problem. The current state of PEMFC technology has been reviewed recently (Mathias et al., 2005).

1.4.3 Phosphoric Acid Fuel Cells (PAFC)

PAFCs use concentrated phosphoric acid as their electrolyte. Their temperatures are in the range of 150 – 200°C and they are classified as low temperature fuel cells. The electrochemical reactions in PAFCs are:

Anode Reaction:

$$H_2 \rightarrow 2\,H^+ + 2\,e^- \qquad (1\text{-}9)$$

Cathode Reaction:-

$$\tfrac{1}{2}\,O_2 + 2\,H^+ + 2\,e^- \rightarrow H_2O \qquad (1\text{-}10)$$

Overall reaction:-

$$H_2 + \tfrac{1}{2}\,O_2 \rightarrow H_2O \qquad (1\text{-}11)$$

Hydrogen ions (protons), produced at the anode according to equation 1-9, migrate through the electrolyte from the anode to the cathode, while electrons travel through an external electrical circuit from the anode to the cathode. Protons, electrons, and oxygen at the cathode form water in accordance with equation 1-10.

More than 250 PAFC units producing 200 kW of electrical power plus heat have been constructed. Several have been in operation for more than 5 years. A Pt catalyst dispersed on carbon was used in the electrodes. Flooding is inhibited in the backing layer and the

catalyst layer by adding PTFE to make them hydrophobic. Savadogo and Beck (1996) have reported that electrodes made from Pt / WO_3 are superior to Pt / C electrodes.

1.4.4 Molten Carbonate Fuel Cells (MCFC)

MCFCs use a combination of alkali (Na, K, and Li) carbonate in molten form as the electrolyte and operate in a temperature range of 600 – 1000°C. They are classified as high temperature fuel cells. The electrochemical reactions in MCFCs are:

Anode Reaction:

$$H_2 + CO_3^{-} \rightarrow H_2O + CO_2 + 2e^{-} \qquad (1\text{-}12)$$

Cathode Reaction:

$$\tfrac{1}{2} O_2 + CO_2 + 2e^{-} \rightarrow CO_3^{-} \qquad (1\text{-}13)$$

Over all reaction:

$$H_2 + \tfrac{1}{2} O_2 \rightarrow H_2O \qquad (1\text{-}14)$$

Carbonate ions form at the cathode and migrate through the electrolyte to the anode where hydrogen is oxidized. The rapid reaction kinetics at the high operating temperatures in MCFCs eliminates the requirement for precious metal catalysts. For example, inexpensive catalysts, such as NiO are often used for oxygen reduction at the cathode and Ni metal catalysts are often used at the anode. Other types of catalyst alloys and electrolytes (Rohland and Jantsch, 1997; Yuh et al., 1995) have also been used.

1.4.5 Solid Oxide Fuel Cells (SOFC)

The electrolyte in SOFCs is typically a mixture of zirconium oxide and calcium oxide that forms a crystal lattice. It is reasonably stable and has an acceptable oxide ion conductivity that increases with temperature over the range of 600 – 1000°C. It is classified as a high temperature fuel cell. The electrochemical reactions in SOFCs are:

Anode Reaction:

$$H_2 + O^{2-} \rightarrow H_2O + 2e^{-} \qquad (1\text{-}15)$$

Cathode Reaction:

$$\tfrac{1}{2} O_2 + 2 e^- \rightarrow O^{2-} \qquad (1\text{-}16)$$

Overall reaction:

$$H_2 + \tfrac{1}{2} O_2 \rightarrow H_2O \qquad (1\text{-}17)$$

The oxygen ions produced at the cathode, according to equation 1-16, migrate through the electrolyte (crystal lattice) to the anode to oxidize the fuel. SOFCs have been demonstrated in combined heat and power applications from 2 kW to multi MW sizes. Several types of anode and cathode catalysts have been tested (Shibuya and Nagamoto 1997; Buchkremer et al., 1997; Doshi et al., 1997). Typically catalysts are (Co-ZrO_2) or (Ni-ZrO_2) cermets at the anode and strontium-doped lanthanum manganite (Sr-La MnO_3) at the cathode.

1.4.6 Direct Methanol Fuel Cells (DMFC)

The direct methanol fuel cell is a promising power source for low power applications and possibly for vehicles. Its characteristics of low emissions, operation near ambient conditions, acceptable efficiency, stability with acidic membranes, and a potentially renewable fuel source make the DMFC a technology of interest. It can be classified as a low temperature fuel cell since it usually operates below 150°C.

DMFCs can be divided into several sections, as shown in figure 1-1 and in the following description:

1.4.6.1 Sections and reactions in the DMFC

The first section is a graphite–plate current collector (used at both the anode and the cathode) having channels through which reactants and products flow when they enter and exit the cell. The second section is the backing layer, sometimes referred to as the gas diffusion layer (located at both the anode and the cathode). It provides mechanical support to

the membrane electrolyte assembly (MEA). It is a porous material that conducts both the electrons and the heat produced at the catalyst layers. It distributes the reactant or fuel from

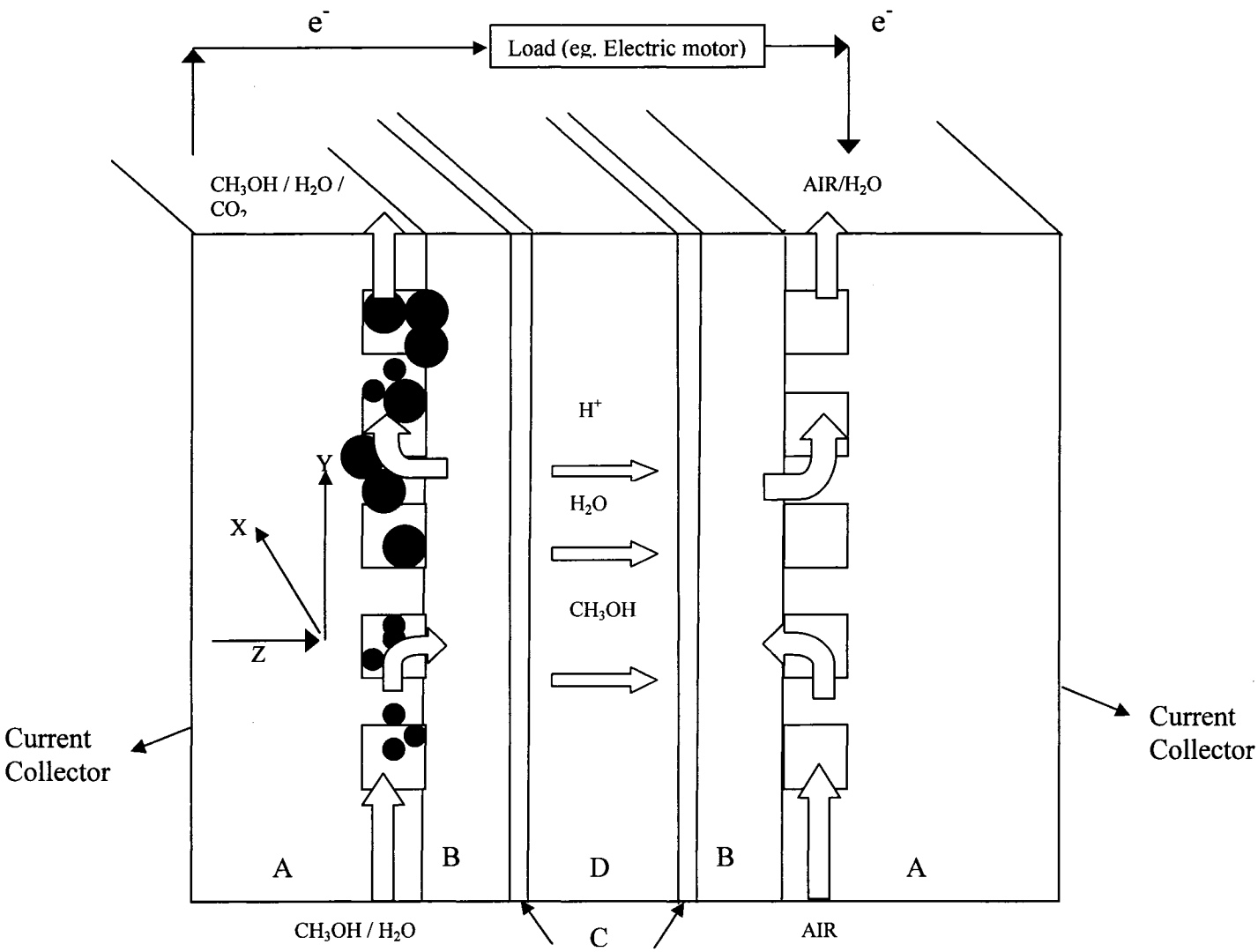

Fig 1-1: Schematic diagram of DMFC, (PEM = Polymer Electrolyte Layer)

A: Is a current collector (bipolar plates), having a flow channel (1 mm) thickness.
B: Is a porous carbon paper backing layer (anode and cathode), 100 μm thickness, each.
C: Is a porous carbon support for the catalyst (anode and cathode catalyst layers), 10 μm thickness, each.
D: Is the polymer electrolyte layer, (usually a Nafion membrane, 200 μm, thickness).

●: Are the bubbles of carbon dioxide formed from the electrochemical reaction at the anode catalyst layer.

□: Flow channel (The flow of fuel at the anode is in the Z-direction across the thickness of the ABL. The flow of air is in the negative Z-direction).

the flow channel to the anode catalyst layer and provides a route to remove the products (CO_2 formed at the anode catalyst layer and H_2O formed at the cathode catalyst layer) from the catalyst layer to the channel.

The third section is a catalyst layer (located at both the anode and the cathode) where at the anode methanol and water react to form carbon dioxide, protons and electrons, according to equation 1-18, and at the cathode the protons and electrons react with oxygen to produce water, according to equation 1-19. The fourth section is the proton exchange membrane that is used to transfer protons from the anode to the cathode, and to minimize the transfer of methanol, oxygen, and electrons between anode and cathode. The electrochemical reactions for DMFCs are:

Anode Reaction:

$$CH_3OH + H_2O \rightarrow CO_2 + 6H^+ + 6e^- \qquad (1\text{-}18)$$

Cathode Reaction:

$$^3/_2\, O_2 + 6\, H^+ + 6e^- \rightarrow 3H_2O \qquad (1\text{-}19)$$

Overall Reaction:

$$CH_3OH + {}^3/_2\, O_2 \rightarrow CO_2 + 2H_2O \qquad (1\text{-}20)$$

Methanol is fed to the anode channel with water in either the liquid or the vapor state. Then it flows through the anode-backing layer to the anode catalyst layer. Air or oxygen is fed to the cathode channel. Then it flows through the cathode-backing layer to the cathode catalyst layer. The transport of molecular reactants and products occurs by a combination of diffusion and convection. The reaction at the anode produces protons that migrate through the Nafion solid electrolyte. As the protons migrate, they drag water and methanol with them (electro-osmotic drag).

1.4.6.2 Advantages and disadvantages of DMFC

DMFCs have both advantages and disadvantages. In addition to producing low emissions, being easy to produce and transport, and being a promising power source for low power applications and possibly for vehicles, methanol has a high energy density (3800

kcal/L) compared to hydrogen (650 kcal/L at 360 atm), (Gurau and Smotkin 2002), where energy density is a measure of the volume necessary for storage. An example is the weight of the fuel that must be carried by a vehicle to travel a defined distance. One of the difficulties for DMFCs is the poor kinetics of the anode reaction, especially at low operating temperatures. That results in larger reactors and greater capital cost. Single methanol fuel cells are combined into stacks containing many cells. Each of the cells has several, cm^2, of cross-sectional area. Stacks can generate larger amounts of electrical power than individual cells. An important development issue is the improvement of catalysts.

A major concern in (DMFC) is the crossover of methanol molecules through the solid membrane from the anode to the cathode. At the cathode the methanol molecules that have crossed-over are oxidized to carbon dioxide without any electrons having been formed, and without conversion of the chemical energy to electrical energy. This causes a mixed potential at the cathode and leads to poor fuel utilization thereby decreasing the performance of the cell. Attempts have been made to develop methanol–tolerant oxygen reduction electro-catalysts. They are catalysts that are active for oxygen reduction and inactive for methanol oxidation. Another approach has been the modification of the membrane properties in order to minimize the methanol crossover. Other suggestions include, increasing the thickness of the membrane to diminish the transport of methanol or increasing the thickness of the anode catalyst layer to increase the fraction of feed methanol that is oxidized before it reaches the interface between the anode catalyst layer and the membrane.

1.4.6.3 Mechanism of methanol electrochemical oxidation

A variety of materials are used in fuel cells. The backing layers are composed of carbon paper or carbon cloth. Platinum is normally used as an oxygen reduction catalyst at the cathode. At the anode the catalyst is either platinum or a platinum alloy such as Pt-Ru. The anode and cathode catalyst layers can be prepared in several ways. The catalyst can be attached to the backing layer by rolling, cold spraying and pressing (Ramkumar and Dheenadayalan, 1997).

A detailed mechanism for methanol electrochemical oxidation on a (Pt- Ru) anode catalyst has been proposed (Ley et al., 1997).

$Pt + CH_3OH \rightarrow Pt^{\bullet}(CH_3OH)_{ads}$

$Pt^{\bullet}(CH_3OH)_{ads} \rightarrow Pt^{\bullet}(CH_3O)_{ads} + H^{+} + e^{-}$

$Pt^{\bullet}(CH_3O)_{ads} \rightarrow Pt^{\bullet}(CH_2O)_{ads} + H^{+} + e^{-}$

$Pt^{\bullet}(CH_2O)_{ads} \rightarrow Pt^{\bullet}(CHO)_{ads} + H^{+} + e^{-}$

$Pt^{\bullet}(CHO)_{ads} \rightarrow Pt^{\bullet}(CO)_{ads} + H^{+} + e^{-}$

$M + H_2O \rightarrow M\bullet(H_2O)_{ads}$

$M\bullet(H_2O)_{ads} \rightarrow M\bullet(HO)_{ads} + H^{+} + e^{-}$

$Pt^{\bullet}(CO)_{ads} + M\bullet(HO)_{ads} \rightarrow Pt + M + CO_2 + H^{+} + e^{-}$

Platinum or platinum-alloys are attractive catalysts for the oxidation of methanol because of their stability and activity. The above mechanism indicates that the oxidation of methanol on Pt based catalysts proceeds by the adsorption of methanol molecules followed by several steps of deprotonation. Following the adsorption and deprotonation steps intermediate adsorbed CO species are formed. They block the surface of the Pt catalyst and inhibit further reaction. A number of studies have been performed with the object of increasing the rate of oxidizing adsorbed CO to CO_2 (Ley et al., 1997, Morimoto and Yeager, 1998). The Pt-Ru alloys have been among the most effective reported to date.

1.4.6.4 Membrane

As indicated above, the membrane electrolyte is an important part of the fuel cell. Nafion membranes are the most widely used electrolytes in DMFCs and they are considered to be one of the most critical materials in the development of DMFCs. Nafion is a sulphonated fluoro–polymer, made from polytetrafluoroethylene (PTFE or Teflon™). In turn the fluoroethylene polymer is made by an ethylene polymerization process in which a fluorine atom is substituted for a hydrogen atom. PTFE is durable and has resistance to chemical attack that results from the strong bond between fluorine and carbon.

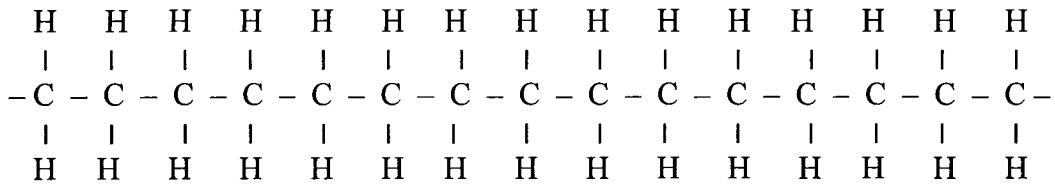

Fig 1-2: Structure of Polyethylene

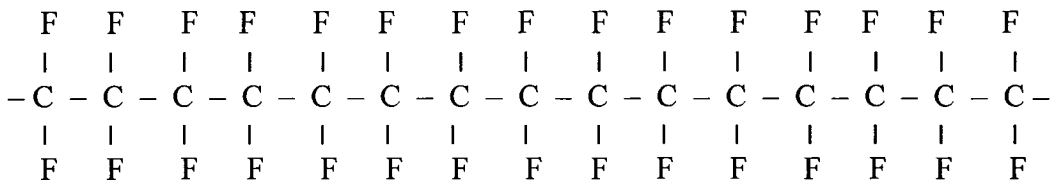

Fig 1-3: Structure of Polytetrafluoroethylene (PTFE)

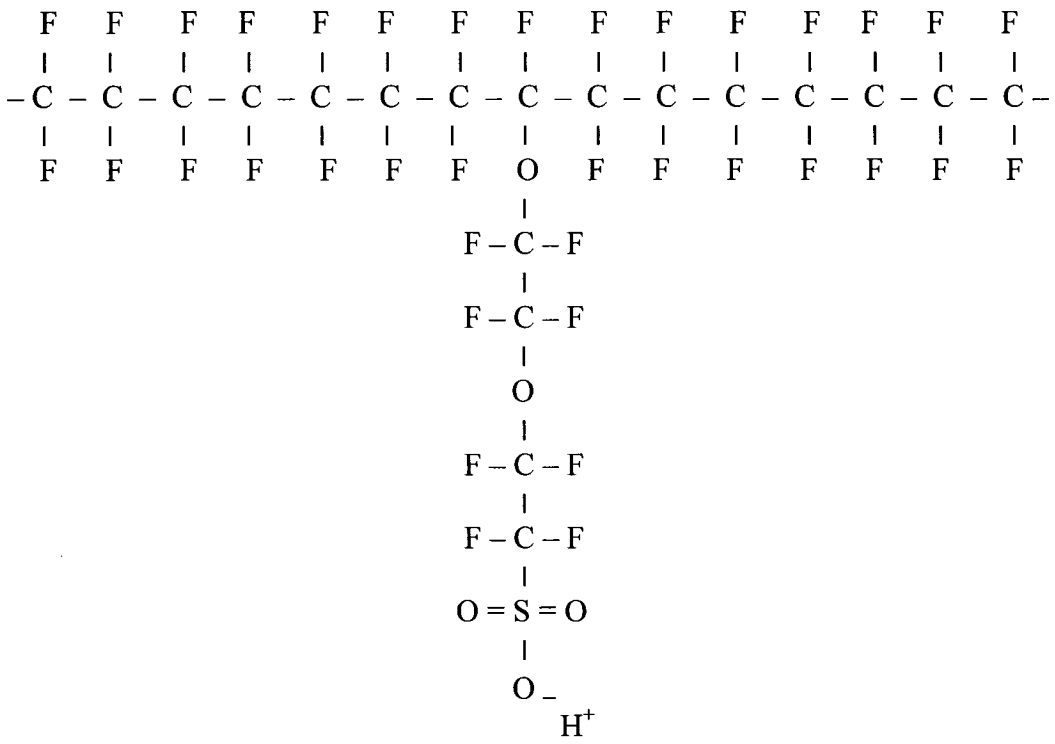

Fig 1-4: Structure of Nafion (Perfluorosulphonic acid PTFE copolymer)

PTFE is a strong hydrophobic polymer and can be used in fuel cell electrodes to prevent flooding. In contrast Nafion is used in fuel cells for the transport of protons. Nafion is made from PTFE polymer by sulphonation that is by adding a side chain ending with a sulphonic acid H+ $SO3^-$ group, where the end of the side chain is actually an SO_3^- ion. The resulting structure is called an ionomer. The presence of these SO_3^- and H^+ ions causes a strong attraction between the + and – charged ions. Therefore the side chains in the polymer tend to cluster within the overall structure of the material.

Sulphonic acid groups are highly hydrophilic, that is they attract water. Therefore Nafion membranes have highly hydrophilic regions that exist within a generally hydrophobic material (PTFE). As a result Nafion can absorb large quantities of water and its dry weight can increase substantially. Desirable properties of DMFC membranes are chemical and electrochemical stability at different operating conditions, mechanical and thermal stability at operating temperatures, with a minimum allowable limit for reactant permeation (cross-over), and of greatest importance large proton conductivity. The membrane is located in the middle of the fuel cell between the anode and cathode catalyst layers. As a result Nafion is often impregnated into the pores of both catalyst layers to assist with the transport of protons.

Because the membrane must remain hydrated for proper fuel cell operation, water management is important. The conductivity of the membrane is directly proportional to its level of hydration. If the membrane dries out the fuel cell operation degrades. Protons (H^+) are produced from the chemical reaction in the anode catalyst layer. Their transport through the membrane is affected by both diffusion, driven by the concentration gradient between the anode the cathode, and by migration, driven by the electrical potential gradient between the anode and the cathode.

There are several mechanisms for water to move through the membrane. For each proton that migrates through the membrane an accompanying shell of water molecules will also be transported with it. This is the electro-osmotic drag phenomenon. A second mechanism is diffusion, driven by the concentration gradient. In a fuel cell, water produced at the cathode by the electro-chemical reaction will diffuse to the anode. Convection is the third mechanism for the transport of water. It arises from the pressure gradient across the membrane between the anode and the cathode.

The same mechanisms that cause the movement of water will also cause the movement of methanol. Both methanol and water can form hydrogen bonds with protons and be transported by electro-osmotic drag. Both methanol and water will be transported by diffusion in response to the concentration gradients. Finally they both can be transported by convection in response to the pressure gradient. The result is that methanol at the interface between the anode catalyst layer and the membrane will cross-over to the cathode.

1.5 Objectives

The overall objective of this investigation paper was to use a mathematical model to describe the anode backing layer in a DMFC, where (1) the liquid feed mixture (methanol and water) is transported from the flow field channel through the liquid-filled pores of the ABL to the anode catalyst layer, and where simultaneously (2) the carbon dioxide produced by the anodic electro-catalytic reaction is transported in the gas-filled pores of the ABL counter currently to the transport of methanol and water in the liquid-filled pores of the ABL. In addition, the effects of the following parameters were to be discussed: current density, methanol concentration, fractional pore volume filled with gas and liquid, wet contact angle of the liquid with the pore walls, and the size of bubbles formed at the interface between the anode channel and the ABL.

References:

K. M. Abraham, V. R. Koch, T. J. Blakley, J. Electrochem. Soc., 147, 1251, (2000).

H.P. Buchkremer, U. Diekmann, L.G.J. de Haart, H. Kabs, U. Stimming, D. Stover

in Proc. Fifth Int. Symp. Solid Oxide Fuel Cells (Eds.: U. Stimming, S. C. Singhal, H. Tagawa, W. Lehnert), Aachen, Germany, 1997, p.160.

R. Doshi, V.L. Richards, M. Krumpelt in Proc. Fifth Int. Symp. Solid Oxide Fuel Cells (Eds.: U. Stimming, S.C. Singhal, H. Tagawa, W. Lehnert), Aachen, Germany, 1997, p.379.

M. Doyle, S. K. Choi, G. Proulx, J. Electrochem. Soc., 147, 34, (2000).

E.D. Geeter, M. Mangan, S. Spaepen, W. Stinissen, G. Vennekens, J. Power Sources, 80, 207, (1999).

B. Gurau, E.S. Smotkin, J. Power Sources, 112, 339, (2002).

Y. Kiros, J. Electrochem. Soc., 143, 2152, (1996).

Y. Kiros, S. Schwartz, J. Power Sources, 87, 101, (2000).

K. Kordesch, J. Gsellmann, M. Cifrain, S. Voss, V. Hacker, R.R. Aronson, C. Fabjan, T. Hezje, J. Daniel-Ivad , J. Power Sources, 80, 190, (1999).

K. Kordesch, V. Hacker, J. Gsellmann, M. Crifrain, G. Falseschini, P. Enzinger, R. Fankhauser, M. Ortner, M. Muhr, R. R. Aronson, J. Power Sources, 86, 162, (2000).

K. Kordesch, G. Simader, Fuel Cells and their Applicantions, VCH, Weinheim, (1996).

K. L. Ley, R. Liu, C. Pu, Q. Fan, N. Leyarovska, C. Segre, E.S. Smoykin,
J. Electrochem Soc., 144, 1543, (1997).

M. F. Mathias, R. Makharia, H.A. Gasteiger, J. J. Conley, T. J. Fuller, C. J. Gittleman, S. S. Kocha, D. P. Miller, C. K. Mittelsteadt, T. Xie, S. G. Yan and P. T. Yu, Interface, 14, 3, (2005).

Y. Morimoto, E. B. Yeager, J. Electroanal. Chem., 444, 95, (1998).

K. M. Nouel, P. S. Fedkiw, Electrochim. Acta, 43, 2381, (1998).

E. Peled, T. Duvdevani, A. Melman, Electrochem. Solid State Lett.1, 210, (1998).

R. Ramkumar, S. Dheenadayalan, J. Power Sources, 69, 75, (1997).

B Rohland, U. Jantsch, in Fourth Int. Symp. Carbonate Fuel Cell Technology (Eds.: J. R. Selman, I. Uchida, H. Wendt, D.A. Shores, T.F. Fuller), Montreal, PQ, (1997), p. 212.

O. Savadogo, P. Beck, J. Electrochem. Soc., 143, 3842, (1996).

Y. Shibuya, H. Nagamoto in Proc.Fifth Int. Symp. Solid Oxide Fuel Cells (Eds.:U. Stimming, S. C. Singhal, H. Tagawa, W. Lehnert), Aachen, Germany (1997), p.510.

C. Yuh, R. Johnsen, M. Farooque, H. Maaru, J. Power Sources, 56, 1, (1995).

CHAPTER TWO

REVIEW OF DMFC MODELING LITERATURE

2.1 An Overview of Fuel Cell Modeling

The possibility of generating electricity by using fuel cells rather than thermal combustion processes has been a dream for many researchers. Examples would be the replacement of the internal combustion engine by fuel cells in automobiles and the replacement of portable batteries with portable fuel cell devices. The current interest in decreasing the amount of pollution has generated additional research in fuel cell technology. Almost all of the current research is directed toward the development of hydrogen fuel cells and direct methanol fuel cells. Those fuel cells that use polymer electrolyte membranes are the ones being described in this investigation. They are considered to be a promising solution because they operate at low temperatures and at near ambient conditions.

In the past twenty years the fuel cell research community has increasingly used mathematical modeling in order to both (a) understand fuel cell performance at different operating conditions and (b) optimize fuel cell design. Three different categories (Cheddie and Munroe, 2005) of fuel cell models have been described:

A) Analytical models: In general approximations are used rather than molecular level descriptions of transport processes and other phenomena. Normally many assumptions that simplify the system are made when an approximate analytical solution is used.

B) Semi – empirical models: Theoretically derived differential and algebraic equations are combined with empirical relationships that are used when the phenomena are complex and difficult to describe theoretically.

C) Theoretical models: Differential and algebraic equations are derived based on the physics and electro chemistry governing all the phenomena that occur in the fuel cell. Some of the first theoretical models for PEMFC were developed for hydrogen fuel cells (Bernardi and Verbrugge, 1991, 1992, and Springer et al., 1991). Several reviews of various fuel cell models have appeared recently (Yao et al., 2004; Cheddie and Munroe, 2005, and Biyikoglu, 2005)

Direct methanol fuel cells have been described in the recent literature (Wasmus and Kuver, 1999; Carrette et al., 2000). They can be divided into those that operate in the gas phase (Scott et al., 1997; Scott et al., 1998; Dohle et al., 2000) and those that operate in the liquid phase. Only those that operate in the liquid phase models are of interest here. Liquid phase mathematical models of direct methanol fuel cells can be divided into two categories; one phase models and two phase models. A more detailed description of these models follows:

2.1.1 Single Phase (Liquid) Models:

One phase DMFC models make the assumption that only the liquid phase needs to be described and that the carbon dioxide gas formed at the anode remains dissolved in the liquid phase. In some of the early work, a simple model was developed (Verbrugge, 1989) in which the liquid phase was described using dilute solution theory. This has progressed to more complicated models of the liquid phase. For example, Myers et al. (2002, 2002a, 2002b) used concentrated solution theory to describe transport in the membrane of a DMFC. The uptake of water vapor by the membrane over the entire range of relative humidities was modeled while the other species were described by a multicomponent equilibrium.

Methanol crossover has been studied in several models. Cruickshank et al. (1998) presented a one-dimensional model that described the permeation of methanol from anode to cathode in DMFC as a function of pressure across the membrane. The need to use different membranes while measuring permeation rates was identified. Sundmacher et al. (1999) showed that methanol mass transfer to the anode catalyst layer is influenced by the formation of bubbles of carbon dioxide vapor, while in contrast the crossover of methanol causes a dramatic drop in cell voltage. They also studied (a) the removal of carbon dioxide from the anode catalyst layer and (b) the poor anode kinetics. Jeng et al. (2002) showed that at low current density and high methanol concentration the methanol crossover causes a serious problem for DMFC at steady-state at isothermal and isobaric conditions. Drake et al. (2004) used an independent transport measurement of carbon dioxide permeation to evaluate the standard assumption by which cathodic carbon dioxide flux is attributed to methanol

cross over. Zhang et al. (2004) used a parallel electrode reaction concept to show that methanol cross over increases the cathode over-potential at low current densities.

The effect of methanol concentration in the liquid fed to the fuel cell has been investigated in several one-dimensional models. Scott et al. (1999) used an empirical model to describe the open circuit voltage and the cathode over-potential to determine the effect of methanol concentration at the catalyst surface on the overall cell voltage and current density response. Limiting current densities were observed to be associated with a diffusion limitation in the flow channel. Sundmacher et al. (2001) studied dynamic changes of methanol feed concentration to predict steady state current voltage characteristics and the fuel cell voltage response. Tae et al. (2005) used a new semi-empirical model to examine the effects of three different concentrations of methanol and a range of cell temperatures on the relationship between cell voltage and current density. Xu et al. (2005) reported a relationship between the methanol feed concentration and the power density at a given current density. Liu et al. (2005) investigated different concentrations of liquid methanol and found that the fuel cell performance improved with increasing methanol concentration and temperature.

Models have also been developed to investigate other phenomena. Baxter et al. (1999) developed a model of the anode catalyst layer, representing the catalyst structure as a thin coating on an ion selective polymer electrolyte. In addition to the assumption of a single liquid phase, they also assumed that the pressure gradient across the anode was negligible, and that the catalyst had a uniform porosity. Andrian et al. (2000) developed a model to examine the fuel cell system efficiency. They found that improvements in cell performance were generally accompanied by decreases in system efficiency. Nordlund et al. (2002) studied the influence of the anode porous structure using a spherical agglomerate model of the electrode. They concluded that the mass transfer limitations in the agglomerates are small. Sandhu et al. (2005) developed a mass flux model to predict the methanol and water molar fluxes, and the concentration profiles of chemical species in the polymer electrolyte.

In contrast to the above one-dimensional models, a few two-dimensional models have been developed. Birgersson et al. (2003) developed a two-dimensional model based on one liquid phase. They studied the effect of methanol feed concentration on methanol mass transfer in the flow channel and on current density. The results indicated that the mass

transfer resistances in both the flow channel and in the adjacent porous backing are important. Kulikovsky (2000) developed a two dimensional numerical model that showed that the pressure gradient effect controls the transport of methanol near the flow channel, whereas transport by diffusion dominates in the catalyst layers and the membrane.

2.1.2 Two Phase (Liquid and Gas) Models:

A number of models have accounted for the presence of a gas phase in addition to the liquid phase that is present in DMFCs. Methanol cross-over is one of the phenomena that have also been studied by models accounting for both phases. Wang et al. (2003) described the relationship between the mixed potential caused by methanol oxidation and methanol crossover to the cathode caused by diffusion, convection, and electro-osmotic drag force. The results showed that at zero and small current densities methanol crossover is dominated by molecular diffusion whereas at high current densities it becomes small. Murgia et al. (2003) used the phenomenological transport equations to describe the catalyst layer, the diffusion layer, and the membrane. The model identified polarization effects caused by methanol crossover.

A variety of other phenomena have been investigated using models that described both gas and liquid phases. Argyropoulos et al. (2000) developed a model that described the hydraulic behavior of internally manifolded fuel cell stacks. The model predicted the pressure drop through the anode and determined the optimum channel depth and width. Argyropoulos et al. (2000a) developed another model to predict the local pressure and chemical composition profiles at the anode and cathode. The results showed that decreasing the methanol concentration could decrease methanol stripping by carbon dioxide gas. Birgersson et al. (2004) accounted for the conservation of momentum and mass in describing a ternary mixture. They found that the presence a gas phase improved the mass transfer of methanol at temperature > 30 °C. Divisek et al. (2003) developed a two dimensional model that treated the backing layer (diffusion layer) as a water – gas system. They accounted for the presence of both hydrophilic and hydrophobic pores. Wang et al. (2001) described transport in the cathode both analytically and numerically. Their model identified both single and two phase regions of the membrane. Conditions for the first

appearance of liquid water and the water distribution at the membrane / cathode interface were identified. Kulikovsky (2005) accounted for both the liquid feed and gaseous bubbles in the anode channel. He found a significant decrease in cell performance with increasing bubble formation.

Although the backing layer (diffusion layer) of fuel cells has not been modeled extensively, a few models have been developed. Bewer et al. (2004) showed that bubble formation influences the flow distribution and therefore the power density of the fuel cell. Their model used a novel method to describe the insitu production of bubbles in which a Perspex test cell had been used to measure the decomposition of a hydrogen peroxide solution to form oxygen and water in. Pasaogullari et al. (2005) compared two phase and single phase transport through a GDL. The results showed that the performance of the fuel cell decreased as a result of flooding and when two phase transport occurred rather than single phase transport. Sun et al. (2005) developed a two-dimensional model of the backing layer.

References:

V. Andrian, Stefanie, J. Meusinger, J. Power Sources, 91, 193, (2000).

P. Argyropoulos, K. Scott, W. M. Taama, J. Appl. Electrochem., 30 (8), 899, (2000).

P. Argyropoulos, K. Scott, W. M. Taama, J. Appl. Electrochem., 78, 29, (2000).

S. F. Baxter, V. S. Battaglia, R. E. White, J. Electrochem. Soc., 146 (2) 437, (1999)

D. M. Bernardi and M. W. Verbrugge, AIChE J., 37, 1151, (1991).

D. M. Bernardi and M. W. Verbrugge, J. Electrochem. Soc., 139, 2477, (1992).

T. Bewer, T. Beckmann, H. Dohle, J. Mergel, D. Stolten, J. Power Sources, 125, 1, (2004).

A. Biyikoglu, Int. J. Hydrogen Energy, 30, 1181, (2005).

E. Birgersson, J. Nordlund, M. Vynnycky, C. Picard, G. Lindbergh, J. Electrochem..Soc., 150, A1368, (2003).

E. Birgersson, J. Nordlund, M. Vynnycky, C. Picard, G. Lindbergh, J. Electrochem. Soc., 151, A2157, (2004).

L. Carrette, K.A. Friedrich, U. Stimming, Chem. Phys. Chem, 1, 162, (2000).

D. Cheddie, N. Munroe, J. Power Sources, 147, 72, (2005).

J. Cruickshank, K. Scott, Journal of Power Sources, 70, 40, (1998).

J. Divisek, J. Fuhrmann, K. Gartner, R. Jung, J. Electrochem. Soc., 150 (6), A811, (2003).

H. Dohle, J. Divisek, R. Jung, J. Power Sources, 86, 469, (2000).

J. Drake, W. Wilson, K. Killeen, J. Electrochem. Soc., 151 (3), A413, (2004).

K. T. Jeng, C. W. Chen, J. Power Sources, 112, 367, (2002).

T. H. Kim, Y. C. Bae, Polymer, 46 (17), 6494, (2005).

A. A. Kulikovsky, J. Appl. Electrochem., 30, 1005, (2000).

A. A. Kulikovsky, Electrochem. Commun, 7, 237, (2005).

J. G. Liu, T. S. Zhao, R. Chen, C. W. Wang, Electrochem. Commun., 7, 288, (2005).

G. Murgia, L. Pisani, A. K. Shukla, K. Scott, J .Electrochem. Soc., 150 (9), A1231, (2003).

J. P. Myers, J. Newman, J. Electrochem. Soc., 149 (6), A710, (2002).

J. P. Myers, J. Newman, J. Electrochem. Soc., 149 (6), A718, (2002a).

J. P. Myers, J. Newman, J. Electrochem. Soc., 149 (6), A729, (2002b).

J. Nordlund, G. Lindbergh, J. Electrochem. Soc., 149 (9), A1107, (2002).

U. Pasaogullari, C. Y. Wang, J. Electrochem. Soc., 152 (2), A380, (2005).

S. S. Sandu, R. O. Crowther, J. P. Fellner, Electrochim. Acta, 50, 3985, (2005). .

K. Scott, W. Taama, J. Cruickshank, J. Appl. Electrochem., 28, 289, (1998).

K. Scott, W. Taama, J. Cruickshank, J. Power Sources, 65, 159, (1997).

K. Scott, P. Argyropoulos, K. Snudmacher, J. Electroanal Chem., 477, 97, (1999).

T.E. Springer, T.A. Zawodzinski, S. Gottesfeld, J. Electrochem. Soc., 138, 2334, (1991).

W. Sun, B.A. Peppley, K. Karan, J. Power Sources, 144, 42, (2005).

K. Sundmacher, K. Scott, Chem. Eng. Sci., 54, 2927, (1999).

K. Sundmacher, T. Schultz, S.Zhou, K. Scott, M. Ginkel, E. D. Gilles, Chem. Eng. Sci., 56, 333, (2001).

M. W. Verbrugge, J. Electrochem. Soc., 136, 417, (1989).

Z. H. Wang, C. Y. Wang, J. Electrochem. Soc., 150 (4) A508, (2003).

Z. H. Wang, C. Y. Wang, K. S. Chen, J. Power Sources, 94, 40, (2001).

S. Wasmus, A. Kuver, J. Electroanal. Chem., 461, 14, (1999).

C. Xu, P.M. Follmann, L.T. Biegler, M. Jhon, Comp. Chem. Eng., 29 (8), 1849, (2005).

K.Z. Yao, K. Karan, K.B. McAuley, P. Oosthuizen, B. Peppley, T. Xie, Fuel Cells, 4, 3, (2004) .

J.Zhang, Y. Wang, Fuel Cells, 4 (1-2), 90, (2004).

S. Zhou, T. Schultz, M. Peglow, K. Sundmacher, Phys. Chem. Chem. Phys., 3, 347, (2001).

CHAPTER THREE

A model of a partially flooded anode backing layer (ABL) in a direct methanol fuel cell (DMFC)

3.1 Abstract

A one-dimensional mathematical model of the anode-backing layer (ABL) in a direct methanol fuel cell (DMFC) has been developed. It describes operation at 40°C with the methanol-water feed in the liquid phase and the carbon dioxide product in the gas phase in combination with a solid polymer electrolyte membrane. Countercurrents flow of gas and liquid by both diffusion and convection mechanisms are described. The volumetric fractions of gas-filled pores and liquid-filled pores in an experimentally determined pore size distribution for a two-layer ABL (a layer of graphitized carbon paper layer plus a layer of carbon particles) were found to be a function of operating conditions. Variations in the following parameters were studied: ABL thickness, current density, methanol concentration, liquid contact angle inside pores, and diameter of gas bubbles formed in the anode channel. The study showed that adjusting the liquid contact angle inside the pores, to make the interior ABL surfaces hydrophilic, would allow the gas to leave with the minimum gas phase pressure gradient across the ABL. In contrast adjusting the liquid contact angle on the ABL interface with the anode channel, to make the exterior face of the ABL hydrophobic, allowed gas bubbles having small diameters to be formed at the anode channel / ABL interface. Having tiny bubbles dispersed in a continuous liquid phase methanol-water feed in the anode channel is preferable to the formation of large gas slugs. The need for bubble management has been recognized, in order to avoid the formation of large gas slugs that can prevent the liquid feed mixture from leaving the anode channel to enter the ABL.

3.2 List of symbols

C_{TL}: Total concentration of the liquid phase (mol m^{-3})

C_{TG}: Total concentration of the gas phase (mol m^{-3})

$D_{E:}$ Effective diffusivity of reactant within agglomerates (m^2 s^{-1})

$D^{E}_{G\,CO2\,/\,H2O}$: The effective binary molecular diffusion coefficient for carbon dioxide and Water vapor (m^2 s^{-1})

$D^{E}_{G\,CH3OH\,/\,H2O}$: The effective binary molecular diffusion coefficient for methanol and water vapor (m^2 s^{-1})

$D^{E}_{G\,CO2\,/\,CH3OH}$: The effective binary molecular diffusion coefficient for carbon dioxide and methanol vapor (m^2 s^{-1})

$D^{E}_{L\,CH3OH\,/\,H2O}$: The effective binary molecular diffusion coefficient for methanol and water liquid (m^2 s^{-1})

$dp_{(G\,/\,L)}$: Transition pore diameter (m)

dp: Diameter of the carbon agglomerate particles (m)

dz: Thickness of the anode backing layer (m)

F: Faraday constant, (96487 C mol^{-1})

j: Cell current density (A m^2)

N_{TG}: Total gas flux (mol m^{-2} s^{-1})

N^{G}_{CO2}: Flux of carbon dioxide in the gas phase (mol m^{-2} s^{-1})

$N^{G}_{H2O:}$ Flux of water in the gas phase (mol m^{-2} s^{-1})

N^{G}_{CH3OH}: Flux of methanol in the gas phase (mol m^{-2} s^{-1})

N_{TL}: Total liquid flux (mol m^{-2} s^{-1})

N^{L}_{H2O}: Flux of water in the liquid phase (mol m^{-2} s^{-1})

N^{L}_{CH3OH}: Flux of methanol in the liquid phase (mol m^{-2} s^{-1})

P_{TG}: Total gas pressure (Pa)

P_{TL}: Total liquid pressure (Pa)

$(P_{H2O})^{SAT}$: Saturated vapor pressure of water (Pa)

$(P_{CH3OH})^{SAT}$: Saturated vapor pressure of methanol (Pa)

$(R_{H2O})^{VAP}$: Rate of vaporization for water (mol m^{-3} s^{-1})

$(R_{CH3OH})^{VAP}$: Rate of vaporization for methanol (mol m^{-3} s^{-1})

x_{CH3OH}: Methanol mole fraction in liquid phase

x_{H2O}: Water mole fraction in the liquid phase

y_{CH3OH}: Methanol mole fraction in the gas phase

y_{CO2}: Carbon dioxide mole fraction in the gas phase

y_{H2O}: Water mole fraction in the gas phase

σ: Surface tension (N m^{-1}) or surface energy (J m^{-2})

ε_S: Solid volumetric in an ideally packed assembly of spheres

ε_v: Cumulative pore volume of the layer (m^3 m^{-3} total)

ε_G: Pore volume filled with gas with respect to the total cumulative void (pore). Volume for E-TEK carbon paper (m^3 m^{-3} total)

ε_L: Pore volume filled with gas with respect to the total cumulative void (pore) volume for E-TEK carbon paper (m^3 m^{-3} total)

μ_G: Vapor phase viscosity of a component or a mixture (mol m^{-1} s^{-1})

μ_L: Liquid phase viscosity of a component or a mixture (mol m^{-1} s^{-1})

3.3 Introduction

The anode-backing layer (ABL) in a direct methanol fuel cell (DMFC) has several specific functions, (a) Electronic conductivity – The electrical potential loss should be minimized. The current density from the adjacent catalyst layer should be distributed evenly. (b) Heat conductivity – The heat generated within the adjacent catalyst layer has to be transferred through the anode backing layer to the bipolar plate, (c) Reactant and product permeability – The reactants entering the DMFC from the flow field channel must have access to the catalyst layer through the ABL. The products formed in the anode catalyst layer must flow through the ABL to the flow field channel in order to leave the DMFC. (d) Mechanical stability – The backing layer has to be strong enough to provide mechanical support for the other layers in the fuel cell, i.e. the membrane electrode assembly (MEA).

Either graphitized carbon fiber paper or woven graphitized carbon cloth (Miwa et al. 1989, Lindstrom 1987) are usually used as the substrate or foundation for both ABL's and cathode backing layers. Carbon paper was described in the computations being reported here. It is used in many of the polymer electrolyte membrane fuel cells (PEMFC) described in the literature because it has the following desirable properties; large porosity, reasonable electrical conductivity, high mechanical strength, and light weight. Polyacrylonitrile (PAN) fibers are the backbone of carbon fiber paper used for fuel cell backing layers.

Polytetrafluoroethylene (PTFE) or Teflon™ is often added to the carbon paper used in cathode backing layers, in order to diminish the problem of flooding by liquid phase water that is formed at the cathode. Sometimes it is also added to the carbon paper used in ABL's. Adding PTFE to backing layers increases their hydrophobicity property and thereby helps to expel liquid water. The carbon paper is dipped into an aqueous PTFE suspension and the excess suspension is allowed to drip off the paper. The remaining solvent is removed first by oven drying, and then by heating above 350 °C to sinter the PTFE particles on the substrate surface. Other techniques are also used, such as spraying and brushing.

A recent review (Antolini, 2004) described three types of PEMFC electrodes that included backing layers, (a) two layer electrodes – a hydrophobic support layer of carbon paper plus a porous catalyst layer, (b) three layer electrodes – a hydrophobic support layer of carbon paper, plus a diffusion layer formed by carbon particles and PTFE, plus a catalyst layer of carbon supported platinum (Pt/C) and ionomer (e.g. Nafion), (c) four layer electrodes – a hydrophobic support layer of carbon paper, plus two diffusion sub layers, one on each side of the carbon paper, plus the catalyst layer. The pores formed between the carbon particles are smaller than the pores between the fibers that constitute the carbon paper (Williams et al. 2004). The diffusion layers contain hydrophilic pores associated with the carbon particles and hydrophobic pores associated with the PTFE. Williams (2004) has characterized backing layers composed of carbon paper / cloth plus a diffusion layer, with a view to understanding the factors that limit oxygen transport in cathode backing layers. According to their measurements, more than 95% of the pore volumes in most commercial backing layers are hydrophobic pores.

A number of experimental studies have been performed in the past few years that included backing layers in PEMFCs primarily with hydrogen as the fuel. The main interest

was in the flooding phenomenon that occurs in the cathode (cathode catalyst layer and cathode backing layer). Those studies were performed by Baschuk et al. (2000), Gurau et al. (1998, 2000), Chu et al. (2002), Lee et al. (2003), Natarajan et al. (2001, 2003), He et al. (2000), Mazumder et al. (2003), Pisani et al. (2002), Nam et al. (2003), You et al. (2002), Berning et al. (2003). Variables of interest included the bulk porosity, wettability, and pore size distribution.

This investigation concerns the use of an ABL in a DMFC. One of the applications for DMFCs is for portable power where fuel cells may become a viable alternative to batteries. Ease of storage is one of the major advantages of a liquid fuel, such as methanol or a liquid hydrocarbon, over a gaseous fuel, such as hydrogen. Comprehensive reviews of methanol fuel cell technology have been published (Wasmus and Kuver, 1999; McNicol et al., 1999; Dillon et al., 2004). Unfortunately methanol fuel cells also have some undesirable characteristics. All DMFC have both slow anode kinetics and methanol crossover. In addition, low temperatures DMFCs have a third undesirable characteristic. The presence of large carbon dioxide bubbles in the anode channels can temporarily block the mass transport of the reactants into the anode-backing layer (ABL) of the fuel cell. Argyropoulos et al. (1999) and Lu and Wang (2004) used transparent fuel cells and photographed the bubble evolution during the operation of DMFCs. Bewer et al. (2004) photographed oxygen bubbles that were formed from the decomposition of hydrogen peroxide in a manner that simulated DMFCs. Recently Kulikovsky (2005) described a two-phase mathematical model of bubbles in a DMFC anode channel.

The overall objective of this investigation was to use a mathematical model to describe the anode backing layer in a DMFC, where (1) the liquid feed mixture (methanol and water) is transported from the flow field channel through the liquid-filled pores of the ABL to the anode catalyst layer, and where simultaneously (2) the carbon dioxide produced by the anodic electro-catalytic reaction is transported in the gas-filled pores of the ABL counter currently to the transport of methanol and water in the liquid-filled pores of the ABL. In addition, the effects of the following parameters were to be discussed: current density, methanol concentration, fractional pore volume filled with gas and liquid, wet contact angle of the liquid with the pore walls, and the size of bubbles formed at the interface between the anode channel and the ABL.

Several reviews of fuel cell mathematical models are available (Yao et al. 2004, Bryikoglu 2005, Sousa and Gonzalez 2005, and Cheddie and Munroe 2005). Verbrugge (1989) developed one of the earlier models of a methanol fuel cell component, the membrane electrolyte layer. There are several mathematical models that describe operation of DMFCs at temperatures sufficient for vapor phase operation (Scott et al. 1997 and 1998, Kulikovsky et al. 2000). Even though there is always a gas phase composed predominantly of carbon dioxide, a number of mathematical models have used the simplifying assumption that carbon dioxide is completely dissolved in the liquid phase that is present in DMFC anodes (Baxter et al. 1999, Zhou et al. 2001, Jeng and Chen 2002, Murgia et al. 2003, Xu et al. 2005).

A thorough literature survey has indicated that this is the first detailed mechanistic model of an ABL in a low-temperature DMFC. Like our model, several models of DMFC anodes (combination of the ABL and the anode catalyst layer) have described two fluid phases, gas and liquid, in the ABL. None of them described the ABL in detail, instead all of those investigations concentrated on the catalyst layer. Specifically, Sundmacher and Scott (1999) did not describe all the concentration gradients in the liquid phase. Kulikovsky (2000) did not present any results for the gas phase in the ABL. Wang and Wang (2003) emphasized methanol crossover and did not present any results for the ABL. Divisek et al. (2003) did not discuss the influences of diffusion and convection on mass flux. Birgersson et al. (2004) presented results for an entire DMFC and specifically did not describe the phenomena in the ABL.

3.4 Mathematical model description

3.4.1 Equations used to model the gas phase in ABL

Table 3-1

Equations	Equation No.
A) Momentum Transport (Ergun Equation)	
$\frac{dP_{TG}}{dz} = \frac{N_{TG}^2}{\rho_G d_p}\left(\frac{\varepsilon_S}{\varepsilon_G^3}\right)\left\{150\left(\frac{(\varepsilon_S)\,\mu_G}{d_P\ N_{TG}}\right) + 1.75\right\}$	(3-1)
B) Mass Transport (Stefan-Maxwell Equations)	
$\frac{dy_{CO2}}{dz} = \frac{1}{C_{TG}}\left[\frac{(y_{CO2}\ N_{G\text{-}H2O} - y_{H2O}\ N_{G\text{-}CO2})}{D^E_{G\ CO2/H2O}} + \frac{(y_{CO2}\ N_{G\text{-}CH3OH} - y_{CH3OH}\ N_{G\text{-}CO2})}{D^E_{G\ CH3OH/H2O}}\right]$	(3-2)
$\frac{dy_{H2O}}{dz} = \frac{1}{C_{TG}}\left[\frac{(y_{H2O}\ N_{G\text{-}CH3OH} - y_{CH3OH}\ N_{G\text{-}H2O})}{D^E_{G\ CH3OH/H2O}} + \frac{(y_{H2O}\ N_{G\text{-}CO2} - y_{CO2}\ N_{G\text{-}H2O})}{D^E_{G\ CO2/H2O}}\right]$	(3-3)
$\frac{dy_{CH3OH}}{dz} = \frac{1}{C_{TG}}\left[\frac{(y_{CH3OH}\ N_{G\text{-}H2O} - y_{H2O}\ N_{G\text{-}CH3OH})}{D^E_{G\ CH3OH/H2O}} + \frac{(y_{CH3OH}\ N_{G\text{-}CO2} - y_{CO2}\ N_{G\text{-}CH3OH})}{D^E_{G\ CH3OH/CO2}}\right]$	(3-4)
$y_{H2O} = \frac{(P^{SAT})_{H2O}}{P_{TG}}\ x_{H2O}$	(3-5)
$y_{CH3OH} = \frac{(P^{SAT})_{CH3OH}}{P_{TG}}\ x_{CH3OH}$	(3-6)
$y_{CO2} = 1 - y_{H2O} - y_{CH3OH}$	(3-7)

$$(R_{H2O})^{VAP} = \frac{dN_{G\text{-}H2O}}{dz} \quad (3\text{-}8)$$

$$(R_{CH3OH})^{VAP} = \frac{dN_{G\text{-}CH3OH}}{dz} \quad (3\text{-}9)$$

$$N^{G}_{CO2} = \frac{j}{6F} \quad (3\text{-}10)$$

$$N_{TG} = N_{G\text{-}CO2} + N_{G\text{-}CH3OH} + N_{G\text{-}H2O} \quad (3\text{-}11)$$

$$D^{E}_{G\text{-}(i/j)} = D^{G}_{(i/j)} * \varepsilon_{G}$$

3.4.2 Equations used to model the liquid phase in ABL

Table 3-2

Equations	Equation No.
A) Momentum Transport (Ergun equation)	
$\frac{dP_{TL}}{dz} = \frac{N_{TL}^2}{\rho_L d_p} \left(\frac{\varepsilon_S}{\varepsilon_L^3}\right) \left\{150 \left(\frac{(\varepsilon_S)\,\mu_L}{d_P\ N_{TL}}\right) + 1.75\right\}$	(3-12)
B) Mass Transport (Fick's Law)	
$\frac{dx_{H2O}}{dz} = \frac{1}{C_{TL}} \left(\frac{(x_{H2O} N_{L\text{-}CH3OH} - x_{CH3OH} N_{L\text{-}H2O})}{D^E_{L\ CH3OH/H2O}}\right)$	(3-13)
$\frac{dx_{CH3OH}}{dz} = \frac{1}{C_{TL}} \left(\frac{(x_{CH3OH} N_{L\text{-}H2O} - x_{H2O} N_{L\text{-}CH3OH})}{D^E_{L\ CH3OH/H2O}}\right)$	(3-14)
$(R_{H2O})^{VAP} + \frac{dN_{L\text{-}H2O}}{dz} = 0.0$	(3-15)
$(R_{CH3OH})^{VAP} + \frac{dN_{L\text{-}CH3OH}}{dz} = 0.0$	(3-16)
$N_{TL} = N_{L\text{-}CH3OH} + N_{L\text{-}H2O}$	(3-17)
$D^E_{L\text{-}(i/j)} = D^L_{(i/j)} * \varepsilon_L$	

3.4.3 Equations used to predict the transition pore diameter and the fractional pore volume filled with liquid and gas in ABL

Table 3-3

Equations	Equation No.
A) Young and Laplace Equation	
$d_{p\,(G/L)} = \dfrac{-4\,\sigma\cos\theta}{P_{TL} - P_{TG}}$	(3-18)
B) Pore volume correlations for liquid and gas	
1) $d_{p\,(G/L)} < 1^{*}\,10^{-8}$ $\varepsilon_G = 0.52 - 2.6444*(1-\exp(0.000001-(d_{p(G/L)}*10^{6})))$ $\varepsilon_L = \varepsilon_v - \varepsilon_G$	(3-19)
2) $d_{p\,(G/L)} > 1^{*}\,10^{-4}$ $\varepsilon_G = 0.018632*\exp\,(1-0.01*(-d_{p(G/L)}*10^{6}))$ $\varepsilon_L = \varepsilon_v - \varepsilon_G$	(3-20)
3) $1*10^{-8} < d_{p\,(G/L)} < 1*10^{-4}$ $\varepsilon_G = 0.20613*\exp\,(((d_{p\,(G/L)}*10^{6})^{16.24})/\,(-3.949e+27)) + 0.47129/\,((d_{p\,(G/L)})*10^{6})^{0.061144}) - 0.337$ $\varepsilon_L = \varepsilon_v - \varepsilon_G$	(3-21)

3.4.4 Boundary conditions at the AC / ABL interface (base calculation)

Table 3-4

$P_{TL} = 1.01325 * 10^{5}$ (Pa)

$N_{CO2} = j / (6*F)$

$N_{TG} = N_{CO2} / y_{CO2}$

$N_{G\text{-}H2O} = y_{H2O} * N_{TG}$

$N_{G\text{-}CH3OH} = y_{CH3OH} * N_{TG}$

$x_{H2O} = 0.98158$

$x_{CH3OH} = 0.01842$

$N_{L\text{-}H2O} = j / (6*96485) + (\lambda * x_{H2O} * j) / 96485 + N_{TG} * y_{H2O}$

$N_{L\text{-}CH3OH} = j / (6*96485) + (\lambda * x_{CH3OH} * j) / 96485 + N_{TG} * y_{CH3OH}$

3.4.5 Guessed boundary conditions at the AC / ABL interface

Table 3-5

P_{TG} = Calculated from Young and Laplace equation

$\varepsilon_G = 0.25$

$dp_{(G/L)}$ = Calculated from Young and Laplace equation

3.4.6 Physical properties

All physical properties used in modeling the ABL are shown in Table 3-6, as a function of temperature.

Table 3-6

Equation	
$T = 313.16$ (K)	
$y_{H2O} = (P^{sat}_{H2O} * x_{H2O}) / P_{TG}$	
$y_{CH3OH} = (P^{sat}_{CH3OH} * x_{CH3OH}) / P_{TG}$	
$y_{CO2} = 1 - y_{H2O} - y_{CH3OH}$	
$\mu_L = \frac{100}{(18.016 * (2.1482 * (T - 281.6) + \sqrt{(8078.4 * (T - 281.6)^2)}) - 120.0)}$	
$D_{L\ CH3OH/H2O} = (6.1*10^{-8} * T) / 10000$	R. C. Ried (1977)
$D^G_{CO2/H2O} = 9.8879 *10^{-6} * (T^{1.75}) / 10000$	
$D^G_{CH3OH/H2O} = 9.98 * 10^{-6} * (T^{1.75}) / 10000$	
$D^G_{CH3OH/CO2} = 6.2638 * 10^{-6} * (T^{1.75}) / 10000$	
$\mu_{H2O} = (1.32158 * 10^{-6} * T^2 + 2.00505 *10^{-2} * T - 0.70217) * 10^{-4}$	
$\mu_{CH3OH} = (-7.45113 * 10^{-7} * T^2 + 1.09785 * 10^{-2} * T - 0.162809) *10^{-4}$	
$\mu_{CO2} = (-2.7812 * 10^{-6} * T^2 + 1.17024 * 10^{-2} * T + 0.204435) * 10^{-4}$	
$P^{sat}_{H2O} = 1.8038e+11*\exp.(-5340.5 / T)$	Perry (1963)
$P^{sat}_{CH3OH} = 1.14203e+11*\exp.(-4701.39 / T)$	
Contact angle (Θ) = 65 °	
Thickness (ABL) = 100 μm.	
$\varepsilon_v = 0.52$	
$\varepsilon_L = \varepsilon_v - \varepsilon_G$	
$\sigma = (- 2.5798e-04* T^2 - 1.1525e-03* T + 92.215) / 1000$	

Equations that describe phenomena in each phase are discussed in the material that follows:

3.4.7 Liquid phase equations

The transport of the two liquid species (water and methanol) can occur by both diffusion and by convection. These fluxes arise from concentration and pressure gradients respectively. At the current densities used in this study, the amount of carbon dioxide dissolved in the liquid phase is sufficiently small that it can be neglected (Kulikovsky, 2005). Therefore the liquid phase was treated as a two-component system that could be described by Fick's Law, equations 3-13 and 3-14. Equations for both components can be rearranged to show the separate terms that describe the contributions of diffusion and convection.

$$N_{(L-CH3OH)} = -C_{TL} D^{E}_{L\ CH3OH/H2O} \frac{dx_{CH3OH}}{dz} + x_{CH3OH} N_{TL} \qquad (3\text{-}14)$$

$$N_{(L-H2O)} = -C_{TL} D^{E}_{L\ CH3OH/H2O} \frac{dx_{H2O}}{dz} + x_{H2O} N_{TL} \qquad (3\text{-}13)$$

Where the first term describes the diffusion mechanism and the second term describes the convection mechanism.

The pressure gradient across the thickness of ABL was calculated using the Ergun equation (Bird et al. 2002), which is shown in equation 3-12, that describes the convective flux phenomena. The Ergun equation was used rather than the Darcy equation. The Darcy equation requires either an estimate of tortuosity (difficult) or an experimental measurement of permeability (material plus fluids at the operating conditions). In contrast, the Ergun equation only requires the measurement of one material property, the cumulative pore

volume (ε_V) to describe the porous medium. The various symbols in the Ergun equation, equation 3-12, are the following: N_{TL} is total liquid flux (mol / m^2 sec) and is equal to the flux of methanol and water. ε_S is the volumetric fraction of the porous solid that is non-porous . ε_L is the volumetric fraction of the porous solid that is filled with liquid. μ_L is the liquid phase viscosity (mol/m sec). d_P is the diameter of the carbon agglomerate particles. Since 97 % of the liquid phase is water, the viscosity of pure liquid water (Perry, 1963a) was used to describe the viscosity of the liquid mixture, Table 3-5. The average density of a liquid phase mixture containing 3 wt % methanol and 97 wt % water, over the temperature range 40-80°C, was 0.98 gm / mL, and it was converted to concentration by dividing it by the molecular weight of water, to give $5.44 * 10^4$ mol /m^3 (Perry, 1963b). This value was used to represent the liquid mixture concentration in equations 3-13 and 3-14.

The fluxes of water and methanol entering the anode-backing layer (ABL) from the anode channel (AC) must be sufficient to supply three requirements. The first is the amounts of methanol and water that are needed for the reaction at the ACL. The second is the amounts of methanol and water that are transported by protons across the electrolyte layer (ELL), ie. the membrane, via electro-osmotic drag to the cathode. The third is the amount of each component that is vaporized from the liquid phase of the ABL and enters the vapor phase. These three requirements are included in the following three equations, which form the boundary conditions for the liquid fluxes,

$$N_{L\text{-}H2O} = j / (6*96485) + (\lambda * x_{H2O} * j) / 96485 + N_{TG} * y_{H2O} \qquad (3\text{-}22)$$

$$N_{L\text{-}CH3OH} = j / (6*96485) + (\lambda * x_{CH3OH} * j) / 96485 + N_{TG} * y_{CH3OH} \qquad (3\text{-}23)$$

$$N_{TL} = N_{L\text{-}H2O} + N_{L\text{-}CH3OH} \qquad (3\text{-}24)$$

Where λ is the electro-osmotic drag coefficient for water or the number of water or methanol molecules attached to each proton ≈ 3 (Choi and Datta, 2003).

Mass balances were performed over each incremental section of the ABL. Within each incremental section, the change in the liquid flux of a component will be equal to the amount vaporized. Therefore the changes in the liquid fluxes of water and methanol, $N_{L\text{-}H2O}$, $N_{L\text{-}CH3OH}$, could be calculated from the rate of vaporization at different positions along the ABL, using equations 3-15 and 3-16.

3.4.8 Gas phase equations

The flux of carbon dioxide through the ABL is virtually constant. There are two factors that cause constant carbon dioxide flux. At steady state a constant flux of carbon dioxide is produced in the anode catalyst layer (ACL), and all of it has to flow through the ABL to leave the fuel cell. Since the amount of carbon dioxide that is soluble in the liquid phase is negligible, the carbon dioxide flux through the ABL must correspond to the carbon dioxide production rate in the ACL as shown in equation 3-10.

The gas phase was assumed to be saturated with water and with methanol vapor. This assumption requires the rate of vaporization to respond rapidly to changes in gas pressure and liquid composition. With this assumption Dalton's law and Raoult's law could be combined to obtain the vapor phase mole fractions for liquid and methanol as shown in equations 3-5 to 3-7.

The gas phase will contain three species, (carbon dioxide saturated with water and methanol) which will be transported by two mechanisms, diffusion and convection. Diffusion phenomena are caused by the change in the carbon dioxide concentration gradient. Convection phenomena are caused by the change in the pressure gradient that is created because the carbon dioxide will continue to accumulate until there is sufficient driving force for it to flow out of the ABL.

The Stefan - Maxwell equations 3-2 to 3-4, were used to describe the gas phase fluxes. The vapor phase compositions were used in calculating the fluxes of water and methanol in the gas phase. The methanol and water fluxes were added to the carbon dioxide flux to obtain the total gas flux. The Ergun equation 3-1 was also used to calculate the pressure gradient in the gas phase. To keep the gas phase saturated with methanol and water, some of the methanol and water in the liquid phase will evaporate. The rate of vaporization was calculated from the difference between the liquid phase methanol or water flux entering a section of the ABL and the corresponding flux leaving the same section of the ABL, as shown in equations 3-8 and 3-9. C_{TG} is the total gas concentration (mol/m^3) and was calculated from the temperature and total pressure using the ideal gas law. $N_{G\text{-}CO2}$, $N_{G\text{-}H2O}$, $N_{G\text{-}CH3OH}$ are the fluxes of the species in the gas phase ($mol / m^2 sec$), and were used in

the calculation of the rate of vaporization for water and methanol. ε_G is the volumetric fraction of the porous solid that is filled with gas. μ_G is the vapor phase viscosity of a component or a mixture (mol / m sec). The viscosities of the pure components were determined as a function of temperature, by fitting empirical equations to experimental data (Hodgman et al., 1962a) as shown in Table 3-6. The viscosity of the gas mixture was obtained by combining the three pure component viscosities using the following mixing rule (Ried et al., 1977).

$$(\mu_{H2O})\ mix = \frac{(y_{H2O} * \mu_{H2O})}{(y_{CO2} * ((MW_{CO2} / MW_{H2O})^{0.5}) + (y_{CH3OH} * ((MW_{CH3OH} / MW_{H2O})^{0.5})}$$

$$(\mu_{CH3OH})\ mix = \frac{(y_{CH3OH} * \mu_{CH3OH})}{(y_{CO2} * ((MW_{CO2} / MW_{CH3OH})^{0.5}) + (y_{H2O} * ((MW_{CH3OH} / MW_{H2O})^{0.5})}$$

$$(\mu_{CO2})\ mix = \frac{(y_{Co2} * \mu_{CO2})}{(y_{CH3OH} * ((MW_{CH3OH} / MW_{CO2})^{0.5}) + (y_{H2O} * ((MW_{H2O} / MW_{CO2})^{0.5})}$$

3.4.9 Linking the gas and liquid phases

The Young and Laplace equation, equation 18, was used to calculate the pore diameter that defines the transition between the vapor and liquid phases. It is calculated using the difference in pressure between the gas phase and the liquid phase. Pores smaller than the transition pore diameters are filled with liquid. Those larger than the transition pore diameter are filled with gas. An experimentally measured pore size distribution (M.V. Williams et al., 2004) of a backing layer composed of carbon paper plus a diffusion layer was used to represent the ABL volumetric void fraction. The transition pore diameter was used in the equation that represented this pore size distribution to determine the volumetric void fraction that was filled with liquid, ε_L, and the volumetric void fraction that was filled with gas, ε_G. The pore size distribution for the ABL was measured by mercury porosimetry. In this method mercury is forced into pores of a solid at a certain pressure. Mercury enters the largest pores first, and as the pressure increases smaller pores are penetrated. The total amount of mercury that penetrates the pores at a given applied pressure can be used to calculate the pore size. The backing layer whose pore size distribution was measured by

mercury porosimetry was E-TEK EFCG containing Toray Paper TGP-H-120 and PTFE. The pore volume was distributed between a pore diameter of 100 μm corresponding to a cumulative pore volume of 0.01 mL/g and a pore diameter of 0.001 μm = 1 nm corresponding to a cumulative pore volume of 0.52 mL/g. Three different correlations, equations 3-19, 3-20, and 3-22 were used to describe three different regions of the pore size distribution.

The surface tension, σ (N m^{-1} or J m^{-2}) for the liquid water-methanol mixture was obtained from an empirical equation that was developed from experimental data for a 3 wt% methanol – 97 wt% water solution (Hodgman, 1962b). The equation is shown below:

$$\sigma = - 2.5798E\text{-}04 * T^2 - 1.1525E\text{-}03 * T + 92.215 \qquad (3\text{-}25)$$

Where T = Temperature (K)

3.4.10) Discussion of Computations

The base case calculation used in this study was performed at the following conditions: wet contact angle Θ = 65°, thickness of anode backing layer = 100 μm, current density j = 200 (mA cm^{-2}), the molarity of methanol in the feed mixture = 1 M). Additional calculations were performed to study the effects of (a) two different current densities (100 and 400 mA cm^{-2}) at the same wet contact angle and ABL thickness, (b) two different molarities for methanol (3 and 5 M) at the same wet contact angle and ABL thickness, (c) two extra wet contact angles (Θ = 45°, and Θ = 85°), to represent a range of contact angles for water on graphite between (Θ = 92.9° (advancing), and Θ = 45.6° (receding)). At each wet contact angle a new transition pore diameter was found $(dp)_{G/L}$ as shown in equation 3-24 , using the same bubble diameter of carbon dioxide $(d_B)_{AC}$ and gas pressure used in the base calculation,

The value used for the bubble diameter was an assumption based on an experimental observation, that the bubble diameter is 2 to 3 times the average pore diameter. Equations 3-25 to 3-27, showed that the wet contact angle and the bubble diameter in the channel are related to each other, and equation 3-27 shows that specifying cos Θ defines the ratio of [

$(dp)_{G/L}$ / $(d_B)_{AC}$]. It also showed that the smallest value of $(dp)_{G/L}$ will occur by combining the smallest value of (cos Θ, where Θ = 85°) with the smallest value of bubble diameter $(d_B)_{AC}$, and the largest value of $(dp)_{G/L}$ will occur by combining the largest value of (cos Θ, where Θ = 45°) with the largest value of bubble diameter $(d_B)_{AC}$.

Other parameters were obtained from established relationships. The boundary condition for the gas phase pressure was determined by assuming a bubble diameter and using that bubble diameter in the equation of Young and Laplace for bubbles in a liquid. The pore size distribution for the ABL was taken from the literature as described above. The average pore diameter as measured by mercury porosimetry is approximately 30 μm.

Photographs of the carbon paper indicate that the pores are really interconnected spaces between fibers. Pasaogullari and Wang (2004) have presented photographs of commercial carbon paper and carbon cloth in which both the fibers and the PTFE can be seen. Lim and Wang (2004) have presented photographs showing carbon paper before and after adding a fluorinated ethylene propylene hydrophobic material. The pore space occupied by PTFE or other hydrophobic materials is vividly apparent. Several studies have discussed usefulness of adding PTFE to the diffusion layer to increase hydrophobicity and to diminish the flooding phenomena in the cathode. The carbon dioxide bubbles start to form at the pores mouths at the ABL / anode channel interface. Subsequently they can coalesce and form large discrete slugs that at some conditions can occupy the entire cross-section of the anode channel. An experimental pore size distribution of the anode backing layer (including the carbon paper and PTFE), figure 3-1, was used to obtain the transition pore diameter, $(d_P)_{G/L}$, between liquid-filled pores and gas-filled pores.

The initial diameters of liquid droplets formed from a capillary tube in a system consisting of two liquid phases were measured by Galinat et al. (2005). Although the diameters varied somewhat with flow conditions, they were generally 2 to 3 times larger than the diameter of the capillary from which they were formed. Argyropoulos et al. (1999) and Lu et al. (2004) also indicated that the bubble diameters are a function of fuel cell operating conditions. Based on the above observations, the initial calculations were performed assuming the carbon dioxide bubble diameter at the anode channel, $(d_B)_{AC}$, was 2.5 * (average pore diameter obtained from pore size distribution for the ABL).

Subsequently, the above bubble diameter at the anode channel, $(d_B)_{AC}$, was used in the equation of Young and Laplace for gas bubbles surrounded by liquid (R. DeFay et al. 1966)

$$P_{TG\text{-}BUBBLE} = P_{TL} + \frac{4\sigma}{(d_B)_{AC}} \qquad (3\text{-}26)$$

to calculate the total gas pressure inside the bubble, ($P_{TG\text{-}BUBBLE}$).

The pressure inside the bubbles, is the same as the total gas phase pressure at the anode channel anode backing layer interface, $(P_{TG})_{INT}$, which is the boundary condition for the total gas pressure at the anode channel / ABL interface. The transition pore diameter, $(d_P)_{G/L}$, between liquid-filled pores and gas-filled pores was calculated using the Young and Laplace for a gas-liquid meniscus in a pore, (J. J. Bikerman et al 1970),

$$(d_P)_{G/L} = \frac{4\sigma\cos\Theta}{(P_{TG})_{INT} - P_{TL}} \qquad (3\text{-}27)$$

The gas pressure in a pore at the anode channel / ABL interface is identical to the gas pressure inside a bubble. By equating the two equations (A and B), the transition pore diameter $(dp)_{G/L}$ can be written in the form of

$$(dp)_{G/L} = (d_B)_{AC} * \cos\Theta \qquad (3\text{-}28)$$

The Young and Laplace equation describes the capillary force that is equal to the pressure difference between the gas and liquid phases. In hydrophilic media, where the wet contact angle $\Theta < 90$, the pressure difference is positive because the gas pressure is greater than the liquid pressure, $P_{TG} > P_{TL}$. The gas exists as the bubbles of a dispersed gas phase within a continuous liquid phase.

In hydrophobic media the dry contact angle, $\Theta > 90$, the pressure difference between the gas and liquid phases is negative because the liquid phase pressure is greater than the gas phase pressure, $P_{TG} < P_{TL}$. The liquid exists as the droplets of a dispersed liquid phase within a continuous gas phase. At the cathode, droplets of water are formed (mist flow)

instead of bubbles of carbon dioxide at the anode. In this case a bubble of carbon dioxide, this is held on the carbon paper surface by a surface tension force. It grows until a sufficient size for detachment occurs and then it becomes an unattached bubble in the anode channel.

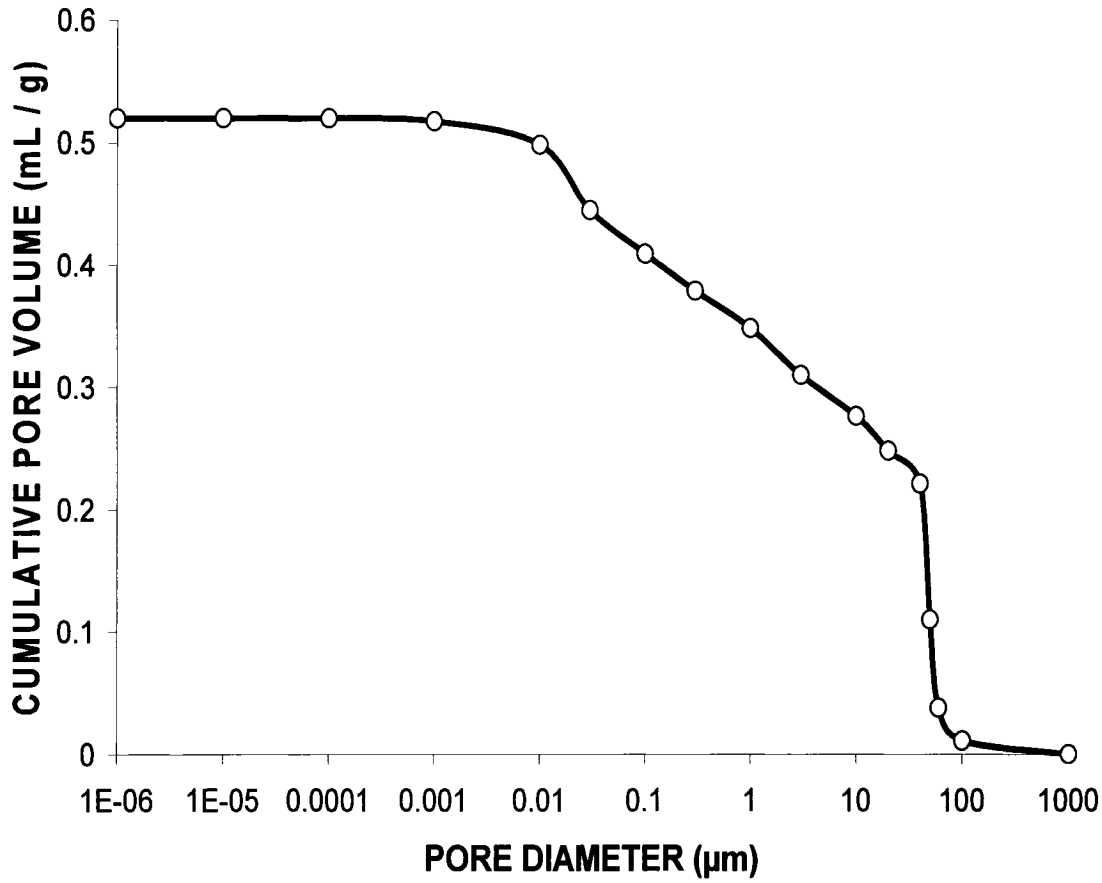

Figure 3-1: Pore Size Distribution of E-TEK Carbon Paper
(Cumulative pore volume (mL/gm) in all pores smaller than the diameter shown versus pore diameter).

Forming bubbles of carbon dioxide in a hydrophobic media is not easy to explain because it does not occur at equilibrium. Weber et al. (2004) observed that the contact angle of water on a dry Nafion membrane had a hydrophobic value of $\Theta = 115°$. This is the same value that Bargeman (1972) found the water contact angle on Teflon, $\Theta = 115°$. In contrast Weber et al. (2004) reported that the water contact angle on a Nafion membrane that was saturated with water had slightly hydrophilic value, $\Theta = 85°$.

The above information provides an explanation for the formation of carbon dioxide bubbles in an initially dry hydrophobic medium that becomes wet. When sufficient water is present, the hydrophobic medium, $\Theta > 90°$ can become a hydrophilic medium, $\Theta < 90°$. Birdi (1982) reported a contact angle for water on graphite of $\Theta = 92.9°$ (advancing) and $\Theta = 45.6°$ (receding). Therefore an average value between advancing and receding wet contact angles, $\Theta = 65°$, was used in the base calculation for this study.

The thickness of anode backing layer is in the range 100-300 μm. The role of the diffusion media is to provide its four functions, electronic conductivity, heat conductivity, reactant permeability, and mechanical strength, with minimum voltage loss. Different thicknesses have been used in different models. Weber et al. (2004), Um et al. (2000), Sun et al. (2005), and Murgia et al. (2003) used an anode backing layer thickness = 250-260 μm. Kulikovsky (2002) used 300 μm. Sundmacher et al. (1999, 2001) used 100 μm. In this study an anode backing layer thickness of 100 μm was used in the base case. Other computations were made with anode backing layer thicknesses of 200 and 300 μm.

The liquid phase pressure was assumed to be 1 atm. The operating temperature in this study, T = 40°, is a desirable temperatures for a portable DMFC that might be used to provide power for a laptop computer or a personal digital assistant.

3.4.11 Values of parameters used in the calculations

Table 3-7

Parameter	Base case	Parameter variation
ABL thickness [μm]	100	200, 300
Current density [mA cm^{-2}]	200	100, 400
CH_3OH concentration [M]	1	3, 5
Contact angle °	65	45, 85
Bubble diameter [μm]	75	15.465, 125.486

3.5 Computational Method

The method used to solve the system of differential-algebraic equations of the two-phase one-dimensional multi-component model of an anode backing layer is described here. Values of boundary and initial conditions for the AC / ABL interface that describe the operation of the anode are shown in tables 3-4, and 3-5.

The differential equations of this system were all rewritten using the finite difference method with a hundred grid pointd across the thickness of the ABL. The global algebraic system so obtained was solved with an iterative method, by walking through the grid points across the ABL starting at the gas channel. The iterative method consists in guessing the solution at the current grid point from the solution at the left neighboring node (using the boundary conditions for the leftmost grid point of the ABL) and updating this guess at the current node to more closely satisfy the equations of the system. Details of the algorithm used are given in table 3-8.

The boundary conditions do not specify all the variables at the gas channel, and some strategy is needed in the iterative method to initiate the calculations in case unknown variables are required in an equation.

By assuming that the effect of diffusion of the gas phase in the anode channel is negligible and the only parameter that affects transport is the convection effect, initial guesses (in the iterative method) for the total gas flux is $N_{TG} = N^G_{CO2} / y_{CO2}$, for the water flux $N^G_{H2O} = y_{H2O} * N_{TG}$, and for the methanol flux $N^G_{CH3OH} = y_{CH3OH} * N_{TG}$. The initial transition pore diameter, $dp_{(G/L)}$, was calculated from equation (3-28) above. Equation (3-26) was then used to find the initial gas pressure. The rest of variables at the anode channel were known.

3.5.1 Algorithm used.

Table 3-8

1) All variables, physical properties and pore volumes are initialized across ABL.
2) Loop over all grid points along the ABL thickness to evaluate gas phase quantities:
2.1) Obtain the gas pressure from the Ergun equation (3-1) discretized using a finite difference method:
$P_{TG}(i) = P_{TG}(i-1) + [a1 * N_{TG} + a2 * N_{TG}^2] * dz$
2.2) Compute new concentration values for all gas species at the grid point using equations (3-5, 6 and 7).
2.3) Compute new values for gas physical properties at the grid point from table 3-6.
2.4) Compute new gas fluxes N_G for species at the grid point using Stefan-Maxwell equations (3-2, 3 and 4) with a finite difference approximation of the derivatives of gas concentrations obtained in Step 2.2.
2.5) Compute a new total gas flux N_{TG} at the grid point from equation (3-11).
3) Repeat the point 2 until the calculated total gas flux N_{TG} before and after the loop in Step 2.5 are within a tolerance of 10^{-8}.
4) Compute the rate of vaporization at all the grid points from equations (3-8 and 9) with a finite difference approximation of the derivatives of gas fluxes obtained in Step 2.4.
5) Loop over all grid points along the ABL thickness to evaluate liquid phase quantities:

5.1) Compute liquid species fluxes at each grid point from equations (3-15 and 16) using the rates of vaporization obtained in point 4.

5.2) Compute new value for liquid concentration at each grid point from Fick's law, equations (3-13, 14 and 17), written in finite difference form using the liquid fluxes obtained in Step 5.1.

6) Compute new values for liquid pressure P_{TL} at all grid points from Ergun equation (3-12) for the liquid phase.

7) Compute new value for the transition pore diameter at all grid points from Young and Laplace equation (3-18).

8) Compute new values for fractional pore volume filled with gas and liquid at all grid points from equations (3-19, 20, and 21) using the transition pore diameter obtained in Step 7.

Repeat Steps 2 to 8 until the fractional pore volume filled with gas calculated from iteration to iteration is within a tolerance of 10^{-8}.

3.6 Results and Discussion

One of the objectives of this work was to identify the separate contributions of diffusion and of convection to mass transport through the ABL. The pressure gradients, shown in Fig 3-2, are the driving forces for convection. Because the liquid methanol-water mixture is circulated through the anode channel, its pressure at the interface between the anode channel and the ABL is known, and is a boundary condition. The pressure of the liquid phase decreases and the pressure of the gas phase increases across the thickness of the ABL, z_{ABL}. Although the change in liquid phase pressure, ΔP_{TL} [kPa] is small, the pressure gradient, $\Delta P_{TL} / \Delta z$ [kPa m^{-2}], is large because the thickness of the ABL is so small [100 μm]. It is reasonable to suggest that the pressure is almost constant, as is done in many mathematical models. However, it is the large value of the pressure gradient that causes the convective flux of the methanol-water liquid mixture through the ABL away from the anode channel to the anode catalyst layer.

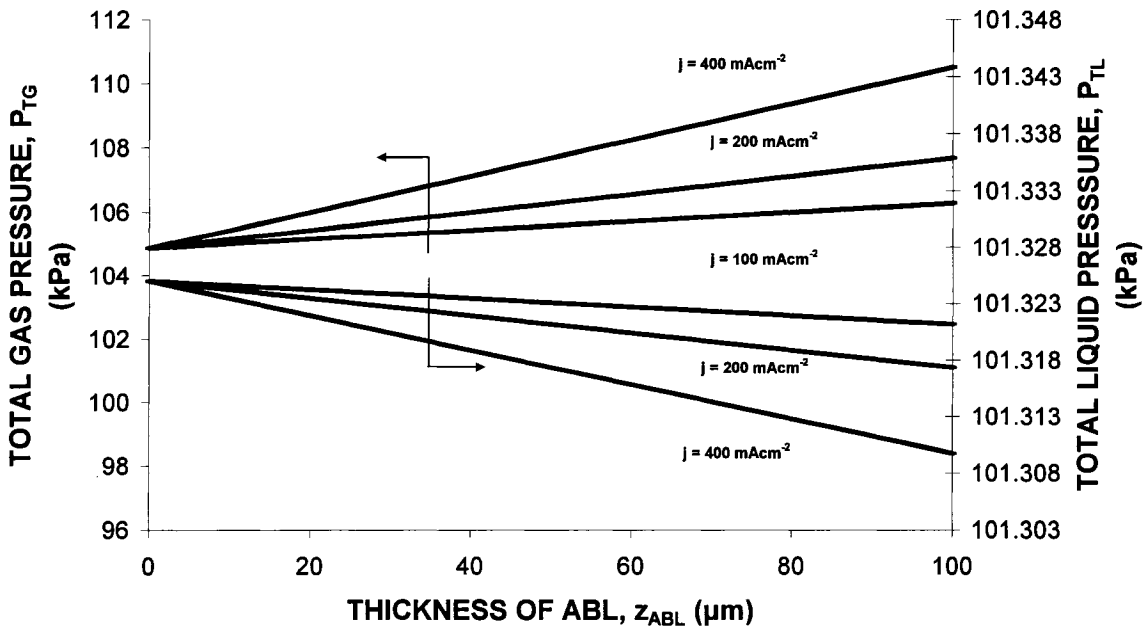

Figure 3-2: The effect of different current density on the total gas and liquid pressure at wet contact angle = 65, and, 1 M across the thickness of backing layer. Position zero is the AC/ABL interface, and position 100 is the ABL/ACL interface

The pressure gradients in Fig 3-2 show that the liquid phase flows from the anode channel ($z_{ABL} = 0$) to the anode catalyst layer ($z_{ABL} = 100$). In contrast, the gas phase flows in the opposite direction. Countercurrent flow of the two different phases is possible because the larger pores are filled with gas, while the smaller pores are filled with liquid. The gas phase is created in the anode catalyst layer when carbon dioxide is generated by the DMFC anode reaction, equation 1-18. The CO_2 leaves the anode catalyst layer by flowing through the ABL and entering the anode channel from which it leaves the DMFC. It is the

pressure gradient $\Delta P_{TG}/\Delta z$ that cause the convective gas flux away from the anode catalyst layer to the anode channel.

The pressure difference between the gas phase and the liquid phase, $P_{TG} - P_{TL}$ determined from Fig 3-2, can be put into equation 3-18 to determine the transition pore diameter, $(d_P)_{G/L}$, where pores larger than $(d_P)_{G/L}$ are filled with gas and those smaller are filled with liquid. The value of $(d_P)_{G/L}$ can be used in equation 3-19 – equation 3-21 to determine the volumetric fractions of the ABL that are filled with gas, ε_G, and with liquid, ε_L, where ε_G is the volumetric fraction of pores having $d_P > (d_P)_{G/L}$ and ε_L is the volumetric fraction of pores having $d_P < (d_P)_{G/L}$. It must be noted that the Equation of Young and Laplace, equation 3-18, describes equilibrium. As the fuel cell current density increases to values greater than zero, the fuel cell operating conditions become further and further from equilibrium values. Therefore the use of equation 3-18 is a limiting condition that becomes less useful as the fuel cell operating conditions depart farther from equilibrium.

The pressure gradients in Fig 3-2 are shown for three different current densities. As the current density, or reaction rate, increases from 100 to 400 mA cm^{-2} the slopes of the lines become steeper. In other words, the pressure gradients become more positive or more negative. For every current density, the difference in pressure between the gas phase and the liquid phase is greater at the anode catalyst interface than at the anode channel interface. Furthermore the pressure difference between phases increases as the current density increases.

The mole fractions of methanol and water in the liquid phase are shown in Fig 3-3. The slopes of these curves, for example $\Delta x_{CH3OH}/\Delta z$, are mole fraction gradients and are the driving forces for diffusion fluxes. The slopes indicate that methanol diffuses from the anode channel through the ABL to the anode catalyst layer. In contrast water diffuses in the opposite direction. Methanol diffusion and methanol convection are in the direction toward the anode catalyst layer. In contrast water convection is toward the anode catalyst layer and water diffusion is away from the anode catalyst layer.

As the current density increases the mole fraction gradients increase. For methanol as the mole fraction gradient increases the methanol diffusion flux increases and that helps to increase the total methanol flux required at larger current densities. However, an increase in the water mole fraction gradient increases the water diffusion flux away from the anode

catalyst layer, and that is in the wrong direction. As a result when the current density increases the pressure gradient, in Fig 3-1, has to increase enough to both provide the additional water that is needed plus compensate for the increased diffusion of water away from the anode catalyst layer.

The mole fractions of methanol and water in the gas phase are shown in Fig 3-4. The balance of the gas mixture is CO_2. It was assumed that the CO_2 gas would be saturated with both methanol and with water. The saturated vapour pressures of the components were used in the equation combining Raoult's Law with Dalton's Law, equation 3-5 and 3-6. From the slopes of the lines in Fig 3-4, it is apparent that both the methanol and the water mole fraction gradients cause diffusion to occur from the anode channel to the anode catalyst layer. In contrast convection of the gas phase is from the anode catalyst layer to the anode channel. Finally the methanol and water gas phase gradients become steeper (more positive) as the current density increases.

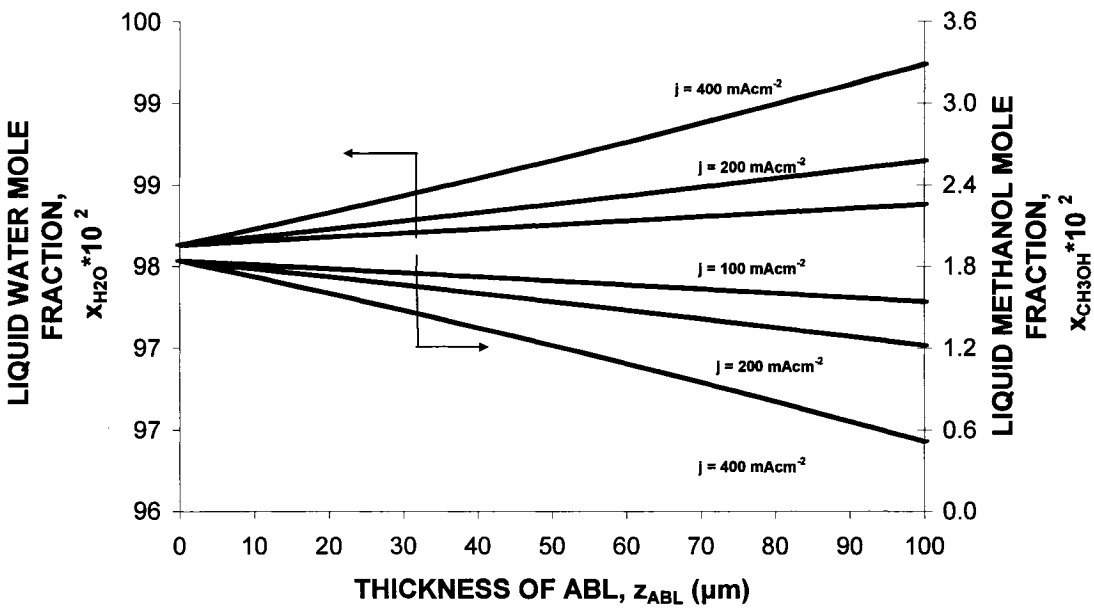

Figure 3-3: The effect of different current density on the concentration of water and methanol in the liquid phase at wet contact angle = 65, and, 1 M across the thickness of backing layer. Position zero is the AC/ABL interface, and position 100 is the ABL/ACL interface

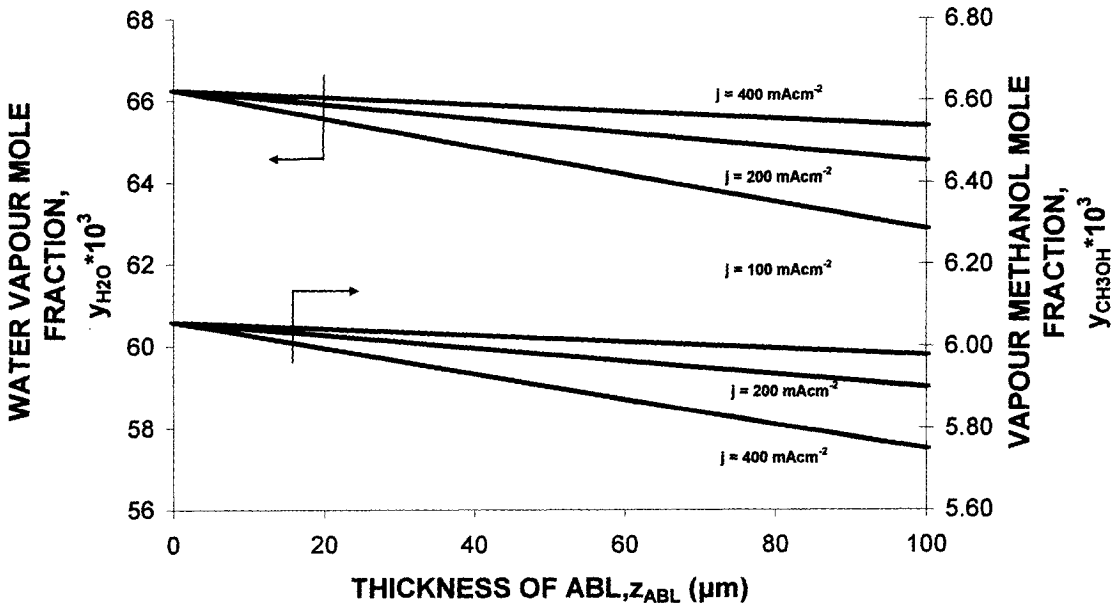

Figure 3-4: The effect of different current density on the concentration of water and methanol in the vapour phase at wet contact angle = 65, and, 1 M across the thickness of backing layer. Position zero is the AC/ABL interface, and position 100 is the ABL/ACL interface

The CO_2 mole fractions are shown in Fig 3-5. As shown by the slope of the lines, the mole fraction gradients cause CO_2 to diffuse from the anode catalyst layer to the anode channel. Therefore both diffusion (concentration gradient in Fig 3-5) and convection (pressure gradient in Fig 3-2) are in the same direction, toward the anode channel. Again the CO_2 mole fraction gradients increase as the current density increases.

The fractional fluxes of diffusion and convection for the liquid phase are shown in Fig's (3-6, and 3-7). For methanol in the liquid phase both diffusion and convection fluxes are positive because both their flows are toward the anode catalyst layer. The fractional value of diffusion and convection with respect to the total liquid methanol flux is also positive in Fig 3-6. It shows that the fractional convection of methanol exceeds the

fractional diffusion. Furthermore it shows that convection is much more important than diffusion near the interface of the ABL with the anode channel.

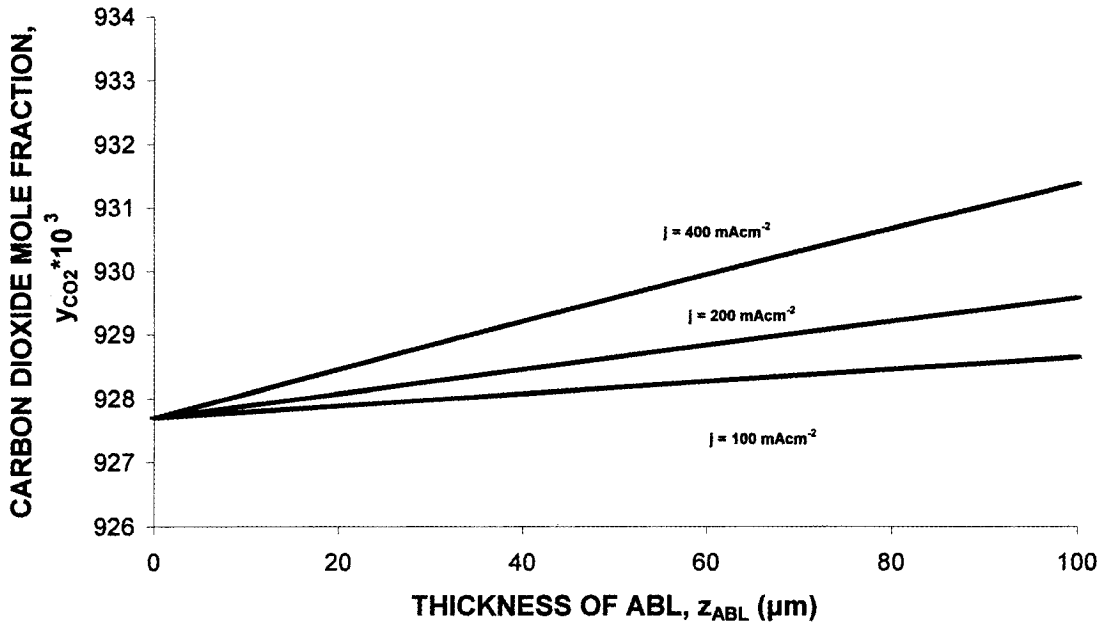

Figure 3-5: The effect of different current density on the concentration on the carbon dioxide at wet contact angle = 65, and, 1 M across the thickness of backing layer.

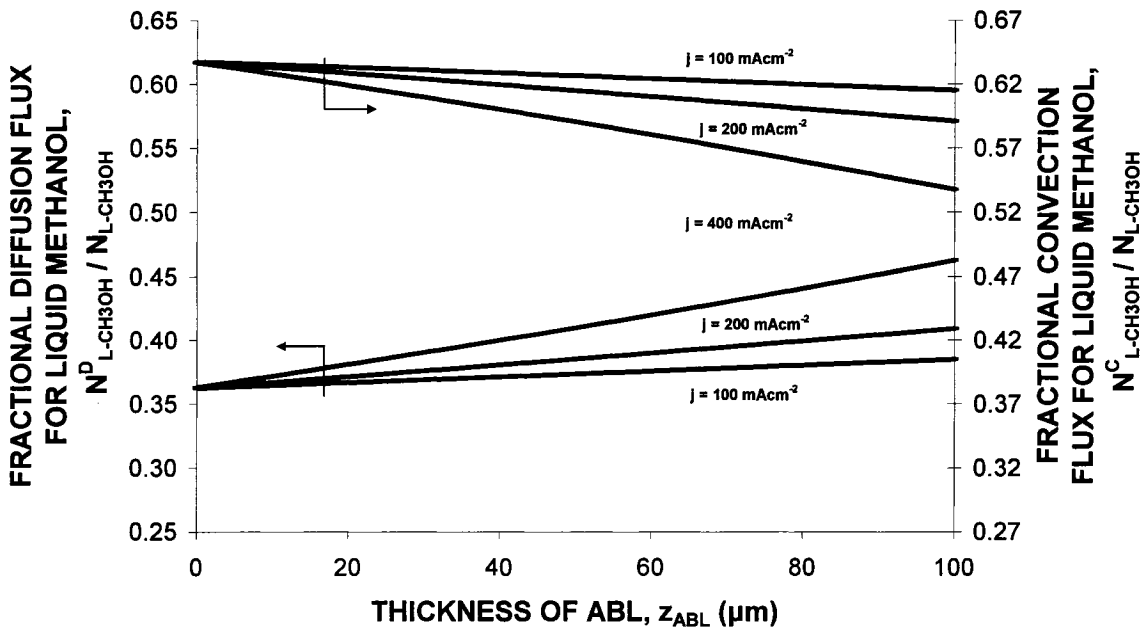

Figure 3-6: The effect of different current density on the fractional diffusion flux and fractional convection flux for liquid methanol at wet contact angle = 65, and, 1 M across the thickness of backing layer.

As the current density increases the concentration gradient of methanol, $\Delta x_{(CH3OH)} / \Delta z$ shown in Fig 3-3 is also increases which is the driving force for diffusion, therefore the fraction of flux caused by diffusion increased about (3 to 10 %) at current density = 400 mA cm^{-2}. For water in the liquid phase, the fraction of flux caused by convection is positive because it is toward the anode catalyst layer and the fraction of flux caused by diffusion is negative because it is toward the anode channel. The ratio formed from a negative number divided by a positive number is negative as shown in Fig 3-7.

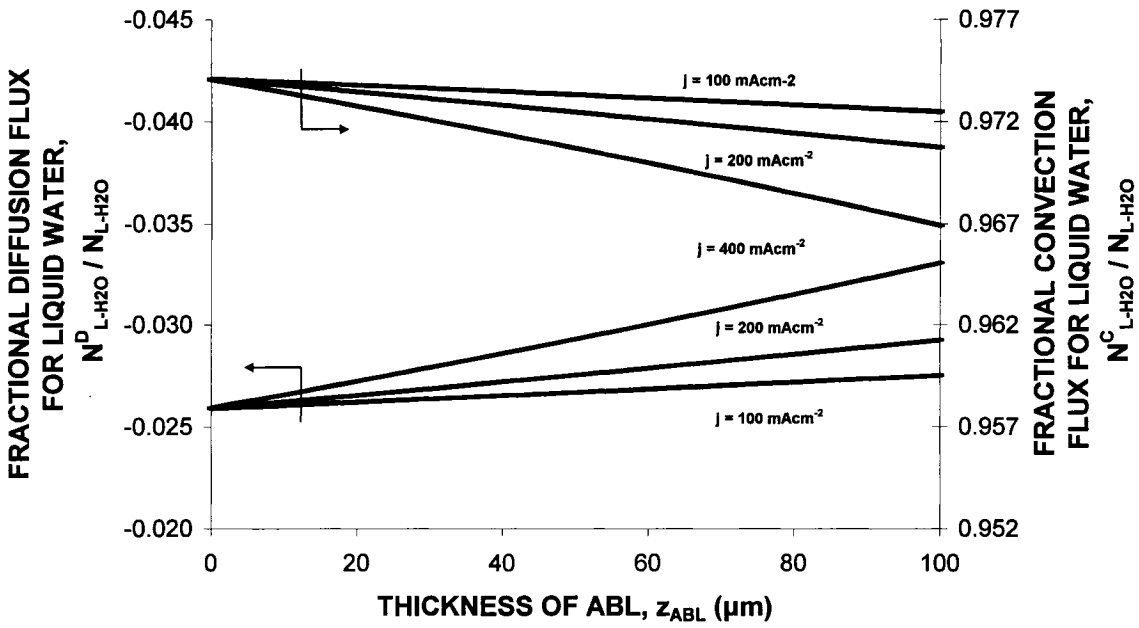

Figure 3-7: The effect of different current density on the fractional diffusion flux and fractional convection flux for liquid water at wet contact angle = 65, and, 1 M across the thickness of backing layer.

The fractions of diffusion and convection flux for methanol and water in the gas phase with respect to the total gas methanol and water fluxes are shown in Fig's 3-8, and 3-9. In the gas phase convection is negative because it is toward the anode channel. Diffusion is positive because it is toward the anode catalyst layer. Therefore the ratios obtained by dividing a negative number by a positive number are negative, as shown in Fig 3-8, and 3-9. Because the diffusion flux is greater than the convection flux both for methanol and for water, the values of the fractional diffusion ratios are large.

The fractions of the total CO_2 flux in the gas phase caused by diffusion and by convection are shown in Fig 3-10. Both the gas phase pressure gradient (the driving force for the convection flux), Fig 3-2, and the CO_2 mole fraction gradient (the driving force for the diffusion flux), Fig 3-5, are negative because both their flows are toward the anode channel. The ratio of two negative quantities is positive, as shown in Fig 3-10. The fraction of total gas phase CO_2 flux caused by convection always exceeds the fraction caused by

diffusion. In addition the fraction caused by convection increases as the location becomes closer to the anode catalyst layer and as the current density increases.

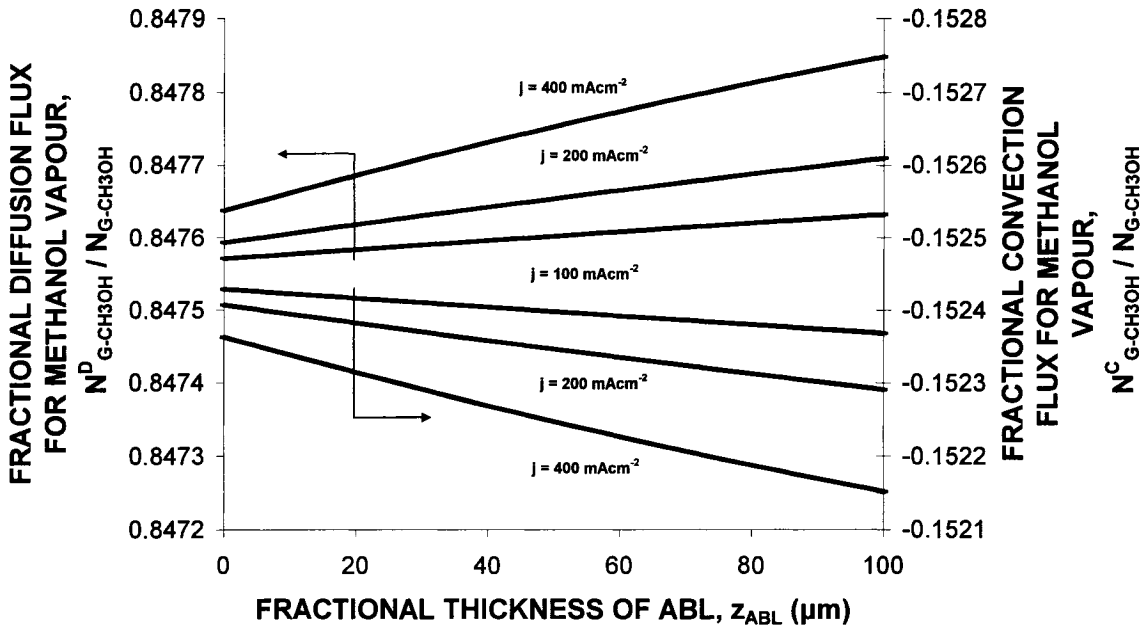

Figure 3-8: The effect of different current density on the fractional diffusion flux and fractional convection flux for methanol vapour at wet contact angle = 65, and, 1 M across the thickness of backing layer.

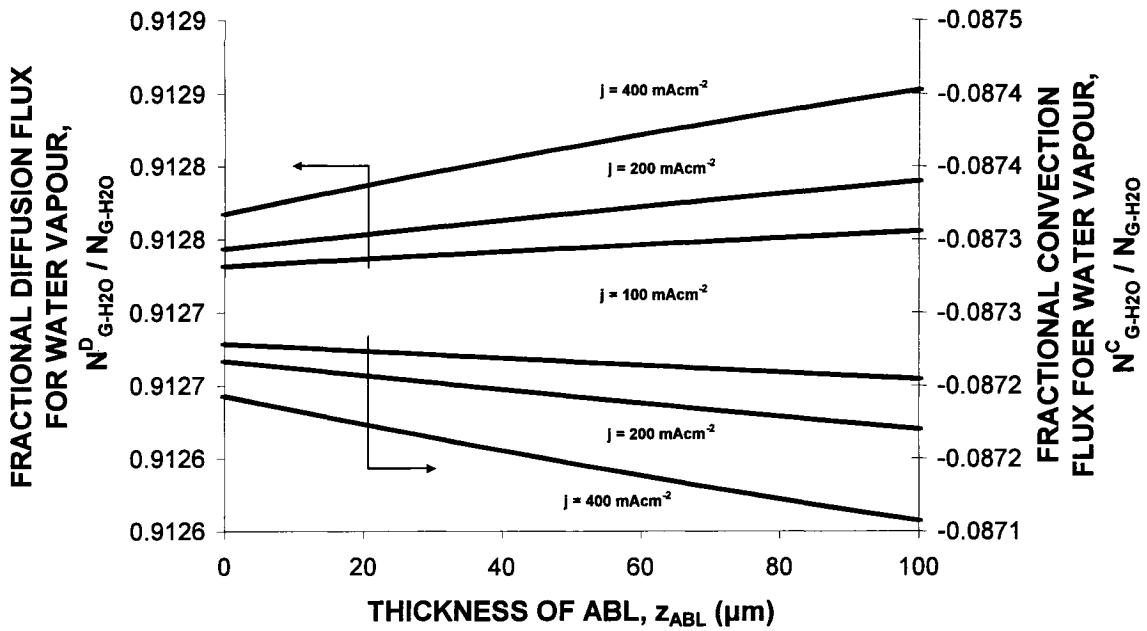

Figure 3-9: The effect of different current density on the fractional diffusion flux and fractional convection flux for water vapour at wet contact angle = 65, and, 1 M across the thickness of backing layer.

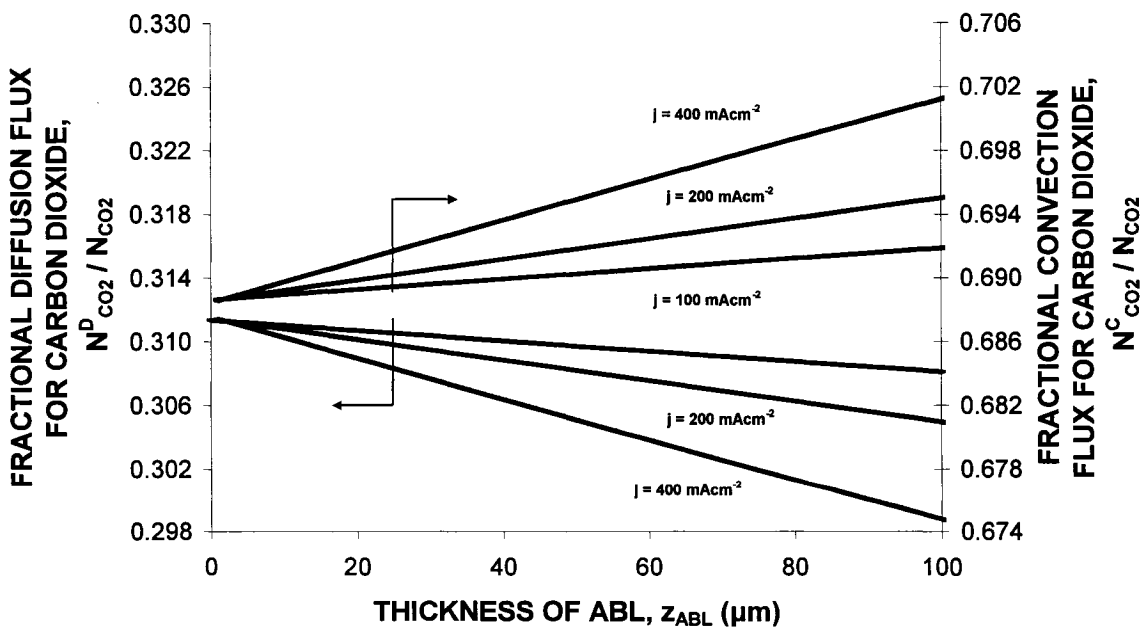

Figure 3-10: The effect of different current density on the fractional diffusion flux and fractional convection flux for carbon dioxide at wet contact angle = 65, and, 1 M across the thickness of backing layer.

The direction of convection and diffusion is controlled by the pressure gradient and the concentration gradient respectively. All species in the ABL for both phases move by both diffusion and convection. The net total flux for liquid or gas is dependant on the net values of the species. The direction of pressure changes for liquid phase, Fig 3-2, the concentration changes, Fig 3-3, and the fractional diffusion and convection fluxes for liquid water and methanol, Fig 3-6 and Fig 3-7, shows that the net flux for the liquid species is from anode channel towards anode catalyst layer, which means that the net total flux of the liquid phase also has the same direction. Fig 3-11 explains this.

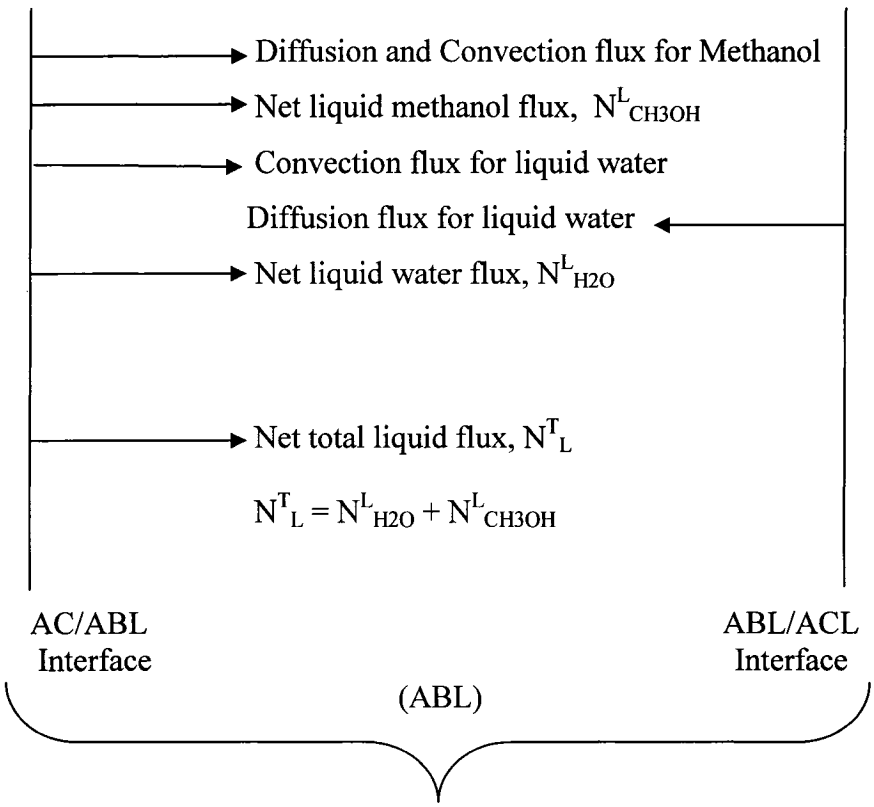

Figure 3-11: The direction of the total liquid flux

The fraction of the total methanol flux that occurs in the gas phase, in contrast to the liquid phase, is shown in Fig 3-12. It is apparent that most of methanol is transported in the liquid phase. Furthermore the amount transported in the liquid phase increases as the location becomes closer to the anode catalyst layer and as the current density increases. These calculations were performed at 40°C. It is possible that as the temperature increases the fraction of methanol transported in the gas phase might increase, since vapor pressures increase with temperature.

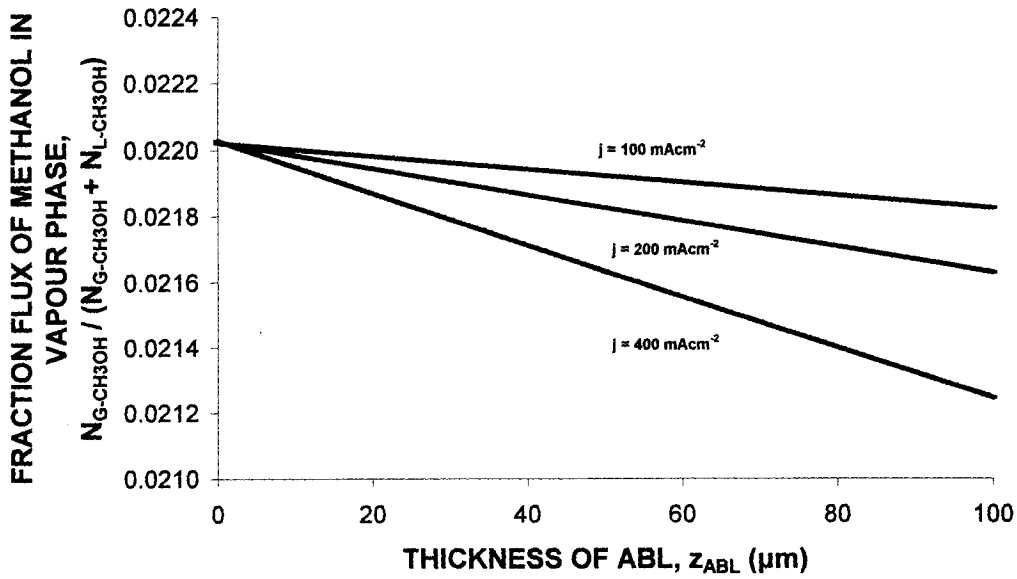

Figure 3-12: The effect of different current density on the fractional flux of methanol in vapour phase at wet contact angle = 65, and, 1 M across the thickness of backing layer.

The effect of anode backing layer thickness on the gas phase and liquid phase pressure drops is shown in Fig 3-13. An increase in thickness caused an increase in the pressure drops in both phases, as would be expected. One of several criteria for ABL performance is its permeability; the transport of reactants and products with minimum pressure drop. On the basis of Fig 3-13 alone, it might be apparent that a thinner thickness is better. Other criteria, such as diffusion perpendicular to the direction of flow must also be considered in optimizing the ABL thickness.

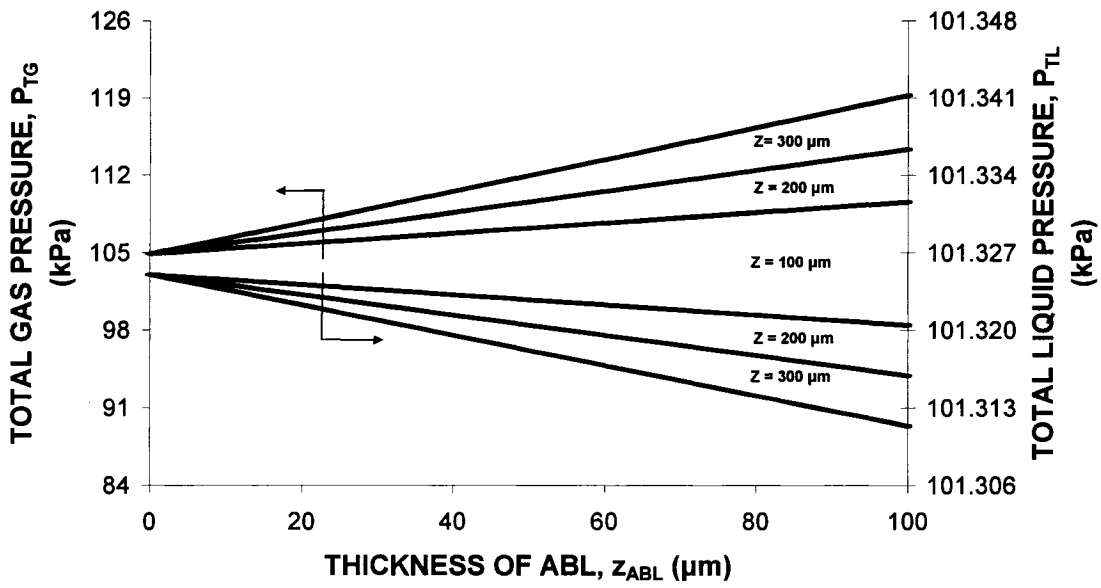

Figure 3-13: The effect of different ABL thicknesses on the total gas and liquid pressure at wet contact angle = 65°, and, 1 M CH_3OH, at the percentage of ABL thickness.

Methanol crossover through the membrane to the cathode catalyst layer is one of the problems that cause a decrease in the performance of DMFCs. Different studies in the literature have shown that this problem can be diminished by using a small concentration of feed methanol. The effect of different methanol molarities in the feed on the pressure drop across the layer is shown Fig 3-14. Increasing the methanol molarity has almost no effect on the liquid phase pressure drop while the gas phase pressure drop across the ABL increases as the methanol molarity decreases.

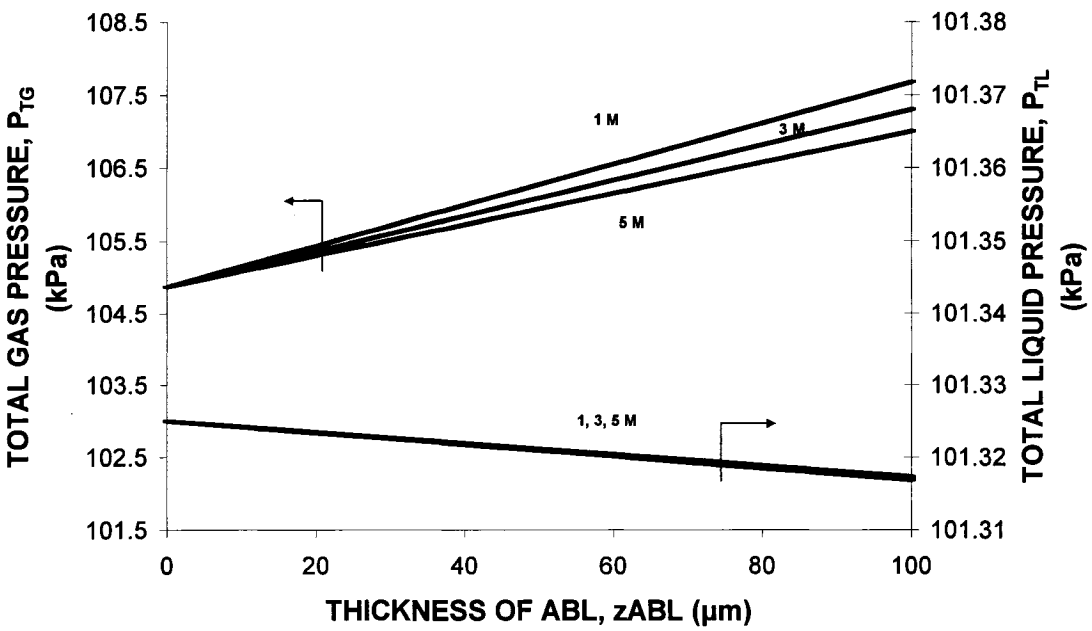

Figure 3-14: The effect of different molarities on the total gas and liquid pressure across the thickness of backing layer at wet contact angle = 65.

The pressure difference between the liquid and gas phases has a direct influence on the transition pore diameter between those pores that are filled with liquid and those that are filled with gas, equation 3-18. In turn the transition pore diameter influences the volumetric void fractions filled with gas and with liquid, equations 3-19 to 3-21. The volumetric fraction filled with liquid is just slightly larger than that filled with gas, as seen in Fig 3-15. The liquid filled fraction decreases as the location moves toward the anode catalyst layer and as the current density increases.

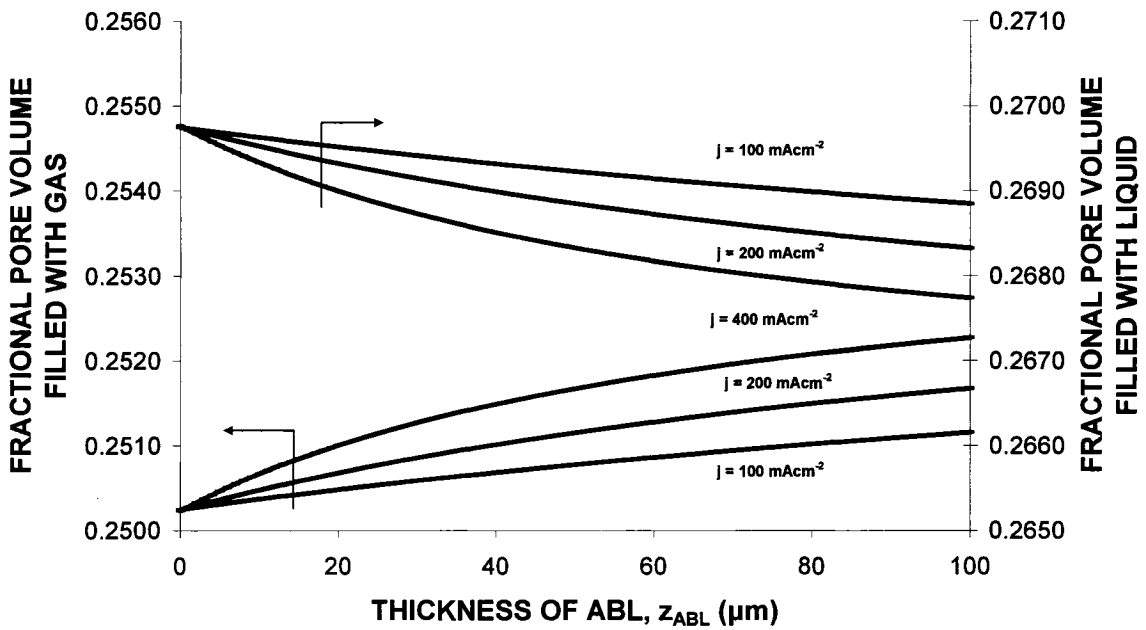

Figure 3-15: The effect of different current density on the fractional pore volume filled with liquid and gas at wet contact angle = 65, and, 1 M.

In order to obtain an understanding of the effects caused by varying contact angle and gas bubble diameter, nine sets of calculations were performed. The resulting variations in volumetric gas fraction are shown in Fig 3-16. As indicated in equation (3-27) above there is a relationship with bubble diameter and the contact angle that involves the pore diameter. At fixed bubble diameter the volumetric fraction filled with gas changed as the contact angle changed. In addition an increase in bubble diameter at constant contact angle caused a change in the volumetric fraction filled with gas. In general a larger fractional pore volume filled with gas was observed at the combination of the smallest bubble diameter and largest contact angle.

Equation (3-26) above shows that the combination of the cosine of the contact angle and the pore diameter will have an influence on the value of the total gas pressure when the total liquid pressure has been identified. It is seen in Fig 3- 17 that when other variables are held constant, the total gas pressure decreases significantly as the gas bubble diameter increases. When other variables are held constant, changes in bubble diameter have little effect on liquid phase pressure, liquid methanol flux, and liquid water flux. This can be seen in Fig 3-18 to 3-20.

However gas bubble diameter does have a minor effect on some variables. The fraction of carbon dioxide flux caused by convection, shown in Fig 3-21 is one of those variables. Fig 3-22 shows the ratio of the flux of methanol in the gas phase to the total flux in both liquid and gas phases. It is another one of those variables. Both of these trends are similar to that of the gas pressure, shown in Fig 3-17

The ratios are constant at constant bubble diameter (pore diameter) for different contact angles while at a constant contact angle a very slight increase in the ratios occur with increasing bubble diameter because of increase in methanol flux in the gas phase.

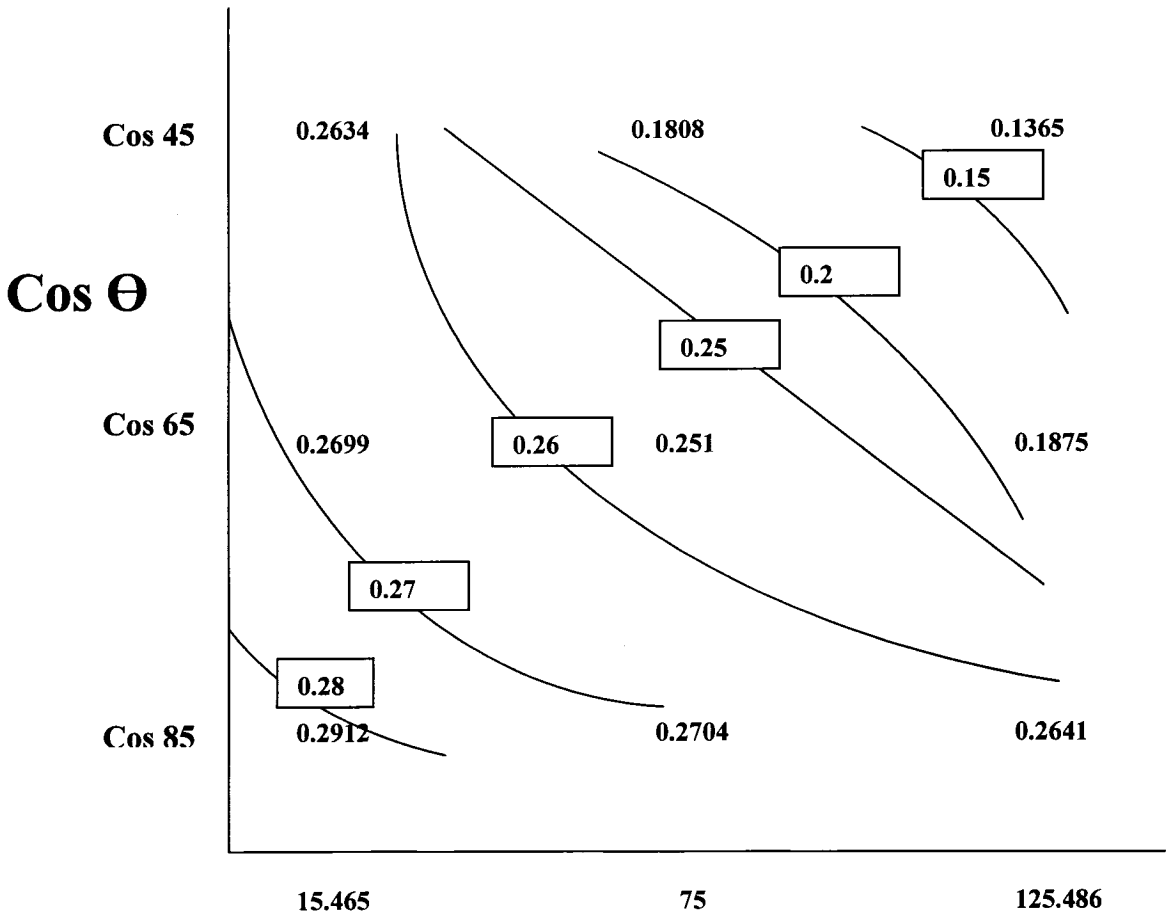

Figure 3-16: Contour plot showing volumetric void fraction, ε_G, as a function of both contact angle, cos Θ, and CO_2 bubble diameter, d_B. (The fractions with 4 significant figures are results obtained from the model, while the fractions with 2 significant figures inside the boxes are lines of constant gas volume fraction that were drawn by interpolation among the results from the model

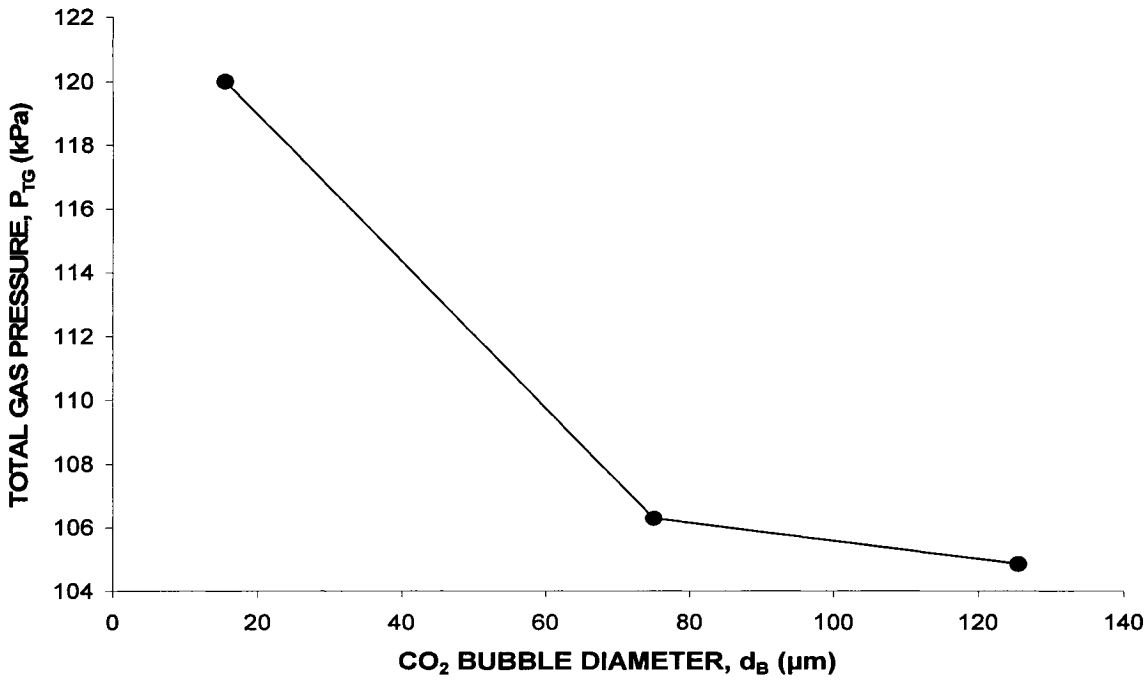

Figure 3-17: The effect of CO_2 bubble diameter on the total gas pressure at 1 M, at the average point between (0 and 100 μm).

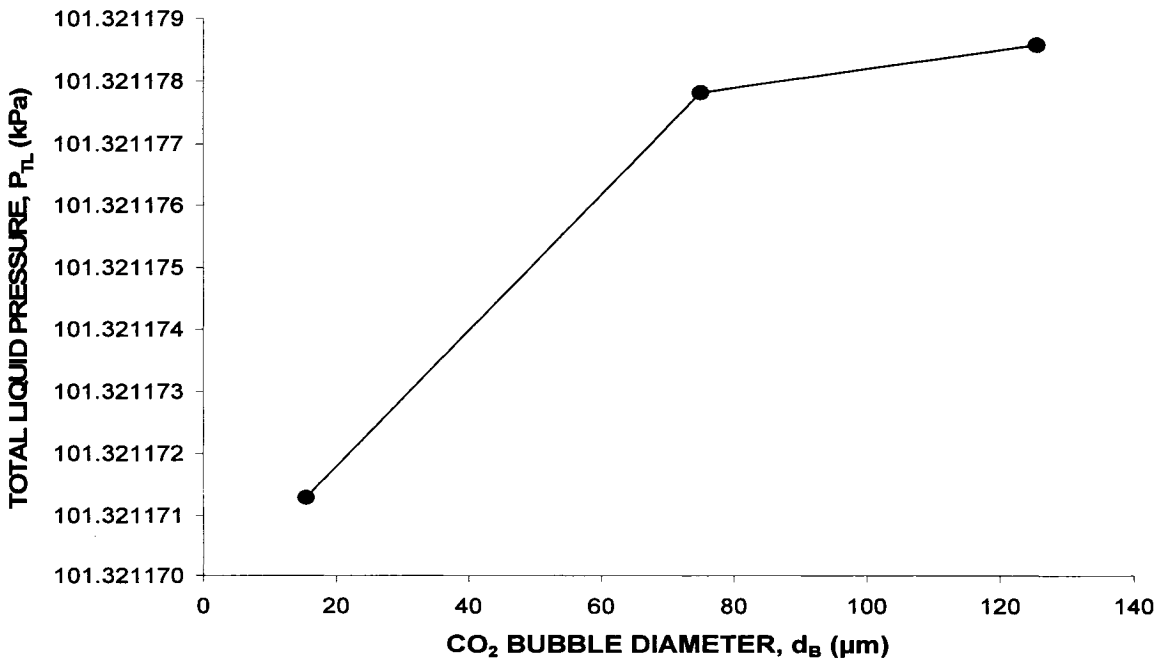

Figure 3-18: The effect of CO_2 bubble diameter on the total liquid pressure at 1 M, at the average point between (0 and 100 μm).

3.6.1 Ratios of methanol flux in the gas phase to the total flux (liquid and gas) phases.

Table 3-9

$\frac{N^{G}_{CH3OH}}{(N^{G}_{CH3OH}+N^{L}_{CH3OH})}$	Pore diameter dp (μm)	Contact Angle	Bubble diameter d_B (μm)
0.0202	10.9	45	15.465
0.0202	6.54	65	15.465
0.0202	1.35	85	15.465
0.0218	53.033	45	75
0.0218	31.7	65	75
0.0218	6.54	85	75
0.022	88.7	45	125.486
0.022	53.033	65	125.486
0.022	10.9	85	125.486

Convection is the dominant transport mechanism for methanol in the liquid phase. By increasing the bubble diameter, at constant contact angle, the transition pore diameter increases. As a result the volume fraction filled with liquid increases, making convection in the liquid phase easier. This explains why there is a slight increase in the fractional convection of liquid phase methanol flux as bubble diameter increases, as shown in Fig 3.20. Similarly, the volume fraction filled with gas decreases, making convection in the gas phase more difficult. As a result, the fractional convection flux of carbon dioxide will decrease, as shown in Fig 3-21, and the fractional diffusion flux for carbon dioxide will increase.

An increase in bubble diameter will decrease the gas pressure, as shown in Fig 3-17. From the equations combining Raoult's and Dalton's Laws, equations 3-5 to 3-7, this will increase the concentration of the methanol and water species and decrease the carbon dioxide concentration. The smaller carbon dioxide concentration will decrease the fraction of the CO_2 flux by convection, as shown in Fig. 3-21.

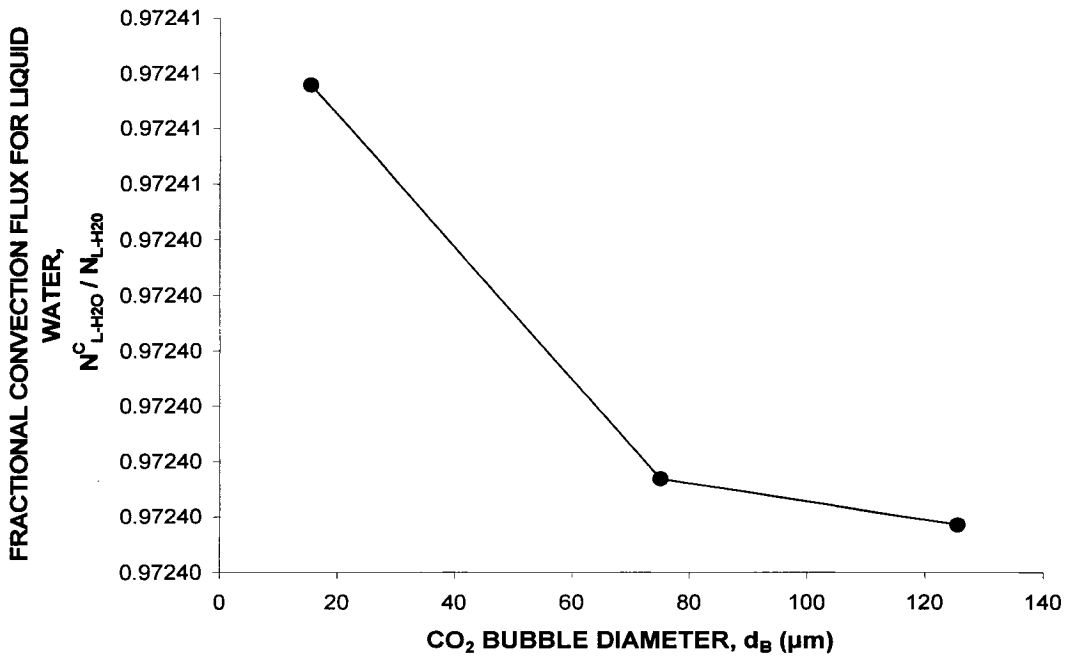

Figure 3-19: The effect of CO_2 bubble diameter on the fractional convection flux for liquid water at 1 M at the average point between (0 and 100 μm).

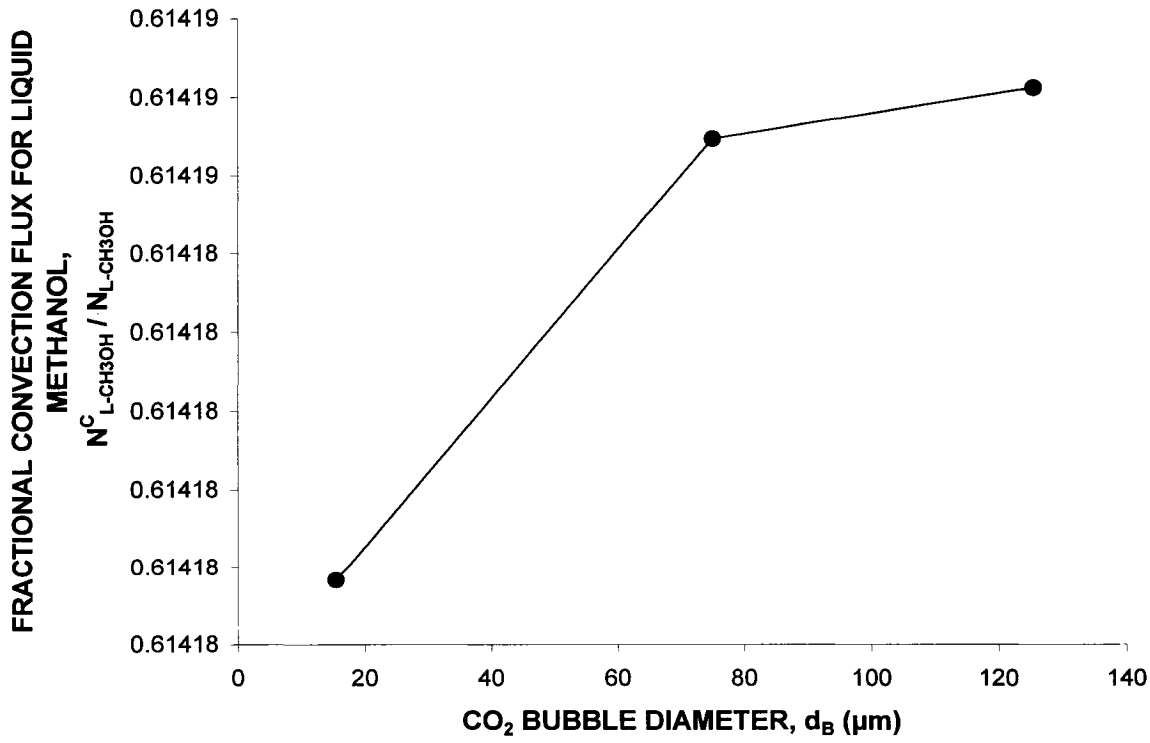

Figure 3-20: The effect of CO_2 bubble diameter on the fractional convection flux for liquid methanol at 1 M at the average point between (0 and 100 μm).

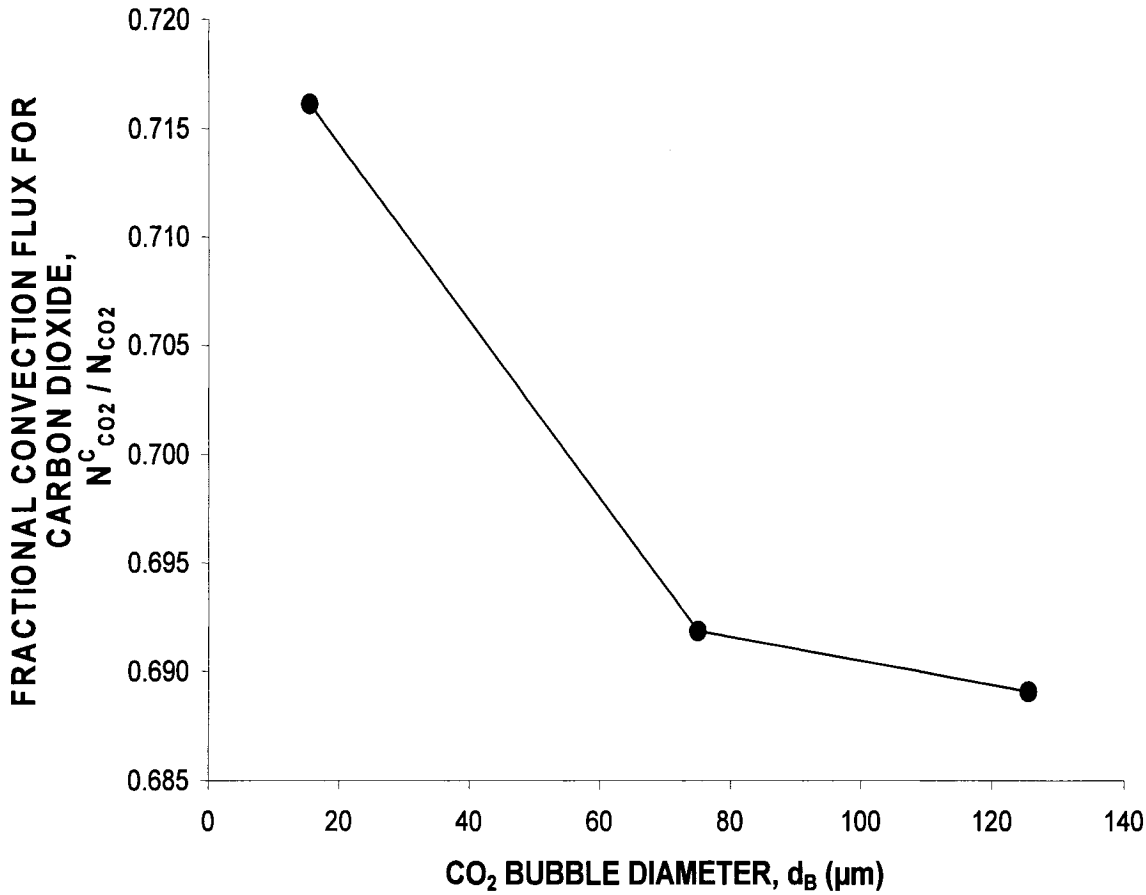

Figure 3-21: The effect of CO_2 bubble diameter on the fractional convection flux for carbon dioxide at 1 M, at the average point between (0 and 100 μm).

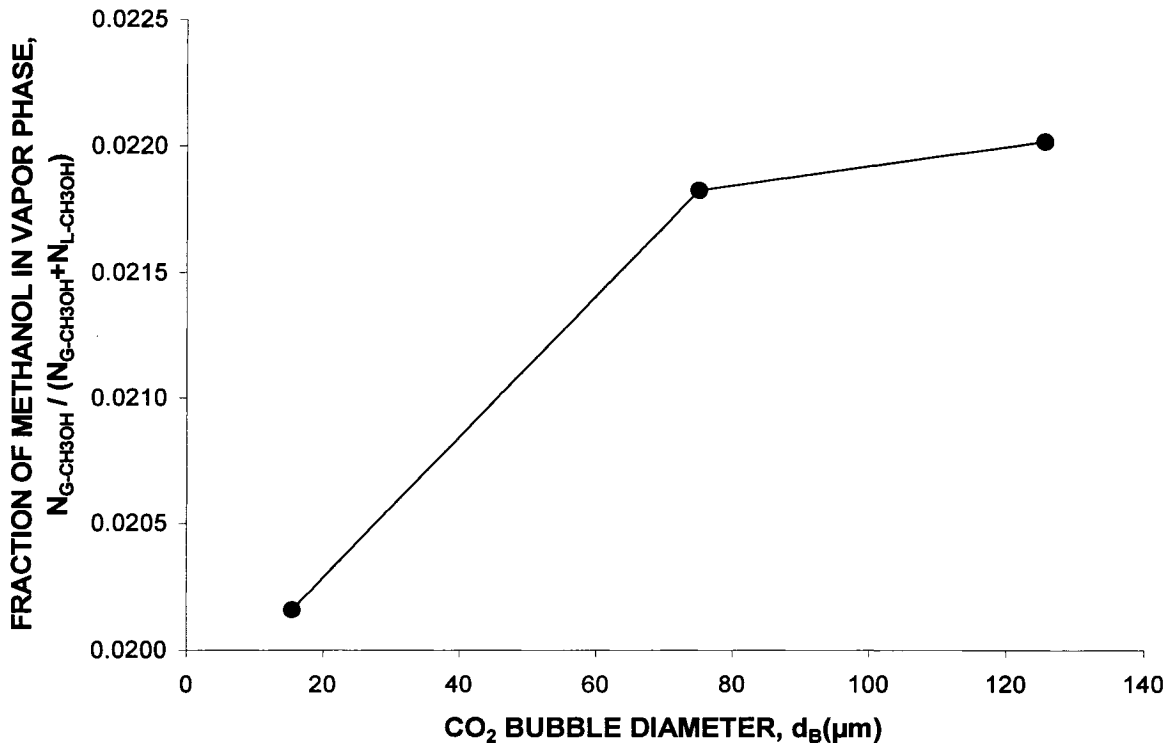

Figure 3-22: The effect of CO_2 bubble diameter on the fraction of methanol flux in the vapour phase at 1 M at the average point between (0 and 100

There are no experimental results published for the ABL by itself that can be used to validate this model. Experimental results are generally reported for entire fuel cells consisting of all layers. They normally report properties of streams (flow rates, concentrations) at the anode and cathode channels, together with current densities. None of those measurements confirm or refute the detailed results reported here. However, a recent study by Neergat and Shulka (2002) confirmed our prediction that the anode backing layer should be hydrophilic. The best results in their study were obtained using a hydrophilic anode backing layer and a hydrophobic cathode backing layer.

References:

E. Antolini, J. Appl. Electrochem., 34, 563, (2004).

P. Argyropoulos, K. Scott, W. M. Taama, J. Appl. Electrochem., 29, 661, (1999).

D. Bargeman, J. Colloid, Interface Sci., 40, 344, (1972).

J. J. Baschuk, X. Li, J. Power Sources, 86, 181, (2000).

S. F. Baxter, V. S. Battaglia, R. E. White, J. Electrochem. Soc., 146 (2), 437, (1999).

T. Berning and N. Djilali, J. Electrochem. Soc., 150, A1598, (2003).

T. Bewer, T. Beckmann, H. Dohle, J. Mergel, D. Stolten, J. Power Sources, 125, 1, (2004).

J. J. Bikerman, Physical Surfaces, Academic Press, New York and London, (1970), p.277.

K. S. Birdi, J. Colloid Interface Sci., 88, 290, (1982).

R. B. Bird, W. E. Stewart, E. N. Lightfoot, Transport Phenomena, 2nd ed., Wiley, New York, (2002), p.192.

E. Birgersson, J. Nordlund, M. Vynnycky, C. Picard, G. Lindberg, J. Electrochem. Soc., 151, A2157, (2004).

A. Biyikoglu, Intern. J. Hydrogen Energy, 30, 1181, (2005).

D. Cheddie, N. Munroe, J. Power Sources, 147, 72, (2005).

H. S. Chu, C. Yeh, F. Chen, J. Power Sources, 123, 1, (2002).

P. Choi, R. Datta, J. Electrochem. Soc., 151, E601, (2003).

R. DeFay, I. Prigogine, A. Bellemans, D. H. Everett, Surface Tension and Adsorption, Longmans, London, (1966), p.7.

R. Dillon, S. Srinivasan, A.S. Arico, V. Antonucci, J. Power Sources, 127, 112, (2004).

J. Divisek, J. Fuhtmann, K. Gartner, R. Jung, J. Electrochem. Soc., 150, A811, (2003).

S. Galinat, O. Masbernat, P. Guiraud, C. Dalmazzone, C. Nolk, Chem. Eng. Sci., 60, 6511, (2005).

V. Guurau, H. Liu, S. Kakac, AIChE J., 44, 2414, (1998).

V. Gurau, F. Barbir, H. Liu, J. Electrochem. Soc., 147, 2468, (2000).

W. He, J. S. Yi, T. V. Nguyen, AIChE J., 46, 2053, (2000).

C. D. Hodgman, R. D. Weast, R. S. Shankland, S. M. Selby, Handbook of Chemistry and Physics, 44th Ed., Rubber Publishing Co., Cleveland, (1962), (a) p. 2265, (b) p. 2238.

K. T. Jeng, C. W. Chen, J. Power Sources, 112, 367, (2002).

A. A. Kulikovsky, Electrochem Commun., 4, 939, (2002).

A. A. Kulikovsky, J. Appl. Electrochem., 30, 1005, (2000).

A. A. Kulikovsky, J. Divisek, A. A. Kornyshev, J. Electrochem. Soc., 147, 953, (2000).

A. A. Kulikovsky, Electrochem. Commun, 7, 237, (2005).

C. Lim, C. Y. Wang, Electrochim. Acta, 49, 4149, (2004).

Lindstrom, (US Patent 4,647,359: Electrolytic Gas Diffusion Electrode Employing Thin Carbon Cloth Layer), issued Mar.3, (1987).

G. Q. Lu, C. Y. Wang, J. Power Sources, 134, 33, (2004).

K. Miwa, K. Shimazu, H. Fukui, (US Patent 4,851,304: Electrode Substrate for Fuel Cell and Process for Producing the same), issued Jul.25, (1989).

S. Mazumder and J. V. Cole, J. Electrochem. Soc., 150, A1510, (2003).

B. D. McNicol, D. A. J. Rand, K. R. Williams, J. Power Sources, 83, 15, (1999).

G. Murgia, I. Pisani, A. K. Shukla, K. Scott, J. Electrochem. Soc., 150, A1231, (2003).

J. H. Nam, M. Kaviany, Int. J. Heat Mass Transfer, 46, 4595, (2003).

D. Natarajan, T. V. Nguyen, J. Electrochem. Soc., 148, A1324, (2001).

D. Natarajan, T. V. Nguyen, J. Power Sources, 115, 66, (2003).

M. Neergat, A.K. Shukla, J. Power Sources, 104, 289 (2002).

U. Pasaogullari, C. Y. Wang, J. Electrochem. Soc., 151, A399, (2004).

R. H. Perry, C. H. Chilton, S. D. Kirkpatrick, Chemical Engineers' Handbook, 4th Ed., McGraw-Hill, New York, (1963), (a) p. 3-201, (b) p. 3-82.

L. Pisani, G. Murgia, M. Valentini, B. D'Aguanno, J. Electrochem. Soc., 149, A898, (2002).

R. C. Ried, J. M. Prausnitz, T. K. Sherwood, The properties of Gases and Liquids, 3rd ed., McGraw-Hill, New York, (1977), p.411-414.

K. Scott, W. Tamma, and J. Cruickshank, J. Power Sources, 65, 159, (1997).

K. Scott, W. Tamma, J. Cruickshank, J. Appl. Electrochem., 28, 289, (1998).

K. Scott, P. Argyropoulos, K. Sundmacher, J. Electroanal. Chem., 477, 97, (1999).

R. Sousa, E. R. Gonzalez, J. Power Sources, 147, 32, (2005).

K. Sundmacher, K. Scott, Chem. Eng. Sci., 54, 2927, (1999).

K. Sundmacher, K.Scott, Chem. Eng. Sci., 54, 2927, (1999).

K. Sundmacher, T. Schultz, S. Zhou, K. Scott, M. Ginkel, E. D. Gilles, Chem.Eng. Sci., 56, 333, (2001).

W. Sun, A. Peppley, K. Karan, J. Power Sources, 144, 42, (2005).

S. Um, Wang, and K. S. Chen, J. Electrochem. Soc., 147, 4485, (2000).

M. W. Verbrugge, J. Electrochem. Soc., 136, 417, (1989).

S. Wasmus, A. Kuver, J. Electroanal. Chem., 461, 14, (1999).

Z. H. Wang, C. Y. Wang, J. Electrochem. Soc., 150 (4), A 508, (2003).

Z. Weber, M. Darling, J. Newman, J. Electrochem. Soc., 151(10), A1715, (2004).

M. V. Williams, E. Begg, L. Bonville, H. R. Kunz, J. M. Fenton, J. Electrochem. Soc., 151(8), A1173, (2004).

C. Xu, P. M. Follmann, F. T. Biegler, M. S. Jhon, Comput. Chem. Eng., 29, 1849, (2005).

L. X. You, H. T. Liu, Int. J. Heat Mass Transfer, 45, 2277, (2002).

K. Z. Yao, K. Karan, K. B. McAuley, P. Oosthuizen, B. Peppley, T. Xie, Fuel Cells 4, 3, (2004).

S. Zhou, T. Schultz, M. Peglow, K. Sundmacher, Phys. Chem. Chem. Phys., 3, 347, (2001).

Figure captions

CHAPTER FOUR

Complete mathematical equations for ACL, ELL, CCL, and CBL

Complete mathematical equations were developed for the other DMFC layers. The transport of all species in both phases was described. An equation for the anode catalyst layer reaction was also developed. The electrochemical reaction occurs in the ACL, producing both (a) charged species (H^+), that move through the electrolyte layer to the cathode side, and (b) electrons (e^-) that move through the conductive layer (ABL), through an external circuit, and then to the cathode side. During the proton transport through the electrolyte layer it drags water and methanol with it (methanol cross-over) causing a mixed potential at the cathode side. In addition to the diffusion and convection transport mechanisms for all species in both phases, two additional transport mechanisms are operative. One is the electro-osmotic drag force that operates on water and methanol. The other is the migration force resulting from the potential gradient, which operates on charged species.

4.1 ANODE CATALYST LAYER

4.1.1 Equations used to model the gas phase in the anode catalyst layer (ACL)

Table (4-10)

Equations	Equation No.
A) Momentum Transport (Ergun Equation)	
$\frac{dP_{TG}}{dz} = \frac{N_{TG}^2}{\rho_G d_p}\left[\frac{\varepsilon_S}{\varepsilon_G^3}\right]\left\{150\left[\frac{(\varepsilon_S)\,\mu_G}{d_P\, N_{TG}}\right] + 1.75\right\}$	(4-1)
B) Mass Transport (Stefan - Maxwell Equations)	
$\frac{dy_{CO2}}{dz} = \frac{1}{C_{TG}}\left[\frac{(y_{CO2}N^G_{H2O} - y_{H2O}N^G_{CO2})}{D^{G\text{-}E}_{CO2/H2O}} + \frac{(y_{CO2}N^G_{CH3OH} - y_{CH3OH}N^G_{CO2})}{D^{G\text{-}E}_{CO2/CH3OH}} + \frac{(y_{CO2}N^G_{O2} - y_{O2}N^G_{CO2})}{D^{G\text{-}E}_{CO2/O2}}\right]$	(4-2)
$\frac{dy_{H2O}}{dz} = \frac{1}{C_{TG}}\left[\frac{(y_{H2O}N^G_{CH3OH} - y_{CH3OH}N^G_{H2O})}{D^{G\text{-}E}_{CH3OH/H2O}} + \frac{(y_{H2O}N^G_{CO2} - y_{CO2}N^G_{H2O})}{D^{G\text{-}E}_{CO2/H2O}} + \frac{(y_{H2O}N^G_{O2} - y_{O2}N^G_{H2O})}{D^{G\text{-}E}_{O2/H2O}}\right]$	(4-3)
$\frac{dy_{CH3OH}}{dz} = \frac{1}{C_{TG}}\left[\frac{(y_{CH3OH}N^G_{H2O} - y_{H2O}N^G_{CH3OH})}{D^{G\text{-}E}_{CH3OH/H2O}} + \frac{(y_{CH3OH}N^G_{CO2} - y_{CO2}N^G_{CH3OH})}{D^{G\text{-}E}_{CH3OH/CO2}} + \frac{(y_{CH3OH}N^G_{O2} - y_{O2}N^G_{CH3OH})}{D^{G\text{-}E}_{CH3OH/O2}}\right]$	(4-4)

$$\frac{dy_{O2}}{dz} = \frac{1}{C_{TG}} \left[\frac{(y_{O2} N^{G}_{H2O} - y_{H2O} N^{G}_{O2})}{D^{G\text{-}E}_{O2/H2O}} + \frac{(y_{O2} N^{G}_{CO2} - y_{CO2} N^{G}_{O2})}{D^{G\text{-}E}_{O2/CO2}} + \frac{(y_{O2} N^{G}_{CH3OH} - y_{CH3OH} N^{G}_{O2})}{D^{G\text{-}E}_{CH3OH/O2}} \right] \quad (4\text{-}5)$$

$$y_{H2O} = \frac{(P^{SAT})_{H2O}}{P_{TG}} x_{H2O} \quad (4\text{-}6)$$

$$y_{CH3OH} = \frac{(P^{SAT})_{CH3OH}}{P_{T}} x_{CH3OH} \quad (4\text{-}7)$$

$$y_{CO2} = 1 - y_{H2O} - y_{CH3OH} - y_{O2} \quad (4\text{-}8)$$

$$N_{TG} = N_{CO2} + N^{G}_{CH3OH} + N^{G}_{H2O} + N^{G}_{O2} \quad (4\text{-}9)$$

$$(R_{H2O})^{VAP} = \frac{dN^{G}_{H2O}}{dz} \quad (4\text{-}10)$$

$$(R_{CH3OH})^{VAP} = \frac{dN^{G}_{CH3OH}}{dz} \quad (4\text{-}11)$$

$$(R_{CO2})^{A\text{-}Rx} = \frac{dN^{G}_{CO2}}{dz} \quad (4\text{-}12)$$

$$(R_{O2})^{VAP} = \frac{dN^{G}_{O2}}{dz} \quad (4\text{-}13)$$

4.1.2 Equations used to model the liquid phase in the anode catalyst layer (ACL)

Table (4-11)

Equations	Equation No.

A) Momentum Transport (Ergun equation)

$$\frac{dP_{TL}}{dz} = \frac{N_{TL}^2}{\rho_L d_p} \left[\frac{\varepsilon_S}{\varepsilon_L^3}\right] \left\{150\left[\frac{(\varepsilon_S)\,\mu_L}{d_P\, N_{TL}}\right] + 1.75\right\} - \rho_{H^+} n_{EQ} F \frac{d\Phi_L}{dz} \qquad (4\text{-}14)$$

Ohm's Law – 2 Equations (liquid phase) and (solid phase)

$$\frac{d\Phi_L}{dz} = j\, R_L \qquad \frac{d\Phi_S}{dz} = 0.0 \quad (R_S = 0.0)$$

B) Mass transport (Fluxes from Stefan - Maxwell Equations)

$$N^L_{H2O} = -\left\{\frac{C_{TL}}{(x_{CH3OH}/D^{L\text{-}E}_{CH3OH/H2O}) + (x_{O2}/D^{L\text{-}E}_{O2/H2O}) + (x_{H^+}/D^{L\text{-}E}_{H^+/H2O})}\right\}\frac{dx_{H2O}}{dz} +$$

$$x_{H2O}\left[\frac{N^L_{CH3OH}}{x_{CH3OH} + x_{O2}(D^{L\text{-}E}_{CH3OH/H2O}/D^{L\text{-}E}_{O2/H2O}) + x_{H^+}(D^{L\text{-}E}_{CH3OH/H2O}/D^{L\text{-}E}_{H^+/H2O})} +\right.$$

$$\frac{N^L_{O2}}{x_{O2} + x_{CH3OH}(D^{L\text{-}E}_{O2/H2O}/D^{L\text{-}E}_{CH3OH/H2O}) + x_{H^+}(D^{L\text{-}E}_{O2/H2O}/D^{L\text{-}E}_{H^+/H2O})} +$$

$$\left.\frac{N^L_{H^+}}{x_{H^+} + x_{CH3OH}(D^{L\text{-}E}_{H^+/H2O}/D^{L\text{-}E}_{CH3OH/H2O}) + x_{O2}(D^{L\text{-}E}_{H^+/H2O}/D^{L\text{-}E}_{O2/H2O})}\right] +$$

$$\lambda_{H2O} * x_{H2O}\frac{j}{F} \qquad (4\text{-}15)$$

$$N^{L}_{H^+} = -\left\{ \frac{C_{TL}}{(x_{CH3OH}/D^{L\text{-}E}_{CH3OH/H^+}) + (x_{H2O}/D^{L\text{-}E}_{H^+/H2O}) + (x_{O2}/D^{L\text{-}E}_{H^+/O2})} \right\} \frac{dx_{H^+}}{dz} +$$

$$x_{H^+} \left[\frac{N^{L}_{CH3OH}}{x_{CH3OH} + x_{H2O}(D^{L\text{-}E}_{CH3OH/H^+}/D^{L\text{-}E}_{H^+/H2O}) + x_{O2}(D^{L\text{-}E}_{CH3OH/H^+}/D^{L\text{-}E}_{H^+/O2})} + \right.$$

$$\frac{N^{L}_{O2}}{x_{O2} + x_{CH3OH}(D^{L\text{-}E}_{O2/H^+}/D^{L\text{-}E}_{CH3OH/H^+}) + x_{H2O}(D^{L\text{-}E}_{O2/H^+}/D^{L\text{-}E}_{H^+/H2O})} +$$

$$\left. \frac{N^{L}_{H2O}}{x_{H2O} + x_{CH3OH}(D^{L\text{-}E}_{H^+/H2O}/D^{L\text{-}E}_{CH3OH/H^+}) + x_{O2}(D^{L\text{-}E}_{H^+/H2O}/D^{L\text{-}E}_{O2/H^+})} \right] +$$

$$\left[-Z\,u\,F\,C\,x_{H^+} \frac{d\Phi^{L}}{dz} \right] \qquad (4\text{-}16)$$

$$N^{L}_{CH3OH} = -\left\{ \frac{C_{TL}}{(x_{H2O}/D^{L\text{-}E}_{CH3OH/H2O}) + (x_{O2}/D^{L\text{-}E}_{CH3OH/O2}) + (x_{H^+}/D^{L\text{-}E}_{H^+/CH3OH})} \right\} \frac{dx_{CH3OH}}{dz}$$

$$+ x_{CH3OH} \left[\frac{N^{L}_{H2O}}{x_{H2O} + x_{H^+}(D^{L\text{-}E}_{CH3OH/H2O}/D^{L\text{-}E}_{H^+/CH3OH}) + x_{O2}(D^{L\text{-}E}_{CH3OH/H2O}/D^{L\text{-}E}_{CH3OH/O2})} + \right.$$

$$\frac{N^{L}_{O2}}{x_{O2} + x_{H2O}(D^{L\text{-}E}_{O2/CH3OH}/D^{L\text{-}E}_{CH3OH/H2O}) + x_{H^+}(D^{L\text{-}E}_{O2/CH3OH}/D^{L\text{-}E}_{H^+/CH3OH})} +$$

$$\left. \frac{N^{L}_{H^+}}{x_{H^+} + x_{H2O}(D^{L\text{-}E}_{H^+/CH3OH}/D^{L\text{-}E}_{CH3OH/H2O}) + x_{O2}(D^{L\text{-}E}_{H^+/CH3OH}/D^{L\text{-}E}_{O2/CH3OH})} \right] +$$

$$\frac{x_{CH3OH}}{x_{CH3OH} + x_{H2O}} \lambda_{H2O} \frac{j}{F} \qquad (4\text{-}17)$$

$$N^{L}_{O2} = -\left\{ \frac{C_{TL}}{(x_{CH3OH}/D^{L\text{-}E}_{CH3OH/O2}) + (x_{H2O}/D^{L\text{-}E}_{O2/H2O}) + (x_{H^+}/D^{L\text{-}E}_{H^+/O2})} \right\} \frac{dx_{O2}}{dz} +$$

$$x_{O2} \left[\frac{N^{L}_{CH3OH}}{x_{CH3OH} + x_{H2O}(D^{L\text{-}E}_{CH3OH/O2}/D^{L\text{-}E}_{O2/H2O}) + x_{H^+}(D^{L\text{-}E}_{CH3OH/O2}/D^{L\text{-}E}_{H^+/O2})} + \right.$$

$$\frac{N^{L}_{H^+}}{x_{H^+} + x_{CH3OH}(D^{L\text{-}E}_{O2/H^+}/D^{L\text{-}E}_{CH3OH/O2}) + x_{H2O}(D^{L\text{-}E}_{O2/H^+}/D^{L\text{-}E}_{O2/H2O})} +$$

$$\left. \frac{N^{L}_{H2O}}{x_{H2O} + x_{CH3OH}(D^{L\text{-}E}_{O2/H2O}/D^{L\text{-}E}_{CH3OH/O2}) + x_{H^+}(D^{L\text{-}E}_{O2/H2O}/D^{L\text{-}E}_{O2/H^+})} \right]$$

(4-18)

$$N_{TL} = N^{L}_{H2O} + N^{L}_{CH3OH} + N^{L}_{H^+} + N^{L}_{O2} \qquad (4\text{-}19)$$

$$\frac{dN^{L}_{H2O}}{dz} + (R_{H2O})^{VAP} + (R_{H2O})^{A\text{-}RX} = 0 \qquad (4\text{-}20)$$

$$\frac{dN^{L}_{CH3OH}}{dz} + (R_{CH3OH})^{VAP} + (R_{CH3OH})^{A\text{-}RX} = 0 \qquad (4\text{-}21)$$

$$\frac{dN^{L}_{H^+}}{dz} + (R_{H^+})^{A\text{-}RX} = 0 \qquad (4\text{-}22)$$

$$\frac{dN^{L}_{O2}}{dz} + (R_{O2})^{MP} + (R_{O2})^{VAP} = 0 \qquad (4\text{-}23)$$

4.1.3 Reaction equations in the Catalyst Layer

$$(R_{CH3OH})^{A\text{-}RX} = N_{AG}\,(R_{AG})^{RX}$$

$$= 4\,\pi\, r_{AG}\, N_{AG} \left[\frac{1}{\frac{1}{D} + \frac{1}{D_E\,(r_{AG}\sqrt{\Psi}\coth(r_{AG}\sqrt{\Psi}) - 1)}} \right] C_{TL}\, x_{CH3OH} \qquad (4\text{-}24)$$

$$\Psi = \frac{K_{F,CH}\, C\, x_{H2O}}{F\, SAV\, D_E} \exp\left[\frac{\alpha_F\, n_{EQ}\, F\, \Delta\Phi_{EQ}}{RT}\right] \left\{ \exp\left[\frac{-\alpha_A\, n_{EQ}\, F\, \eta_A}{RT}\right] - \exp\left[\frac{-\alpha_C\, n_{EQ}\, F\, \eta_C}{RT}\right] \right\}$$

$$(R^{L}_{H2O})^{A\text{-}RX} = (R^{L}_{CH3OH})^{A\text{-}RX} \qquad (4\text{-}25)$$

$$(R^{G}_{CO2})^{A\text{-}RX} = (R^{L}_{CH3OH})^{A\text{-}RX} \qquad (4\text{-}26)$$

$$(R^{L}_{H^+})^{A\text{-}RX} = -(R^{L}_{H^+})^{C\text{-}RX} = 6 * (R^{L}_{CH3OH})^{A\text{-}RX} \qquad (4\text{-}27)$$

$$(R^{G}_{O2})^{C\text{-}RX} = -3/2 * (R^{L}_{CH3OH})^{A\text{-}RX} \qquad (4\text{-}28)$$

$$(R^{L}_{H2O})^{C\text{-}RX} = -3 * (R^{L}_{CH3OH})^{A\text{-}RX} \qquad (4\text{-}29)$$

$$(R^{G}_{CO2})^{A\text{-}RX} = (R^{L}_{CH3OH})^{A\text{-}RX} \qquad (4\text{-}30)$$

4.2 Electrolyte Layer

4.2.1 Equations used to model the Electrolyte layer (liquid only)

Table (4-12)

Equations	Equation No.

A) Momentum Transport (Ergun equation)

$$\frac{dP_{TL}}{dz} = \frac{N_{TL}^2}{\rho_L d_p}\left[\frac{\varepsilon_S}{\varepsilon_L^3}\right]\left\{150\left[\frac{(\varepsilon_S)\,\mu_L}{d_P\,N_{TL}}\right] + 1.75\right\} - \rho_H{}^{+} n_{EQ} F \frac{d\Phi_L}{dz} \quad (4\text{-}31)$$

B) Mass transport (Fluxes from Stefan - Maxwell Equations)

$$N^L_{H2O} = -\left\{\frac{C_{TL}}{(x_{CH3OH}/D^{L\text{-}E}_{CH3OH/H2O}) + (x_{O2}/D^{L\text{-}E}_{O2/H2O}) + (x_{H^+}/D^{L\text{-}E}_{H^+/H2O})}\right\}\frac{dx_{H2O}}{dz} +$$

$$x_{H2O}\left[\frac{N^L_{CH3OH}}{x_{CH3OH} + x_{O2}(D^{L\text{-}E}_{CH3OH/H2O}/D^{L\text{-}E}_{O2/H2O}) + x_{H^+}(D^{L\text{-}E}_{CH3OH/H2O}/D^{L\text{-}E}_{H^+/H2O})} + \right.$$

$$\frac{N^L_{O2}}{x_{O2} + x_{CH3OH}(D^{L\text{-}E}_{O2/H2O}/D^{L\text{-}E}_{CH3OH/H2O}) + x_{H^+}(D^{L\text{-}E}_{O2/H2O}/D^{L\text{-}E}_{H^+/H2O})} +$$

$$\left.\frac{N^L_{H^+}}{x_{H^+} + x_{CH3OH}(D^{L\text{-}E}_{H^+/H2O}/D^{L\text{-}E}_{CH3OH/H2O}) + x_{O2}(D^{L\text{-}E}_{H^+/H2O}/D^{L\text{-}E}_{O2/H2O})}\right] +$$

$$\lambda_{H2O} * x_{H2O}\frac{j}{F} \quad (4\text{-}32)$$

$$N^{L}_{H^+} = -\left\{ \frac{C_{TL}}{(x_{CH3OH}/D^{L\text{-}E}_{CH3OH/H+}) + (x_{H2O}/D^{L\text{-}E}_{H^+/H2O}) + (x_{O2}/D^{L\text{-}E}_{H^+/O2})} \right\} \frac{dx_{H^+}}{dz} +$$

$$x_{H^+} \left[\frac{N^{L}_{CH3OH}}{x_{CH3OH} + x_{H2O}(D^{L\text{-}E}_{CH3OH/H^+}/D^{L\text{-}E}_{H^+/H2O}) + x_{O2}(D^{L\text{-}E}_{CH3OH/H^+}/D^{L\text{-}E}_{H^+/O2})} + \right.$$

$$\frac{N^{L}_{O2}}{x_{O2} + x_{CH3OH}(D^{L\text{-}E}_{O2/H^+}/D^{L\text{-}E}_{CH3OH/H^+}) + x_{H2O}(D^{L\text{-}E}_{O2/H^+}/D^{L\text{-}E}_{H^+/H2O})} +$$

$$\left. \frac{N^{L}_{H2O}}{x_{H2O} + x_{CH3OH}(D^{L\text{-}E}_{H^+/H2O}/D^{L\text{-}E}_{CH3OH/H^+}) + x_{O2}(D^{L\text{-}E}_{H^+/H2O}/D^{L\text{-}E}_{O2/H^+})} \right] +$$

$$\left[-Z\,u\,F\,C\,x_{H^+} \frac{d\Phi^{L}}{dz} \right] \qquad (4\text{-}33)$$

$$N^{L}_{CH3OH} = -\left\{ \frac{C_{TL}}{(x_{H2O}/D^{L\text{-}E}_{CH3OH/H2O}) + (x_{O2}/D^{L\text{-}E}_{CH3OH/O2}) + (x_{H^+}/D^{L\text{-}E}_{H^+/CH3OH})} \right\} \frac{dx_{CH3OH}}{dz}$$

$$+ x_{CH3OH} \left[\frac{N^{L}_{H2O}}{x_{H2O} + x_{H^+}(D^{L\text{-}E}_{CH3OH/H2O}/D^{L\text{-}E}_{H^+/CH3OH}) + x_{O2}(D^{L\text{-}E}_{CH3OH/H2O}/D^{L\text{-}E}_{CH3OH/O2})} \right.$$

$$\frac{N^{L}_{O2}}{x_{O2} + x_{H2O}(D^{L\text{-}E}_{O2/CH3OH}/D^{L\text{-}E}_{CH3OH/H2O}) + x_{H^+}(D^{L\text{-}E}_{O2/CH3OH}/D^{L\text{-}E}_{H^+/CH3OH})} +$$

$$\left. \frac{N^{L}_{H^+}}{x_{H^+} + x_{H2O}(D^{L\text{-}E}_{H^+/CH3OH}/D^{L\text{-}E}_{CH3OH/H2O}) + x_{O2}(D^{L\text{-}E}_{H^+/CH3OH}/D^{L\text{-}E}_{O2/CH3OH})} \right]$$

$$+ \frac{x_{CH3OH}}{x_{CH3OH} + x_{H2O}} \lambda_{H2O} \frac{j}{F} \qquad (4\text{-}34)$$

$$N^{L}_{O2} = -\left\{ \frac{C_{TL}}{(x_{CH3OH}/D^{L\text{-}E}_{CH3OH/O2}) + (x_{H2O}/D^{L\text{-}E}_{O2/H2O}) + (x_{H^+}/D^{L\text{-}E}_{H^+/O2})} \right\} \frac{dx_{O2}}{dz} +$$

$$x_{O2} \left[\frac{N^{L}_{CH3OH}}{x_{CH3OH} + x_{H2O}(D^{L\text{-}E}_{CH3OH/O2}/D^{L\text{-}E}_{O2/H2O}) + x_{H^+}(D^{L\text{-}E}_{CH3OH/O2}/D^{L\text{-}E}_{H^+/O2})} + \right.$$

$$\frac{N^{L}_{H^+}}{x_{H^+} + x_{CH3OH}(D^{L\text{-}E}_{O2/H^+}/D^{L\text{-}E}_{CH3OH/O2}) + x_{H2O}(D^{L\text{-}E}_{O2/H^+}/D^{L\text{-}E}_{O2/H2O})} +$$

$$\left. \frac{N^{L}_{H2O}}{x_{H2O} + x_{CH3OH}(D^{L\text{-}E}_{O2/H2O}/D^{L\text{-}E}_{CH3OH/O2}) + x_{H^+}(D^{L\text{-}E}_{O2/H2O}/D^{L\text{-}E}_{O2/H^+})} \right]$$

(4-35)

$$N_{TL} = N^{L}_{H2O} + N^{L}_{CH3OH} + N^{L}_{H^+} + N^{L}_{O2} \qquad (4\text{-}36)$$

4.3 CATHODE CATALYST LAYER

4.3.1 Equations used to model the gas phase in the cathode catalyst layer (CCL)

Table (4-13)

Equations	Equation No.

A) Momentum Transport (Ergun Equation)

$$\frac{dP_{TG}}{dz} = \frac{N_{TG}^2}{\rho_G d_p}\left[\frac{\varepsilon_S}{\varepsilon_G^3}\right]\left\{150\left[\frac{(\varepsilon_S)\,\mu_G}{d_P\, N_{TG}}\right] + 1.75\right\} \qquad (4\text{-}37)$$

B) Mass Transport (Stefan - Maxwell Equations)

$$\frac{dy_{O2}}{dz} = \frac{1}{C_{TG}}\left[\frac{(y_{O2}N^G_{H2O} - y_{H2O}N^G_{O2})}{D^{G\text{-}E}_{O2/H2O}} + \frac{(y_{O2}N^G_{CH3OH} - y_{CH3OH}N^G_{O2})}{D^{G\text{-}E}_{O2/CH3OH}} + \frac{(y_{O2}N^G_{CO2} - y_{CO2}N^G_{O2})}{D^{G\text{-}E}_{CO2/O2}} + \frac{(y_{O2}N^G_{N2} - y_{N2}N^G_{O2})}{D^{G\text{-}E}_{O2/N2}}\right] \qquad (4\text{-}38)$$

$$\frac{dy_{N2}}{dz} = \frac{1}{C_{TG}}\left[\frac{(y_{N2}N^G_{H2O} - y_{H2O}N^G_{N2})}{D^{G\text{-}E}_{N2/H2O}} + \frac{(y_{N2}N^G_{CH3OH} - y_{CH3OH}N^G_{N2})}{D^{G\text{-}E}_{N2/CH3OH}} + \frac{(y_{N2}N^G_{CO2} - y_{CO2}N^G_{N2})}{D^{G\text{-}E}_{CO2/N2}} + \frac{(y_{N2}N^G_{O2} - y_{O2}N^G_{N2})}{D^{G\text{-}E}_{O2/N2}}\right] \qquad (4\text{-}39)$$

$$\frac{dy_{H2O}}{dz} = \frac{1}{C_{TG}}\left[\frac{(y_{H2O}N^G_{CH3OH} - y_{CH3OH}N^G_{H2O})}{D^{G\text{-}E}_{CH3OH/H2O}} + \frac{(y_{H2O}N^G_{CO2} - y_{CO2}N^G_{H2O})}{D^{G\text{-}E}_{CO2/H2O}} + \frac{(y_{H2O}N^G_{O2} - y_{O2}N^G_{H2O})}{D^{G\text{-}E}_{O2/H2O}} + \frac{(y_{H2O}N^G_{N2} - y_{N2}N^G_{H2O})}{D^{G\text{-}E}_{N2/H2O}}\right] \qquad (4\text{-}40)$$

$$\frac{dy_{CO2}}{dz} = \frac{1}{C_{TG}}\left[\frac{(y_{CO2}N^{G}_{H2O} - y_{H2O}N^{G}_{CO2})}{D^{G\text{-}E}_{CO2/H2O}} + \frac{(y_{CO2}N^{G}_{CH3OH} - y_{CH3OH}N^{G}_{CO2})}{D^{G\text{-}E}_{CO2/CH3OH}} + \frac{(y_{CO2}N^{G}_{O2} - y_{O2}N^{G}_{CO2})}{D^{G\text{-}E}_{CO2/O2}} + \frac{(y_{CO2}N^{G}_{N2} - y_{N2}N^{G}_{CO2})}{D^{G\text{-}E}_{CO2/N2}}\right] \quad (4\text{-}41)$$

$$\frac{dy_{CH3OH}}{dz} = \frac{1}{C_{TG}}\left[\frac{(y_{CH3OH}N^{G}_{H2O} - y_{H2O}N^{G}_{CH3OH})}{D^{G\text{-}E}_{CH3OH/H2O}} + \frac{(y_{CH3OH}N^{G}_{CO2} - y_{CO2}N^{G}_{CH3OH})}{D^{G\text{-}E}_{CO2/CH3OH}} + \frac{(y_{CH3OH}N^{G}_{O2} - y_{O2}N^{G}_{CH3OH})}{D^{G\text{-}E}_{CH3OH/O2}} + \frac{(y_{CH3OH}N^{G}_{N2} - y_{N2}N^{G}_{CH3OH})}{D^{G\text{-}E}_{CH3OH/N2}}\right] \quad (4\text{-}42)$$

$$y_{H2O} = \frac{(P^{SAT})_{H2O}}{P_{TG}} x_{H2O} \quad (4\text{-}43)$$

$$y_{CH3OH} = \frac{(P^{SAT})_{CH3OH}}{P_{TG}} x_{CH3OH} \quad (4\text{-}44)$$

$$y_{CO2} = 1 - y_{H2O} - y_{CH3OH} - y_{O2} - y_{N2} \quad (4\text{-}45)$$

$$(R_{H2O})^{VAP} = \frac{dN^{G}_{H2O}}{dz} \quad (4\text{-}46)$$

$$(R_{CH3OH})^{VAP} = \frac{dN^{G}_{CH3OH}}{dz} \quad (4\text{-}47)$$

$$(R_{O2})^{C\text{-}RX} = \frac{dN^{G}_{O2}}{dz} \quad (4\text{-}48)$$

$$(R_{CO2})^{C\text{-}MP} = \frac{dN^{G}_{CO2}}{dz} \quad (4\text{-}49)$$

$$N_{TG} = N_{CO2} + N^{G}_{CH3OH} + N^{G}_{H2O} + N^{G}_{O2} + N^{G}_{N2} \quad (4\text{-}50)$$

4.3.2 Equations used to model the liquid phase in the cathode catalyst layer (CCL)

Table (4-14)

Equations	Equation No.

A) Momentum Transport (Ergun equation)

$$\frac{dP_{TL}}{dz} = \frac{N_{TL}^2}{\rho_L d_p}\left[\frac{\varepsilon_S}{\varepsilon_L^3}\right]\left\{150\left[\frac{(\varepsilon_S)\,\mu_L}{d_P\, N_{TL}}\right] + 1.75\right\} - \rho_{H^+} n_{EQ} F \frac{d\Phi_L}{dz} \qquad (4\text{-}51)$$

B) Mass transport (Fluxes from Stefan - Maxwell Equations)

$$N^L_{H2O} = -\left[\frac{C_{TL}}{(x_{CH3OH}/D^{L\text{-}E}_{CH3OH/H2O}) + (x_{O2}/D^{L\text{-}E}_{O2/H2O}) + (x_{H^+}/D^{L\text{-}E}_{H^+/H2O})}\right]\frac{dx_{H2O}}{dz} +$$

$$x_{H2O}\left[\frac{N^L_{CH3OH}}{x_{CH3OH} + x_{O2}(D^{L\text{-}E}_{CH3OH/H2O}/D^{L\text{-}E}_{O2/H2O}) + x_{H^+}(D^{L\text{-}E}_{CH3OH/H2O}/D^{L\text{-}E}_{H^+/H2O})} +\right.$$

$$\frac{N^L_{O2}}{x_{O2} + x_{CH3OH}(D^{L}_{O2/H2O}/D^{L}_{CH3OH/H2O}) + x_{H^+}(D^{L}_{O2/H2O}/D^{L}_{H^+/H2O})} +$$

$$\left.\frac{N^L_{H^+}}{x_{H^+} + x_{CH3OH}(D^{L\text{-}E}_{H^+/H2O}/D^{L\text{-}E}_{CH3OH/H2O}) + x_{O2}(D^{L\text{-}E}_{H^+/H2O}/D^{L\text{-}E}_{O2/H2O})}\right] +$$

$$\lambda_{H2O} * x_{H2O}\frac{j}{F} \qquad (4\text{-}52)$$

$$N^{L}_{H^+} = -\left\{\frac{C_{TL}}{(x_{CH3OH}/D^{L\text{-}E}_{CH3OH/H+}) + (x_{H2O}/D^{L\text{-}E}_{H^+/H2O}) + (x_{O2}/D^{L\text{-}E}_{H^+/O2})}\right\}\frac{dx_{H^+}}{dz} +$$

$$x_{H^+}\left[\frac{N^{L}_{CH3OH}}{x_{CH3OH} + x_{H2O}(D^{L\text{-}E}_{CH3OH/H^+}/D^{L\text{-}E}_{H^+/H2O}) + x_{O2}(D^{L\text{-}E}_{CH3OH/H^+}/D^{L\text{-}E}_{H^+/O2})} +\right.$$

$$\frac{N^{L}_{O2}}{x_{O2} + x_{CH3OH}(D^{L\text{-}E}_{O2/H^+}/D^{L\text{-}E}_{CH3OH/H^+}) + x_{H2O}(D^{L\text{-}E}_{O2/H^+}/D^{L\text{-}E}_{H^+/H2O})} +$$

$$\left.\frac{N^{L}_{H2O}}{x_{H2O} + x_{CH3OH}(D^{L\text{-}E}_{H^+/H2O}/D^{L\text{-}E}_{CH3OH/H^+}) + x_{O2}(D^{L\text{-}E}_{H^+/H2O}/D^{L\text{-}E}_{O2/H^+})}\right] +$$

$$\left[-Z\,u\,F\,C\,x_{H^+}\frac{d\Phi^{L}}{dz}\right] \qquad (4\text{-}53)$$

$$N^{L}_{CH3OH} = -\left\{\frac{C_{TL}}{(x_{H2O}/D^{L\text{-}E}_{CH3OH/H2O}) + (x_{O2}/D^{L\text{-}E}_{CH3OH/O2}) + (x_{H^+}/D^{L\text{-}E}_{H^+/CH3OH})}\right\}\frac{dx_{CH3OH}}{dz}$$

$$+ x_{CH3OH}\left\{\frac{N^{L}_{H2O}}{x_{H2O} + x_{H^+}(D^{L\text{-}E}_{CH3OH/H2O}/D^{L\text{-}E}_{H^+/CH3OH}) + x_{O2}(D^{L\text{-}E}_{CH3OH/H2O}/D^{L\text{-}E}_{CH3OH/O2})} +\right.$$

$$\frac{N^{L}_{O2}}{x_{O2} + x_{H2O}(D^{L\text{-}E}_{O2/CH3OH}/D^{L\text{-}E}_{CH3OH/H2O}) + x_{H^+}(D^{L\text{-}E}_{O2/CH3OH}/D^{L\text{-}E}_{H^+/CH3OH})} +$$

$$\left.\frac{N^{L}_{H^+}}{x_{H^+} + x_{H2O}(D^{L\text{-}E}_{H^+/CH3OH}/D^{L\text{-}E}_{CH3OH/H2O}) + x_{O2}(D^{L\text{-}E}_{H^+/CH3OH}/D^{L\text{-}E}_{O2/CH3OH})}\right] +$$

$$\frac{x_{CH3OH}}{x_{CH3OH} + x_{H2O}}\lambda_{H2O}\frac{j}{F} \qquad (4\text{-}54)$$

$$N^{L}_{O2} = -\left\{ \frac{C_{TL}}{(x_{CH3OH}/D^{L\text{-}E}_{CH3OH/O2}) + (x_{H2O}/D^{L\text{-}E}_{O2/H2O}) + (x_{H^+}/D^{L\text{-}E}_{H^+/O2})} \right\} \frac{dx_{O2}}{dz} +$$

$$x_{O2} \left[\frac{N^{L}_{CH3OH}}{x_{CH3OH} + x_{H2O}(D^{L\text{-}E}_{CH3OH/O2}/D^{L\text{-}E}_{O2/H2O}) + x_{H^+}(D^{L\text{-}E}_{CH3OH/O2}/D^{L\text{-}E}_{H^+/O2})} + \right.$$

$$\frac{N^{L}_{H^+}}{x_{H^+} + x_{CH3OH}(D^{L\text{-}E}_{O2/H^+}/D^{L\text{-}E}_{CH3OH/O2}) + x_{H2O}(D^{L\text{-}E}_{O2/H^+}/D^{L\text{-}E}_{O2/H2O})} +$$

$$\left. \frac{N^{L}_{H2O}}{x_{H2O} + x_{CH3OH}(D^{L\text{-}E}_{O2/H2O}/D^{L\text{-}E}_{CH3OH/O2}) + x_{H^+}(D^{L\text{-}E}_{O2/H2O}/D^{L\text{-}E}_{O2/H^+})} \right]$$

(4-55)

$$N_{TL} = N^{L}_{H2O} + N^{L}_{CH3OH} + N^{L}_{H^+} + N^{L}_{O2} \quad (4\text{-}56)$$

$$x_{CH3OH} = 1 - x_{H2O} - x_{H^+} - x_{O2} \quad (4\text{-}57)$$

$$\frac{dN^{L}_{H2O}}{dz} + (R_{H2O})^{VAP} - (R_{H2O})^{C\text{-}RX} - (R_{H2O})^{C\text{-}MP} = 0 \quad (4\text{-}58)$$

$$\frac{dN^{L}_{CH3OH}}{dz} + (R_{CH3OH})^{VAP} + (R_{CH3OH})^{C\text{-}MP} = 0 \quad (4\text{-}59)$$

$$\frac{dN^{L}_{H^+}}{dz} + (R_{H^+})^{C\text{-}RX} = 0 \quad (4\text{-}60)$$

4.4 CATHODE BACKING LAYER

4.4.1 Equations used to model the gas phase in the cathode-backing layer (CBL)

Table (4-15)

Equations	Equation No.
A) Momentum Transport (Ergun Equation)	
$\frac{dP_{TG}}{dz} = \frac{N_{TG}^2}{\rho_G d_p} \left[\frac{\varepsilon_S}{\varepsilon_G^3}\right] \left\{150 \left[\frac{(\varepsilon_S)\,\mu_G}{d_P\, N_{TG}}\right] + 1.75\right\}$	(4-61)
B) Mass Transport (Stefan - Maxwell Equations)	
$\frac{dy_{O2}}{dz} = \frac{1}{C_{TG}} \left[\frac{(y_{O2} N^G_{H2O} - y_{H2O} N^G_{O2})}{D^{G\text{-}E}_{O2/H2O}} + \frac{(y_{O2} N^G_{CO2} - y_{CO2} N^G_{O2})}{D^{G\text{-}E}_{O2/CO2}} + \frac{(y_{O2} N^G_{N2} - y_{N2} N^G_{O2})}{D^{G\text{-}E}_{N2/O2}}\right]$	(4-62)
$\frac{dy_{N2}}{dz} = \frac{1}{C_{TG}} \left[\frac{(y_{N2} N^G_{H2O} - y_{H2O} N^G_{N2})}{D^{G\text{-}E}_{N2/H2O}} + \frac{(y_{N2} N^G_{CO2} - y_{CO2} N^G_{N2})}{D^{G\text{-}E}_{N2/CO2}} + \frac{(y_{N2} N^G_{O2} - y_{O2} N^G_{N2})}{D^{G\text{-}E}_{O2/N2}}\right]$	(4-63)

$$\frac{dy_{H2O}}{dz} = \frac{1}{C_{TG}} \left[\frac{(y_{H2O} N^{G}_{O2} - y_{O2} N^{G}_{H2O})}{D^{G\text{-}E}_{O2/H2O}} + \frac{(y_{H2O} N^{G}_{CO2} - y_{CO2} N^{G}_{H2O})}{D^{G\text{-}E}_{CO2/H2O}} + \frac{(y_{H2O} N^{G}_{N2} - y_{N2} N^{G}_{H2O})}{D^{G\text{-}E}_{N2/H2O}} \right] \quad (4\text{-}64)$$

$$\frac{dy_{CO2}}{dz} = \frac{1}{C_{TG}} \left[\frac{(y_{CO2} N^{G}_{H2O} - y_{H2O} N^{G}_{CO2})}{D^{G\text{-}E}_{CO2/H2O}} + \frac{(y_{CO2} N^{G}_{O2} - y_{O2} N^{G}_{CO2})}{D^{G\text{-}E}_{CO2/O2}} + \frac{(y_{CO2} N^{G}_{N2} - y_{N2} N^{G}_{CO2})}{D^{G\text{-}E}_{CO2/N2}} \right] \quad (4\text{-}65)$$

$$y_{H2O} = \frac{(P^{SAT})_{H2O}}{P_{TG}} x_{H2O} \quad (4\text{-}66)$$

$$y_{CO2} = 1 - y_{H2O} - y_{O2} - y_{N2} \quad (4\text{-}67)$$

$$(R_{H2O})^{VAP} = \frac{dN^{G}_{H2O}}{dz} \quad (4\text{-}68)$$

$$N_{TG} = N_{CO2} + N^{G}_{H2O} + N^{G}_{O2} + N^{G}_{N2} \quad (4\text{-}69)$$

4.4.2 Equations used to model the liquid phase in the cathode-backing layer (CBL)

Table (4-16)

Equations	Equation No.
A) Momentum Transport (Ergun equation)	
$\frac{dP_{TL}}{dz} = \frac{N_{TL}^2}{\rho_L d_p} \left[\frac{\varepsilon_S}{\varepsilon_L^3}\right] \left\{150 \left[\frac{(\varepsilon_S)\,\mu_L}{d_P\, N_{T\,L}}\right] + 1.75\right\}$	(4-70)
B) Mass Transport (Fick's Law Equations)	
$N_{TL} = N^L_{H2O}$ Where $x_{H2O} = 1$	(4-71)
$(R_{H2O})^{VAP} = \frac{dN^L_{H2O}}{dz}$	(4-72)

4.5 Equations used to predict the transition pore diameter and the fractional pore volume filled with liquid and gas in (ACL, CCL, and CBL)

Table (4-17)

Equations	Equation No.
A) Young and Laplace Equation	
$P_{TL} - P_{TG} = \frac{-4\,\sigma \cos\theta}{d_{p\,(G/L)}}$	(4-73)
B) Pore volume correlations for liquid and gas	
1) $d_{p\,(G/L)} < 1 * 10^{-8}$	
$\varepsilon_G = 0.52 - 2.6444 * (1\text{-}\exp(0.000001 - (d_{p\,(G/L)} * 10^{6})))$	(4-74)
$\varepsilon_L = \varepsilon_V - \varepsilon_G$	
2) $d_{p\,(G/L)} > 1 * 10^{-4}$	
$\varepsilon_G = 0.018632 * \exp(1\text{-}0.01 * (-d_{p\,(G/L)} * 10^{6}))$	(4-75)
$\varepsilon_L = \varepsilon_V - \varepsilon_G$	
3) $1*10^{-8} < d_{p\,(G/L)} < 1*10^{-4}$	
$\varepsilon_G = 0.20613 * \exp(((d_{p\,(G/L)} * 10^{6})^{16.24}) / (-3.949\ e{+}27)) + 0.47129 / ((d_{p\,(G/L)}) * 10^{6})^{0.061144}) - 0.337$	(4-76)
$\varepsilon_L = \varepsilon_V - \varepsilon_G$	

$D^{G\text{-}E}{}_{(i/j)} = D^{G}{}_{(i/j)} * \varepsilon_G$

$D^{G\text{-}L}{}_{(i/j)} = D^{L}{}_{(i/j)} * \varepsilon_L$

4.6 Boundary Conditions

4.6.1 Anode backing layer, anode catalyst layer interface (ABL/ACL):

$N^{G}_{CO2} = j / 6F$

$N^{L}_{H^+} = 0.0$

$N^{G}_{O2} = N^{L}_{O2} = 0.0$

4.6.2 Anode catalyst layer, Electrolyte layer interface (ACL / ELL):

$N^{G}_{CO2} = N^{L}_{CO2} = 0.0$

$N_{H^+} = j / F$

$P_{O2\,(ACL\,/\,ELL)} = (K_H)_{O2} * C_{TG} * X_{O2\,(ELL\,/\,ACL)}$

4.6.3 Electrolyte layer, Cathode catalyst layer interface (ELL / CCL):

$N^{G}_{O2} = 0.0$

$N^{G}_{N2} = N^{L}_{N2} = 0.0$

$N_{H^+} = j / F$

$N^{G}_{CO2} = 0.0$

$X_{O2\,(ELL\,/\,CCL)} = P_{O2\,(CCL\,/\,ELL)} / (K_H)_{O2} * C_{TG}$

4.6.4 Cathode catalyst layer, Cathode backing layer interface (CCL / CBL):

$N^{G}_{CH3OH} = N^{L}_{CH3OH} = 0.0$

$N^{G}_{CO2} = j / F$

$N^{L}_{H^+} = 0.0$

4.6.5 Cathode backing layer, cathode channel interface (CBL / CC):

$T = 40\ ^{\circ}C$

$$y_{H2O} = \frac{(P^{SAT})_{H2O}}{P_{TG}} \; x_{H2O}$$

$y_{CO2} = 1 - y_{H2O} - y_{O2} - y_{N2}$

$X_{H2O} = 1$

$N^{G}_{H2O} = y_{H2O} * N_{TG}$

$N^{G}_{CH3OH} = y_{CH3OH} * N_{TG}$

$N_{O2} = j / F + (N_{O2})^{MP}$

$N_{TG} = N^{G}_{CO2} + N^{G}_{H2O} + N^{G}_{N2} + N^{G}_{O2}$

List of symbols

$D_{E:}$ Effective diffusivity of reactant within agglomerates ($m^2\ s^{-1}$)

$D^{G-E}{}_{CO2\,/\,O2:}$ The effective binary molecular diffusion coefficient for carbon dioxide and oxygen vapor ($m^2\ s^{-1}$)

$D^{G-E}{}_{O2\,/\,H2O:}$ The effective binary molecular diffusion coefficient for water and oxygen vapor ($m^2\ s^{-1}$)

$D^{G-E}{}_{CH3OH\,/\,O2:}$ The effective binary molecular diffusion coefficient for methanol and oxygen vapor ($m^2\ s^{-1}$)

$D^{G-E}{}_{N2\,/\,O2\ :}$ The effective binary molecular diffusion coefficient for nitrogen and oxygen vapor ($m^2\ s^{-1}$)

$D^{G-E}{}_{N2\,/\,H2O\ :}$ The effective binary molecular diffusion coefficient for nitrogen and water vapor ($m^2\ s^{-1}$)

$D^{G-E}{}_{CH3OH\,/\,N2:}$ The effective binary molecular diffusion coefficient for methanol and nitrogen vapor ($m^2\ s^{-1}$)

$D^{G-E}{}_{N2\,/\,CO2:}$ The effective binary molecular diffusion coefficient for nitrogen and carbon dioxide vapor ($m^2\ s^{-1}$)

$D^{L-E}{}_{O2/\,H2O:}$ The effective binary molecular diffusion coefficient for oxygen and water liquid ($m^2\ s^{-1}$)

$D^{L-E}{}_{H^+\,/\,CH3OH:}$ The effective binary molecular diffusion coefficient for protons methanol liquid ($m^2\ s^{-1}$)

$D^{L-E}{}_{H^+\,/\,H2O:}$ The effective binary molecular diffusion coefficient for protons and water liquid ($m^2\ s^{-1}$)

$D^{L-E}{}_{O2\,/\,CH3OH:}$ The effective binary molecular diffusion coefficient for oxygen and methanol liquid ($m^2\ s^{-1}$)

$D^{L-E}{}_{O2\,/\,H^+:}$ The effective binary molecular diffusion coefficient for oxygen and protons liquid ($m^2\ s^{-1}$)

$K_{H:}$ Henry's law constant for oxygen

$K_{F,\,CH:}$ Forward reaction constant.

$N^{L}{}_{H^+:}$ Flux of protons in liquid phase (mol $m^{-2}\ s^{-1}$)

$N^{L}{}_{O2:}$ Flux of oxygen in liquid phase (mol $m^{-2}\ s^{-1}$)

N^{G}_{O2}: Flux of oxygen in gas phase (mol m^{-2} s^{-1})

N^{G}_{N2} : Flux of nitrogen in gas phase (mol m^{-2} s^{-1})

P_{O2}: Oxygen partial pressure (kPa)

R_L: Resistance of the liquid phase (Ohm)

R_S: Resistance of the solid phase (Ohm)

$(R^{G}_{CO2})^{A\text{-}RX}$: Volumetric reaction rate for carbon dioxide in the ACL (mol m^{-3} s^{-1})

$(R_{CO2})^{C\text{-}MP}$: Volumetric reaction rate for carbon dioxide in the cathode catalyst layer of mixed potential (mol m^{-3} s^{-1})

$(R^{L}_{CH3OH})^{A\text{-}RX}$: Volumetric reaction rate for methanol in the ACL (mol m^{-3} s^{-1})

$(R^{L}_{H^+})^{A\text{-}RX}$: Volumetric reaction rate for protons in the ACL (mol m^{-3} s^{-1})

$(R^{L}_{H2O})^{A\text{-}RX}$: Volumetric reaction rate for water in the ACL (mol m^{-3} s^{-1})

$(R^{L}_{H2O})^{C\text{-}RX}$: Volumetric reaction rate for water in the CCL (mol m^{-3} s^{-1})

$(R^{G}_{O2})^{C\text{-}RX}$: Volumetric reaction rate for carbon oxygen in the CCL (mol m^{-3} s^{-1})

$(R_{O2})^{VAP}$: Rate of vaporization for oxygen (mol m^{-3} s^{-1})

$(R_{AG})^{RX}$: Reaction rate in one agglomerate = moles reactant consumed in one agglomerate / unit time (mol s^{-1})

r_{AG}: Coordinate within agglomerate (measured from centre)

R: Ideal gas constant (8.314 J mol^{-1} K^{-1})

SAV: Surface area of the catalyst per unit volume in the catalyst layer (m^2 face area m^{-3})

T: Temperature (K)

x_{H^+}: Protons mole fraction in the liquid phase

x_{O2}: Oxygen mole fraction in the liquid phase

y_{N2}: Nitrogen mole fraction in the gas phase

y_{O2}: Oxygen mole fraction in the gas phase

u: Mobility of the species (cm^2 mol J^{-1} s^{-1})

Z: Charge number of the species

λ_{H2O}: Electro-osmotic drag coefficient of water

α_A: Anodic transfer coefficient for the reaction

α_C: Cathodic transfer coefficient for the reaction

η_A: Local over potential for the anode side (volts)

η_C : Local over potential for the cathode side (volts)

$\Delta\Phi_{EQ}$: Equilibrium potential for methanol oxidation reaction

ρ_{H^+}: Density of protons (gm cm^{-3})

Φ_L: Electrical potential of the liquid phase (volts)

Φ_S: Electrical potential of the solid phase (volts)

ε_G: Pore volume filled with gas with respect to the total cumulative void (pore) volume for E-TEK carbon paper (m^3 m^{-3} total)

ε_L: Pore volume filled with gas with respect to the total cumulative void (pore) volume for E-TEK carbon paper (m^3 m^{-3} total)

ε_V: The cumulative pore volume of the ABL (m^3 void / m^3 layer)

CHAPTER FIVE

Conclusions

A one-dimensional mathematical model of the anode backing layer of a DMFC operating at 40°C has been developed. Both gas and liquid phases have been described. The pore size distribution was also described. The relative effects of diffusion and convection transport mechanisms were identified in both phases. The phenomena in the ABL at different conditions such as current density and methanol molarity were identified. The volumetric fractions of the ABL filled with gas and with liquid were among the variables investigated. The relationships between the gas bubble diameters, the transition pore diameter between liquid filled and gas filled pores, the pressure difference between the gas phase and the liquid phase, and the volumetric fractions of the ABL filled with liquid and with gas were identified.

The results of the model showed that although pressure drops across the ABL for gas and liquid are small, the pressure gradients are large. The transport of all species occurs by both diffusion and convection mechanisms. Diffusion is the dominant mechanism for the following fluxes: (a) Methanol vapor from the AC to the ACL, (b) Water vapor from the AC to the ACL. Convection is the dominant for the following fluxes: (a) Liquid methanol from the AC to the ACL, (b) Liquid water from the AC to the ACL and, (c) CO_2 gas from the ACL to the AC. Increasing the current density causes an increase in the pressure gradient which causes convection to increase relative to diffusion. The fraction of the ABL volume filled with gas increased when more CO_2 was produced at greater current densities and therefore the total gas flux increased. Increasing contact angle increases the pore volume filled with gas.

CHAPTER SIX

Contributions to knowledge

This thesis describes the first detailed mechanistic two-phase mathematical model of the anode-backing layer (ABL) in a low temperature DMFC. The movements of all species were described in terms of both diffusion and convection phenomena. Two values of pressure were determined at each position, one for the liquid phase and one for the gas phase. The gas pressure was higher than the liquid pressure. The liquid and gas phases moved counter-currently. Values for the concentrations of all species were calculated.

This is the first time that the relative contributions of diffusion and convection mechanisms to mass transport in a low-temperature DMFC have been identified. Changes in the values of the absolute pressures and concentrations across the thickness of the anode-backing layer were small. However, the pressure gradients and concentration gradients that cause diffusion and convection across the thickness of the ABL (100 μm) were high. Total gas flux, total liquid flux, and the flux of each species in both phases were calculated.

This is the first time that the proportion of each species being transported in the gas phase has been quantitatively compared to that transported in the liquid phase, for a low-temperature DMFC. For example, it was shown that that most of the methanol was transported in the liquid phase.

This is the first time that the porosity of an anode-backing layer was described by using a pore size distribution for the carbon paper that is the major constituent of an anode-backing layer. The fractions of pore volume filled with liquid and filled with gas were calculated for various diameters of carbon dioxide bubbles, and for various wet contact angles inside the pores. The results showed that the anode-backing layer should be hydrophilic and that there is no need to add Teflon, as is required for the cathode-backing layer.

APPENDICES

The computer Code for anode backing layer (ABL)

```
Format long e
Format compact


for i = 1
%Tch=temperature in the anode channel [k]
Tch=313.16;
T (i) =Tch;

MW_CO2 = 44.01;
MW_H2O = 18.016;
MW_CH3OH = 32.04;

%ptgch=total gas pressure [Pa] in the anode channel
%ptLch=total liquid pressure [Pa] in the anode channel

Ptgch= (104874.15);
PtLch= (101325);
ptg(i)= Ptgch;
ptL(i)= PtLch;

%xwch = mol fraction of water vapour in the anode channel
 xwch=0.98158;

%xmch = mol fraction of methanol vapour in the anode channel
xmch=0.01842;

%xw (i) = mol fraction H2O in section i
xw (i) =xwch;
%xm (i) = mol fraction CH3OH in section i
xm(i)=xmch;

%CDch = current density in the anode channel [mA/cm2]
%CD = current density [A/m2]

CDch=2000;
CD=CDch;

%NCO2 = CO2 flux [gmol/m2 s]
%NCO2= (CD [A/m2] *[Coul/A s])/ (6[g-equiv/gmol CH3OH] *96485[Coul/g-equiv]

NCO2 (i) =-CD/ (6*96485);

%THabl = thickness of the anode backing layer [cm]
%define the thickness, dz, of a section in the anode backing layer
THabl=100*10^-6;
```

```
dz= THabl/100;

%saturated vapour pressures [Pa]

PsatH2O (i) = 1.8038e+11*exp (-5340.5/T (i));
PsatCH3OH (i) = 1.14203e+11*exp (-4701.39/T (i));

%Raoult's law to calculate the mole fractions

yH2O (i) = (PsatH2O (i)*xw (i))/ptg (i);
yCH3OH (i) = (PsatCH3OH (i)*(1-xw (i)))/ptg (i);
yCO2 (i) = 1 - yH2O (i) - yCH3OH (i);

%ep_s = solid volumetric fraction in an ideally packed assembly of spheres
%ep_v = cumulative void (pore) volume curve for E-TEK carbon paper
%ep_g = fractional volume filled with gas
%ep_L = fractional volume filled with liquid
%dpGL = transition pore diameter
ep_v(i) = 0.52;
ep_s(i) = 1-ep_v(i);
ep_g(i) = 0.25;
ep_L(i) = ep_v(i) - ep_g(i);
dpGL(i)=0.0000317;

% Ngt = total gas flux [gmol/(m^2 s)]
%NgH2O= the flux of water in the gas phase [gmol/ (m^2 s)]
%NgCH3OH = the flux of methanol in the gas phase [gmol/ (m^2 s)]
Ntg(i) =NCO2(i)/yCO2(i);
NgH2O (i) =yH2O (i)*Ntg(i);
NgCH3OH (i) =yCH3OH (i)*Ntg(i);

% Liquid H2O flux = H2O for Rx + H2O for electro-osmotic drag + H2O for vapourization
%from liquid to gas

NLH2O (i) = CD/ (6*96485) + (3*xw (i)*CD)/96485 + Ntg(i)*yH2O(i);
NLCH3OH (i) = CD/ (6*96485) + (3*xm(i)*CD)/96485 + Ntg(i)*yCH3OH(i);
NtL(i) = NLH2O(i) + NLCH3OH(i);

%Vden_mix =P/RT = density of vapour phase mixture
%units Vden_mix {Pa*1N/ (m^2Pa)}/ [{J/ (gmol K)}*1 (N m)/J* K] =gmol/m^3

Vden_mix(i) = ptg(i)/(8.314 *T(i));

%d_ag = 1 micron = 10^-6 [m] = agglomerate diameter

d_ag(i)=1*10^-6;
```

```
end

 for i=2:101

ptg (i)=ptg(i-1);
ptL(i)=ptL(i-1);
T (i) =T (i-1);
xw (i) = xw (i-1);
xm(i)=xm(i-1);
xwcal (i) =xw (i);
yCO2 (i) =yCO2 (i-1);
yH2O (i) =yH2O (i-1);
yCH3OH (i) =yCH3OH (i-1);
d_ag(i)=d_ag(i-1);
Ntg(i) = Ntg(i-1);
NCO2 (i) =NCO2 (i-1);
NgH2O (i) =NgH2O (i-1);
NgCH3OH (i) =NgCH3OH (i-1);
ep_s(i) = ep_s(i-1);
ep_v(i) = ep_v(i-1);
ep_g(i) = ep_g(i-1);
ep_L(i)=ep_L(i-1);
ep_gcal (i) = ep_g(i);
ep_Lcal (i) =ep_L(i);
dpGL (i) =dpGL (i-1);
Vden_mix (i) =Vden_mix (i-1);
R=8.314;

%Diff coeff units = [m^2/s)

DifH2O_CO2 (i) = (9.8879e-06*(T (i) ^1.75))/10000;
DifCO2_CH3OH (i) = (6.2638e-06*(T (i) ^1.75))/10000;
DifH2O_CH3OH (i) = (9.98e-06*(T (i) ^1.75))/10000;
PsatH2O (i) = 1.8038e+11*exp (-5340.5/T (i));
PsatCH3OH (i) = 1.14203e+11*exp (-4701.39/T (i));

%Vvisc = vapour phase viscosity of a component or mixture [gmol/(m s)]

Vvisc_H2O (i) = (1.32158e-06*T (i) ^2 + 2.00505e-02*T (i) - 0.70217)*10^-4;
Vvisc_CH3OH (i) = (-7.45113e-07*T (i) ^2 + 1.09785e-02*T (i) - 0.162809)*10^-4;
Vvisc_CO2 (i) = (-2.7812e-06*T (i) ^2 + 1.17024e-02*T (i) + 0.204435)*10^-4;
vm1 (i) = (yCO2 (i)*Vvisc_CO2 (i))/ (yH2O (i)* (MW_H2O/MW_CO2) ^0.5 +
          yCH3OH (i)*(MW_CH3OH/MW_CO2) ^0.5);
vm2 (i) = (yH2O (i)*Vvisc_H2O (i))/ (yCO2 (i)* (MW_CO2/MW_H2O) ^0.5 +
          yCH3OH (i)*(MW_CH3OH/MW_H2O) ^0.5);
```

```
vm3 (i) = (yCH3OH (i)*Vvisc_CH3OH (i))/ (yH2O (i)*(MW_H2O/MW_CH3OH) ^0.5 +
          yCO2 (i)*(MW_CO2/MW_CH3OH) ^0.5);

Vvisc_mix(i) = vm1(i) + vm2(i) + vm3(i);

MWav(i) = yCO2(i)*44.01 + yH2O(i)*18.016 + yCH3OH(i)*32.04;

%units MWav = [{gmol(i)/gmol_mix}*g(i)/gmol(i) = g_mix/gmol_mix]
%Ergun equation calculation to find ptg(i)
%Ptg(i) = Ptg(i-1) - dz*( a1*Ntg + a2*(Ntg^2) )
%Ptg(i) [Pa = N/m^2 = (kg m/s^2)/m^2 = kg/(s^2 m) ]

%a1*Ntg= [{(150*Ntg*(ep_s^2)*Vvisc_mix) /
          (den_mix*(d_ag^2)*(ep_g^3)}]*(MWav/1000)

%units a1*Ntg= [{gmol/ (m^2 s)}*{gmol/ (m s)}] / [(gmol/m^3)*m^2)]*
                (g/gmol)*(1 kg/1000g)

%units a1*Ntg = (kg / (m^2 s^2)    dz*a1*Ntg = Pa

%a1= [{((150*ep_s^2)*Vvisc_mix)/ (den_mix*(d_ag^2)*(ep_g^3)}] *(MWav/1000)

%a2*Ntg^2= [(1.75*Ntg^2*ep_s) / {den_mix*d_ag*(ep_g^3)}]*(MWav/1000)

%units a2*Ntg^2 = [{gmol/ (m^2 s)} ^2/ {m*gmol/m^3}]*(g/gmol)*(1 kg/1000g)
%               = kg/ (m^2s^2) dz*a2*Ntg^2 = Pa

%a2= [(1.75*ep_s) / {den_mix*d_ag*(ep_g^3)}]*(MWav/1000)

ptg(i)=ptg(i-1)-dz*
       (((150*Vvisc_mix(i)*(ep_s(i))^2*Ntg(i))/(Vden_mix(i)*d_ag(i)^2*ep_gcal(i)^3)+
       (1.75*(ep_s(i))*Ntg(i)^2)/(Vden_mix(i)*d_ag(i)*ep_gcal(i)^3))*MWav(i)/1000);

ptg(i)=(ptg(i)+ptg(i-1))/2;

yH2O (i) = (PsatH2O (i)*xw (i))/ptg(i);
yCH3OH (i) = (PsatCH3OH (i)*(1-xw (i)))/ptg(i);
yCO2 (i) = 1 - yH2O (i) - yCH3OH (i);
CG (i) =ptg(i)/(R*T(i));
DyH2O (i) = (yH2O (i)-yH2O (i-1))/dz;
DyCH3OH (i) = (yCH3OH (i)-yCH3OH (i-1))/dz;
DyCO2 (i) = (yCO2 (i)-yCO2 (i-1))/dz;
DifH2O_CO2 (i) = (9.8879e-06*(T (i) ^1.75))/10000;
DifCO2_CH3OH (i) = (6.2638e-06*(T (i) ^1.75))/10000;
DifH2O_CH3OH (i) = (9.98e-06*(T (i) ^1.75))/10000;
```

```
%use Stefan-Maxwell Eq to find NgH2O (i) and NgCH3OH (i). NgCO2 is known

A1 (i) = ((-CG (i)*ep_gcal (i)*ep_gcal (i)*DifH2O_CH3OH (i)*
       DifH2O_CO2 (i))/ (yCH3OH (i)*ep_gcal (i)*DifH2O_CO2 (i) +
       yCO2 (i)*ep_gcal (i)*DifH2O_CH3OH (i)))*DyH2O (i);

A2 (i) = ((NgCH3OH (i)*ep_gcal (i)*DifH2O_CO2 (i) +NCO2 (i)*ep_gcal (i)*
       DifH2O_CH3OH (i))/ (yCH3OH (i)*ep_gcal (i)*DifH2O_CO2 (i) +yCO2 (i)*
       ep_gcal (i)*DifH2O_CH3OH (i)))*yH2O (i);

NgH2Ocal (i) =A1 (i) + A2 (i);
NgH2Ocal (i) = (NgH2Ocal (i) +NgH2O (i-1))/2;

B1(i)=((-CG(i)*ep_gcal(i)*ep_gcal(i)* DifH2O_CH3OH(i)*
       DifCO2_CH3OH(i))/(yH2O(i)*ep_gcal(i)*DifCO2_CH3OH(i)+
       yCO2 (i)*ep_gcal (i)*DifH2O_CH3OH (i)))*DyCH3OH (i);

B2 (i) = ((NgH2O (i)*ep_gcal (i)*DifCO2_CH3OH (i) +NCO2 (i)*ep_gcal (i)*
       DifH2O_CH3OH (i))/ (yH2O (i)*ep_gcal (i)*DifCO2_CH3OH (i) +yCO2 (i)*
       ep_gcal (i)*DifH2O_CH3OH (i)))*yCH3OH (i);

NgCH3OHcal (i) =B1 (i) + B2 (i);
NgCH3OHcal (i) = (NgCH3OHcal (i) +NgCH3OH (i-1))/2;

Ntgcal(i)=NgH2O(i)+NgCH3OH(i)+NCO2(i);
Ntgcal(i)=(Ntgcal(i)+Ntg(i-1))/2;

   end

for i=2:101

        RDIFF (i) =1;
    While RDIFF (i)>0.000000001

%the while loop adjusts the value of Ntgcal(total gas flux) at position "i" and determines
ptg(total gas pressure)
ep_gguess (i) =ep_gcal (i)
xw_guess(i)=xw(i);
Ntg_guess(i)=Ntgcal(i);
Ntgavg(i)=(Ntg_guess(i)+Ntg(i-1))/2;
Ntg_old(i)=Ntg_guess(i);
NgH2Oavg (i) = (NgH2Ocal (i) +NgH2O (i-1))/2;
NgCH3OHavg (i) = (NgCH3OHcal (i) +NgCH3OH (i-1))/2;
yH2Oavg (i) = (yH2O (i) +yH2O (i-1))/2;
yCH3OHavg (i) = (yCH3OH (i) +yCH3OH (i-1))/2;
yCO2avg (i) =1-yCH3OHavg (i)-yH2Oavg (i);
```

```
ptgavg(i)=(ptg(i)+ptg(i-1))/2;
Vden_mixavg(i) =(ptg(i)+ptg(i-1))/2/(8.314 *T(i));

DifH2O_CO2 (i) = (9.8879e-06*(T (i) ^1.75))/10000;
DifCO2_CH3OH (i) = (6.2638e-06*(T (i) ^1.75))/10000;
DifH2O_CH3OH (i) = (9.98e-06*(T (i) ^1.75))/10000;
PsatH2O (i) = 1.8038e+11*exp (-5340.5/T (i));
PsatCH3OH (i) = 1.14203e+11*exp (-4701.39/T (i));

Vvisc_H2O (i) = (1.32158e-06*T (i) ^2 + 2.00505e-02*T (i) - 0.70217)*10^-4;
Vvisc_CH3OH (i) = (-7.45113e-07*T (i) ^2 + 1.09785e-02*T (i) - 0.162809)*10^-4;
Vvisc_CO2 (i) = (-2.7812e-06*T (i) ^2 + 1.17024e-02*T (i) + 0.204435)*10^-4;

vm11 (i) = (yCO2avg (i)*Vvisc_CO2 (i))/ (yH2Oavg (i)* (MW_H2O/MW_CO2) ^0.5 +
          yCH3OHavg (i)*(MW_CH3OH/MW_CO2) ^0.5);
vm22 (i) = (yH2Oavg (i)*Vvisc_H2O (i))/ (yCO2avg (i)* (MW_CO2/MW_H2O) ^0.5 +
          yCH3OHavg (i)*(MW_CH3OH/MW_H2O) ^0.5);
vm33 (i) = (yCH3OHavg (i)*Vvisc_CH3OH (i))/ (yH2Oavg (i)*
          (MW_H2O/MW_CH3OH)^0.5 + yCO2avg (i)*(MW_CO2/MW_CH3OH) ^0.5);

Vvisc_mixavg(i) = vm11(i) + vm22(i) + vm33(i);
MWav1 (i) = yCO2avg (i)*44.01 + yH2Oavg (i)*18.016 + yCH3OHavg (i)*32.04;

ptg(i)=ptgavg(i)-dz*
      (((150*Vvisc_mixavg(i)*(ep_s(i))^2*Ntgavg(i))/(Vden_mixavg(i)*d_ag(i)^2*
      ep_gcal(i)^3+(1.75*(ep_s(i))*Ntgavg(i)^2)/(Vden_mixavg(i)*d_ag(i)*ep_gcal(i)^3))
      *MWav1(i)/1000);

ptg(i)=(ptg(i)+ptg(i-1))/2;

yH2O (i) = (PsatH2O (i)*xw (i))/ptg(i);
yCH3OH (i) = (PsatCH3OH (i)*(1-xw (i)))/ptg(i);
yCO2 (i) = 1 - yH2O (i) - yCH3OH (i);
CG (i) =ptg(i)/(R*T(i));
DyH2O (i) = (yH2O (i)-yH2O (i-1))/dz;
DyCH3OH (i) = (yCH3OH (i)-yCH3OH (i-1))/dz;
DyCO2 (i) = (yCO2 (i)-yCO2 (i-1))/dz;
DifH2O_CO2 (i) = (9.8879e-06*(T (i) ^1.75))/10000;
DifCO2_CH3OH (i) = (6.2638e-06*(T (i) ^1.75))/10000;
DifH2O_CH3OH (i) = (9.98e-06*(T (i) ^1.75))/10000;

A11 (i) = ((-CG (i)*ep_gcal (i)*ep_gcal (i)*DifH2O_CH3OH (i)*
          DifH2O_CO2(i))/(yCH3OH(i)*ep_gcal(i)*DifH2O_CO2(i)+yCO2(i)*ep_gcal(i)*
          DifH2O_CH3OH(i)))*DyH2O(i);

A22 (i) = ((NgCH3OHavg (i)*ep_gcal (i)*DifH2O_CO2 (i) +NCO2 (i)*ep_gcal (i)*
```

```
        DifH2O_CH3OH(i))/(yCH3OH(i)*ep_gcal(i)*DifH2O_CO2(i)+yCO2(i)*ep_gcal(i)
        *DifH2O_CH3OH(i)))*yH2O(i);

NgH2Ocal (i) =A11 (i) + A22 (i);
NgH2Ocal (i) = (NgH2Ocal (i) +NgH2O (i-1))/2;

B11(i)=((-CG(i)*ep_gcal(i)*ep_gcal(i)*DifH2O_CH3OH(i)*
        DifCO2_CH3OH(i))/(yH2O(i)*ep_gcal(i)*DifCO2_CH3OH(i)+yCO2(i)*ep_gcal(i)
        *DifH2O_CH3OH(i)))*DyCH3OH(i);

B22 (i) = ((NgH2Oavg (i)*ep_gcal (i)*DifCO2_CH3OH (i) +NCO2 (i)*ep_gcal (i)*
        DifH2O_CH3OH (i))/ (yH2O (i)*ep_gcal (i)*DifCO2_CH3OH (i) +yCO2 (i)*
        ep_gcal (i)*DifH2O_CH3OH (i)))*yCH3OH (i);

NgCH3OHcal (i) =B11 (i) + B22 (i);
NgCH3OHcal (i) = (NgCH3OHcal (i) +NgCH3OH (i-1))/2;

Ntgcal(i)=NgH2Ocal(i)+NgCH3OHcal(i)+NCO2(i);
Ntgcal(i)=(Ntgcal(i)+Ntg(i-1))/2;

DCO2 (i) =NCO2 (i)-(yCO2 (i)*Ntgcal(i));
CCO2 (i) =NCO2 (i)-DCO2 (i);
NCO2 (i) =DCO2 (i) +CCO2 (i);
DgH2O (i) =NgH2Ocal (i)-(yH2O (i)*Ntgcal(i));
CgH2O (i) =NgH2Ocal (i)-DgH2O (i);
NgH2Ocal (i) =DgH2O (i) +CgH2O (i);
DgCH3OH (i) =NgCH3OHcal (i)-(yCH3OH (i)*Ntgcal(i));
CgCH3OH (i) =NgCH3OHcal (i)-DgCH3OH (i);
NgCH3OHcal (i) =DgCH3OH (i) +CgCH3OH (i);
Ntgcal(i)=NgH2Ocal(i)+NgCH3OHcal(i)+NCO2(i);
DIFF (i) =Ntgcal(i)-Ntg_old(i);
RDIFF (i) =abs (DIFF (i)/Ntgcal(i));

Ntgcal(i)=(Ntgcal(i)+Ntg_guess(i))/2;
Ntg_guess(i)=Ntgcal(i);

end

%RH2Ovap = rate at which H2O is added to the gas phase [gmol/ (m3 s)]
%RCH3OHvap = rate of CH3OH evap into the gas phase [gmol/ (m3 s)]

RH2Ovap (i) = (NgH2Ocal (i)-NgH2Ocal (i-1))/dz;
RCH3OHvap (i) = (NgCH3OHcal (i)-NgCH3OHcal (i-1))/dz;

%Lden_H2O = liquid phase denisty [gmol/m3]
Lden_H2O (i) =5.44e+4;
```

```
CL (i) =Lden_H2O (i);

%Lvisc_H2O = liquid phase viscosity [gmol/ (m s)]
Lvisc_H2O (i) =100/ (18.016*(2.1482*(T (i)-281.6) + sqrt(8078.4*(T(i)-281.6)^2))- 120.0);
Lvisc_mix (i) = Lvisc_H2O (i);

%Diff coeff units = [m^2/s)
DifH2O_CH3OHL (i) = (6.1*10^-8*T (i))/10000;

%calculating the liquid fluxes from the rate of vaporization

NLH2O (i) =NLH2O (i-1)-(RH2Ovap (i)*dz);
NLH2O (i) = (NLH2O (i) +NLH2O (i-1))/2;

NLCH3OH (i) =NLCH3OH (i-1)-(RCH3OHvap (i)*dz);
NLCH3OH (i) = (NLCH3OH (i) +NLCH3OH (i-1))/2;

NtL (i) =NLH2O (i) +NLCH3OH (i);

%updating the liquid water mole fraction using Fick's Law

xwcal(i)=(NLH2O(i)*dz-CL(i)*ep_Lcal(i)*DifH2O_CH3OHL(i)*xw(i-1))/(NtL(i)*dz-
        CL(i)*ep_Lcal(i)*DifH2O_CH3OHL(i));

NLH2Ocal (i) =-CL (i)* ep_Lcal (i)* DifH2O_CH3OHL (i)*
                (xwcal (i)-xw (i-1))/dz+xwcal (i)*NtL(i);

NLH2Ocal (i) = (NLH2Ocal (i) +NLH2O (i-1))/2;

NLCH3OHcal (i) =-CL (i)*ep_Lcal (i)*DifH2O_CH3OHL (i)*
                  ((1-xwcal (i))-(1-xw (i-1)))/dz+ (1-xwcal (i))*NtL(i);

NLCH3OHcal (i) = (NLCH3OHcal (i) +NLCH3OH (i-1))/2;

NtLcal (i) =NLCH3OHcal (i) +NLH2Ocal (i);

xwcal (i) = (xwcal (i) +xw (i-1))/2;

%the while loop adjusts the value of xwcal (water mole fraction) at position "i" and
%determines ptL(total gas pressure)

  RDIFF1 (i) =1;

     While RDIFF1 (i)>0.000000001
```

```
xwavg(i)=(xw_guess(i)+xw(i-1))/2;

NLH2Oavg (i) = (NLH2Ocal (i) +NLH2O (i-1))/2;
NLCH3OHavg (i) = (NLCH3OHcal (i) +NLCH3OH (i-1))/2;

NtLavg(i)=(NtLcal(i)+NtL(i-1))/2;
xw_old(i)=xwcal(i);

xwcal (i) = (NLH2Oavg (i)*dz-CL (i)*ep_Lcal (i)*DifH2O_CH3OHL (i)*
        xw (i-1))/ (NtLavg(i)*dz-CL(i)*ep_Lcal(i)*DifH2O_CH3OHL(i));

NLH2Ocal (i) =-CL (i)*ep_Lcal (i)* DifH2O_CH3OHL (i)*
              (xwcal (i)-xw (i-1))/dz+xwcal(i)*NtLavg(i);

NLH2Ocal (i) = (NLH2Ocal (i) +NLH2O (i-1))/2;

NLCH3OHcal (i) =-CL (i)*ep_Lcal (i)*DifH2O_CH3OHL (i)*
                ((1-xwcal (i))-(1-xw (i-1)))/dz+ (1-xwcal (i))*NtLavg(i);

NLCH3OHcal (i) = (NLCH3OHcal (i) +NLCH3OH (i-1))/2;

NtLcal (i) =NLCH3OHcal (i) +NLH2Ocal (i);

xwcal (i) = (xwcal (i) +xw (i-1))/2;

DIFF1 (i) =xwcal (i)-xw_old(i);
RDIFF1 (i) =abs (DIFF1 (i)/xwcal (i));

xwcal (i) = (xwcal (i) +xw_old(i))/2;
xw (i) =xwcal (i);
xm(i)=1-xw(i);
xw_guess(i)=xw(i);

end

DLH2O (i) =-CL (i)*ep_Lcal (i)* DifH2O_CH3OHL (i)*(xw (i)-xw (i-1))/dz;
CLH2O (i) =NLH2Ocal (i)-DLH2O (i);
NLH2Ocal (i) =DLH2O (i) +CLH2O (i);
DLCH3OH (i) =-CL (i)* ep_Lcal (i)*DifH2O_CH3OHL (i)*(xm (i)-xm (i-1))/dz;
CLCH3OH (i) =NLCH3OHcal (i)-DLCH3OH (i);
NLCH3OHcal (i) =DLCH3OH (i) +CLCH3OH (i);
NtLcal (i) =NLCH3OHcal (i) +NLH2Ocal (i);

MWavg(i) =xw(i)*18.016 +(1 - xw(i) )*32.04;

%Ergun eq for the liquid phase
```

```
ptL(i)=ptL(i-1)-dz*(((150*Lvisc_H2O(i)*(ep_s(i))^2*NtLcal(i))/(Lden_H2O(i)*d_ag(i)^2*
        ep_Lcal(i)^3))*MWavg(i)/1000+((1.75*(ep_s(i))*NtLcal(i)^2)/(Lden_H2O(i)*
        d_ag(i)*ep_Lcal(i)^3))*MWavg(i)/1000);

%ST = surface tension [N/m] or surface energy [J/m2]
 ST (i) = (- 2.5798e-04*T (i) ^2 - 1.1525e-03*T (i) + 92.215)/1000;

ptgavg(i)=(ptg(i)+ptg(i-1))/2;
ptLavg(i)=(ptL(i)+ptL(i-1))/2;

dpGLcal (i) = - (4*ST (i)*(0.4226))/ (ptLavg (i) - ptgavg(i) );
dpGLcal (i) = (dpGLcal (i) +dpGL (i-1))/2;

  RDIFF2 (i) =1;

   While RDIFF2 (i)>0.000000001

   dpGLavg(i)=(dpGLcal(i)+dpGL(i-1))/2;
    If dpGLavg (i) < 0.000000001

ep_gcal (i) = 0.52-2.6444*(1-exp (0.000001-(dpGLavg*10^6)));
ep_Lcal (i) = ep_v(i) - ep_gcal(i);
ep_gold (i) =ep_gguess (i);
DIFF2 (i) =ep_gcal (i)-ep_gold (i);
RDIFF2 (i) =abs (DIFF2 (i)/ep_gcal (i));
ep_gcal (i) = (ep_gcal (i) +ep_gold (i))/2;
ep_gguess (i) =ep_gcal (i);

      elseif dpGLavg(i) > 0.0001

ep_gcal (i) = 0.018632*exp (1-0.01*(dpGLavg*10^6));
ep_Lcal (i) = ep_v(i) - ep_gcal(i);
ep_gold (i) =ep_gguess (i);
DIFF2 (i) =ep_gcal (i)-ep_gold (i);
RDIFF2 (i) =abs (DIFF2 (i)/ep_gcal (i));
ep_gcal (i) = (ep_gcal (i) +ep_gold (i))/2;
ep_gguess (i) =ep_gcal (i);

       else

ep_gcal (i) = 0.20613*exp (((dpGLavg (i)*10^6) ^16.24)/ (-3.949e+27)) +
              0.47129/ ((dpGLavg(i)*10^6)^0.061144) - 0.337;
ep_gcal (i) = (ep_gcal (i) +ep_g(i-1))/2;
ep_Lcal (i) = ep_v(i) - ep_gcal(i);
ep_old(i)=ep_gguess(i);
DIFF2 (i) =ep_gcal (i)-ep_old(i);
```

```
RDIFF2 (i) =abs (DIFF2 (i)/ep_gcal (i));
ep_gcal (i) = (ep_gcal (i) +ep_old(i))/2;
ep_gguess (i) =ep_gcal (i);

end
end
end
end
end

ptg= [ptg']
ptL=[ptL']
yCO2= [yCO2']
yCH3OH= [yCH3OH']
yH2O= [yH2O']
Nco2= [NCO2']
Ntgcal= [Ntgcal']
Ntg=[Ntg']
NgH2Ocal= [NgH2Ocal']
NgCH3OHcal= [NgCH3OHcal']
RH2Ovap= [RH2Ovap']
RCH3OHvap= [RCH3OHvap']
xwcal= [xwcal']
xm=[xm']
xw=[xw']
NLH2Ocal= [NLH2Ocal']
NLCH3OHcal= [NLCH3OHcal']
NtLcal= [NtLcal']
dpGLcal= [dpGLcal']
ep_gcal= [ep_gcal']
ep_Lcal= [ep_Lcal']
DLH20= [DLH2O']
CLH2O= [CLH2O']
DLCH3OH= [DLCH3OH']
CLCH3OH= [CLCH3OH']
DCO2= [DCO2']
CCO2= [CCO2']
NCO2= [NCO2']
DgH20= [DgH2O']
CgH2O= [CgH2O']
DgCH3OH= [DgCH3OH']
CgCH3OH= [CgCH3OH']
```